



INSIDE

Stadtwerke München GmbH
Innovative Energie Pullach
Karlsruher Institut für Technologie

Verbundvorhaben: Induzierte Seismizität & Bodendeformation als Interferenzaspekte beim Betrieb von Geothermieranlagen in der süddeutschen Molasse – Untersuchungen zu einem verbesserten Prozessverständnis im tiefen Untergrund und Maßnahmen zur Risikominimierung

SPARKER SURVEY AT SCHÄFTLARNSTRAßE: DESIGN, FIELD ACQUISITION AND DATA PROCESSING

Supported by:



Federal Ministry
for Economic Affairs
and Climate Action



on the basis of a decision
by the German Bundestag

Grant agreement number

Karlsruher Institut für Technologie:	03EE4008A
SWM Services GmbH:	03EE4008B
Innovative Energie für Pullach GmbH:	03EE4008C

The authors are responsible for the content of this publication.

Verbundvorhaben:	Induzierte Seismizität & Bodendeformation als Interferenzaspekte beim Betrieb von Geothermieanlagen in der süddeutschen Molasse
Teilvorhaben:	Koordination, Datenerfassung und -bearbeitung, Modellierung
Ausführende Stelle:	Karlsruher Institut für Technologie (KIT) – Institut für Angewandte Geowissenschaften – Campus Süd – Abt. Geothermie & Reservoir-Technologie
Förderkennzeichen:	03EE4008A
Laufzeit des Vorhabens:	01.09.2019 – 31.08.2022

Titel:	Sparker survey at Schäftlarnstraße: Design, Field acquisition and Data processing
Arbeitspaket:	AP1.3: Bohrlochmessungen
Meilenstein:	(M1.3.2)
Fälligkeitsdatum:	/
Tatsächliches Datum:	/
Ansprechpartner:	Emmanuel Gaucher, emmanuel.gaucher@kit.edu
Autoren:	Jérôme Azzola, jerome.azzola@kit.edu Emmanuel Gaucher, emmanuel.gaucher@kit.edu
Version:	1

Version	Datum	Beschreibung der Ergänzungen, Änderungen, Überprüfungen
1	30.04.2021	Initial version

TABLE OF CONTENT

1	BACKGROUND	8
1.1	INTRODUCTION	8
1.2	DISTRIBUTED ACOUSTIC SENSING (DAS).....	9
1.3	SPARKER BOREHOLE SEISMIC SOURCE.....	11
2	SURVEY DESIGN.....	13
3	DATA ACQUISITION	14
3.1	OVERVIEW	14
3.1	RECEIVER CHARACTERISTICS.....	16
3.1.1	<i>Surface seismometers</i>	<i>16</i>
3.1.2	<i>Fibre-optic cables and DAS-acquisition</i>	<i>17</i>
3.2	SHOOTING AND ACQUISITION PROCEDURE	19
3.2.1	<i>Source characteristics.....</i>	<i>19</i>
3.2.2	<i>Shooting sequence and acquisition parameters</i>	<i>19</i>
3.2.3	<i>Explanation of the shooting and acquisition procedure.....</i>	<i>23</i>
4	SEISMOMETERS DATA	27
5	PRE-PROCESSING OF THE DAS RAW DATA.....	29
5.1	PRINCIPLE	29
5.2	PRE-PROCESSING RESULTS	29
5.3	STACKING PROCEDURE QUALITY-CONTROL	32
6	PROCESSING AND ANALYSIS OF THE STRAIN-RATE DATA	34
6.1	PURPOSE AND MEANS	34
6.2	CONTRIBUTIONS OF THE SURVEY SIMULATIONS	34
6.3	TAP-TEST ANALYSIS (TH4)	35
6.3.1	<i>Time domain</i>	<i>36</i>
6.3.2	<i>Frequency domain.....</i>	<i>38</i>
6.4	SPARKER SHOT-POINT RESULTS AND INTERPRETATION	40
6.4.1	<i>Time domain</i>	<i>41</i>
6.4.2	<i>Frequency domain.....</i>	<i>42</i>
6.4.3	<i>Coherency analysis</i>	<i>43</i>
7	FINAL DISCUSSION AND CONCLUSION.....	47
8	APPENDICES	49
8.1	APPENDIX 1: OTDR MEASUREMENTS ON THE TH3 AND TH4 FIBRES.....	49
8.2	APPENDIX 2: CROSS-WELL SURVEY SIMULATIONS.....	53
8.3	APPENDIX 3: GL = 5 M, DATA ACQUIRED IN TH4 ON 20/11, SOURCE AT 1200 M	59
8.4	APPENDIX 4: GL = 5 M, DATA ACQUIRED IN TH4 ON 19-20/11, SOURCE AT 1200 M.....	62
8.5	APPENDIX 5: GL = 5 M, DATA ACQUIRED IN TH3 ON 19/11, SOURCE AT 920 M	65
8.6	APPENDIX 6: GL = 10 M, DATA ACQUIRED IN TH3 AND TH4 ON 17/11, SOURCE AT 400 M.....	68

LIST OF FIGURES

Figure 1-1: Location of the Schäftlarnstraße geothermal field, in the Munich area (Sendling) and trajectory of the six wells. The red curves shows the well, SLS Th6, in which the source was run. The blue curves show the wells, SLS Th3 and SLS Th4, which acquired the data using with fibre-optic cables deployed over the sections shown by the purple arrows.....	8
Figure 1-2: Overview of the subsurface of the SLS geothermal field. The main layers/horizons identified above the reservoir thanks to the 3D-seismic survey performed in the framework of the GRAME project (further information on mw.tum.de/es/forschung/projekte/abgeschlossene-projekte/grame/) are shown with the six well trajectories.....	9
Figure 1-3: Principle of the Febus DAS-interrogator. Source: http://www.febus-optics.com/en/	10
Figure 1-4: Schematic of the parameters used to set-up a DAS-acquisition. A pulse, with a given power and spatial width, is propagating through the interrogated fibre and is back-scattered by random heterogeneities. The temporal and spatial sampling of the raw optical data is distinguished from the discretization of the strain rate measurements, which are obtained by temporal and spatial differentiation. Source: Febus Optics.....	11
Figure 1-5: Advanced Sparker Tool (AST) of Avalon Sciences Ltd. Source: https://avalonsciences.com/	12
Figure 2-1: For the six wells, evolution of the offset from wellhead as a function of the true vertical depth (TVD). The black dots highlight the depth levels at which the well inclination reaches the 58° limit.....	13
Figure 3-1: Top - Overview of the fieldwork context, at the Schäftlarnstraße geothermal site, with position of the control room, of the crane and of the wireline truck. Bottom - Illustrative picture, Th6 is the last well of the row.....	14
Figure 3-2: Schematic (top) and pictures (bottom) showing the deployment and the routing of the AST assembly in the Th6 borehole.....	15
Figure 3-3: Position of the three seismometers at the Schäftlarnstraße geothermal site.....	16
Figure 3-4: Top – Station SLS1. Bottom – Station SLS3, in the cellar of the well SLS-Th2a.....	17
Figure 3-5: Schematic of the arrangement of the fibre-optic cables in the Th3 and Th4 wells. The schematic shows a configuration where the DAS interrogator, in the control room, acquires the signals along the Th3 and Th4 FOCs in series. The position of sensitive points (splices, microbend) where light pulses may suffer energy loss (which deteriorates the acquired data quality) are highlighted.....	17
Figure 3-6: Firing and DAS acquisition / pre-processing procedure.....	18
Figure 3-7: AST control panel in the wireline truck, with fibre stretcher used for the recording of time-break signals on the top (left). DAS-unit, data-storage device and Pc-Febus in the control room (right).....	19
Figure 3-8: Chronology of the number of shots (top) and source position (bottom). The source position in Th6 is given in m MD and the dates are in UTC time (local time = UTC+01). The vertical lines in the upper subplot indicate changes in the source position. The replacement of the firing head occurred at the dates indicated by the arrows at the bottom of the figure.....	20
Figure 3-9: Evolution with depth (m MD) of the source-receiver distance, in Th4 (top panels) and Th3 (bottom panels). Source positions: 400, 920 or 1200 m MD in Th6.....	23
Figure 3-10: Th6 borehole stratigraphy (left), completion (middle) and trajectory (right). The completion highlights the presence of a tie-back, down to 768 m (the end of the first section of the well), which could behave as a wave guide for the seismic signal generated by the AST. The well trajectory enables to identify depths at which the AST could lay against the well, which could improve the coupling to the ground.....	24
Figure 4-1: Stacked traces (non-filtered) obtained from the recordings of the three channels of the SLS3 seismometer. Position of the source: 1200 m MD in Th6.....	27
Figure 4-2: Power spectral densities of the stacked traces of the three components of SLS3.....	27
Figure 4-3: Stacked and filtered traces of the three components of SLS3. A third order Butterworth bandpass filter has been applied in the frequency range 5-20Hz (left) and 60-100Hz (right).....	28
Figure 5-1: Source at 1200 m MD. Strain-rate stacks of 901 shots (20/11). GL equals 5 m (top), 10 m (middle) and 20 m (bottom), DT = 2 s. The origin of the Y-axis is positioned at the wellhead. $t = 0$ s is the firing time break. The grey-scale shows the strain-rate amplitude, which covers, for each subplot, the inter-quartile range of the strain-rate amplitudes (i.e. the [Q1, Q3] range, where Q1 and Q3 are the first and third quartiles respectively). The box-plots on the left show basic statistics on the amplitudes shown on the right: the blue box is limited by Q1 and Q3, the red segment shows the median (Q2) and the red points below and above the whiskers show the outliers above and below the upper inner fence and the lower inner fence respectively.....	31

Figure 5-2: Source at 1200 m MD. Top – Strain-rate for one shot (20/11). Bottom – Strain-rate after stack of 1446 shots (19+20/11). The grey-scale shows the strain-rate amplitude, the range varies for both datasets. .	32
Figure 5-3: Two seconds strain-rate data-window (unstacked), from the connector plugged to the DAS-interrogator to 600 m downstream. The Th4 wellhead is located at 320 m. GL = 5 m.	33
Figure 5-4: Same as Figure 5-3 but stack of 901 shots.	33
Figure 6-1: Simulation of a source at 1200 m TVD in Th6. Left - dynamic displacements (meters) computed from the simulations in both receiver-wells (Th3, downward on top slice – Th4, downward, on bottom slice). The red dots indicate the maximum amplitude of the first arrivals. Right - evolution with depth of the maximal amplitude of the first arrivals, normalized by the absolute maximum over the whole dataset, in Th3 (top) and Th4 (bottom).	35
Figure 6-2: Picture of the tap-test performed on the Th4 wellhead.	35
Figure 6-3: Top: Strain-rate data produced during the tap-test (left) and corresponding box-plot (right, see Figure 5-1 for details). The 600-m depth range excludes the strong noise recorded at the surface due to the environment of the fibre. Bottom: strain-rate traces extracted at the depths of 300, 330, 360 and 385 m after the control room respectively. Horizontal lines in the top plot highlight these depths. Note the change of strain-rate scale for the trace at 385 m.	36
Figure 6-4: Enhanced visualization of strain-rate by data whitening. Top-right: original dataset. Bottom-right: dataset after whitening all strain-rate values within the inter-quartile range. The colour map for both plots are set according to the boxplot of the dataset after removal of the whitened values (bottom-left).	37
Figure 6-5: Zoom on the first hit displayed Figure 6-4. The white line, with a slope of 5000 m/s, highlights the propagation velocity of the acoustic signal along the FOC and is consistent with propagation in steel material.	38
Figure 6-6: Power spectral densities of the strain-rate along depth recorded during the tap-test. Left: PSDs represented with different colour-scale limits. Top-right: Spectrogram after whitening the amplitudes smaller than Q3.	38
Figure 6-7: Illustration of the normalization procedure to remove acquisition-related noise. The spectra computed from the strain-rate data (top-left) are normalized (top-bottom) and tapered using a Hamming window centred on the requested frequency band – here 150 – 250 Hz – (top-right). A normalized strain-rate is obtained after inverse Fourier transform of the tapered normalized spectrum (bottom-right).	39
Figure 6-8: The four traces of Figure 6-3 after spectral normalization.	39
Figure 6-9: Strain-rate generated by the second hammer strike at 300 m (see Figure 6-8) before spectral normalization (red) and after spectral normalization (black). For comparison, both signals are normalized by their respective maximum value.	40
Figure 6-10: Tap-test data of Figure 6-3 after [50, 150] Hz band-pass filtering using a third-order Butterworth filter. Left: grey scale corresponds to the inter-quartile range. Right: full colour scale but values below Q3 were whitened.	40
Figure 6-11: Strain-rate, GL = 10 m, stack of 901 shots recorded in Th4 on 20/11/20, source at 1200 m MD in Th6. Right: The black vertical line, at $t = 0$ s, indicates the firing time; the red line shows the expected time of arrival of the P-wave as calculated by the simulations; the grey colour scale ranges between Q1 and Q3 of the strain-rate. Left: box-plot of the strain rate values shown on the right-hand side.	41
Figure 6-12: Enhanced visualisation of strain-rate data of Figure 6-11. Top-right: strain-rate amplitudes; the red line indicates the simulated P-wave arrival times. Bottom-right: same as top-right but the strain-rate amplitude within the inter-quartile range are whitened. In both images, the colour map covers the full range of strain-rate amplitudes. Bottom-left: box-plot of the strain-rate amplitude after removal of the whitened values.	42
Figure 6-13: Three representations of the spectrograms of the strain-rate shown in Figure 6-11. Top left: the colour scale is bounded by the upper-inner-fence of the samples. Bottom left: the colour scale is bounded by the Q3 of the samples. Top right: – Data with amplitudes below Q3 are whitened and the colour scale adapted accordingly.	42
Figure 6-14: Strain-rate, GL = 10 m, stack of 901 shots recorded in Th4 on 20/11/20, source at 1200 m MD in Th6. The top-left and bottom-right panels show the dataset and the central position (simulated P-wave arrival time) of each window. They are shown to ease the understanding of the correlation matrix, which is displayed on the top-right. The correlation matrix gives the maximum cross-correlation coefficient between two windows at given depths. Consequently, it is symmetric and the diagonal elements equal one because this corresponds	

to the auto-correlation of the trace. The plot on the bottom-left is a zoom of the correlation matrix in the black square. 44

Figure 6-15: Strain-rate, GL = 10 m, stack of 901 shots recorded in Th4 on 20/11/20, source at 1200 m MD in Th6. Top-left: the blue horizontal lines, at 900 m and 1500 m respectively, and the black vertical line, at 0 s time, limit the zone of interest. The 0.2 s reference window (in red) is centred on the simulated P-wave arrival time at 1000 m depth. Top-right: correlation coefficients computed over the zone of interest. , which is computed for each window comparison, in the queried area. The plot on the bottom-right is a zoom of the correlation coefficients around the reference trace (black square). 45

Figure 6-16: Tap-test. Top-left: a 0.8 s window is selected in the dataset (red segment) and compared by correlation to successive windows selected within the depth interval ranging from 280 to 400 m (black horizontal lines). Bottom-left: strain-rate trace of the tap-test at 330m; the reference window is highlighted in red. Right: maximum correlation coefficient between the reference trace and the rest of the signal over depth and time..... 46

Figure 8-1: Results of the OTDR test: fibre Th3 – SM1, downward and upward. Used wavelength: 1550 nm. The table highlights the main losses identified along the fibre. The 1.3 dB loss #4 is positioned at the microbend (i.e. the turning point of the fibre behind the casing)..... 50

Figure 8-2: Results of the OTDR test: fibre Th4 – SM1. Used wavelength: 1550 nm. The table highlights the main losses identified along the fibre. The trace highlights the energy loss along the fibre, with a cumulative loss of about 0.69 dB at the end of the fibre..... 51

Figure 8-3: Results of the OTDR test: fibre Th3 – SM1 downward + upward connected to fibre Th4 – SM1. Used wavelength: 1550 nm. The table highlights the main losses identified along the fibre. The 1.3 dB loss #3 is positioned at the microbend located in Th3. The connection of Th3 and Th4 fibres brings an additional 0.55 dB loss (#5). The cumulative loss at the end of the fibre reaches 3.7 dB..... 52

Figure 8-4: Schematic of the impact of two physical processes on the amplitude of DAS-measurements..... 53

Figure 8-5: The horizons of the GRAME project are used with the trajectories and sonic-logs of the SLS wells to setup a 3D-blocky velocity model..... 54

Figure 8-6: Evolution of the horizontal particle velocity (in $m.s^{-1}$) with depth (here represented as the receiver #) in both Th3 (downward and upward, for the top and middle sections respectively) and Th4 (lower section) wells. The source is located at 400 m TVD in Th6. 54

Figure 8-7: Evolution, with measured depth, of the angle between the wavefront and the well-trajectory (in black). The source is positioned in Th6 at 1200 m TVD (top-left), 400 m (top-right) or 920 m (bottom panels – in Th3 on the left, in Th4 on the right). The red curve indicates the theoretical sensitivity of DAS measurements toward longitudinal waves: sensitivity is null for longitudinal waves propagating orthogonally to the fibre.... 55

Figure 8-8: Left– Evolution with depth (here with # of receiver) of the dynamic displacement (in m – top panel) or of the strain rate (in $m.m^{-1}.s^{-1}$ – bottom panel), in Th3 and Th4. The source is located at a depth of 1200 m TVD in Th6 (top panel) or at 400 m (bottom panel). The time at which the amplitude of the first arrivals is maximal is highlighted for each trace by a red point. Right – Evolution with measured depth, in both Th3 and Th4, of the maximal amplitude, divided by the absolute maximal amplitude (observed for all the traces). These measurements are representative of the attenuation of the DAS-measurements, caused by the source energy geometrical spreading and the directional sensitivity of the receiving fibres. 56

Figure 8-9: Minimum number of shots (represented by the colours) necessary to identify the source signal positioned along Th6 (horizontal axis) on the fibres (vertical axis) in Th3 (left subplot) and Th4 (right subplot). The colour map is saturated between 500 and 1000 shots and limited to 1000 shots. See text for the assumptions..... 57

Figure 8-10: Prediction of the range of receivers in Th4 (horizontal axis in m MD) that can detect the signal of a source positioned in Th6 at different depths, S_TVD (horizontal subplots), as a function of the number of shots (Y axis of each subplot). See text for the assumptions..... 58

Figure 8-11: Stacked strain-rate, 901 shots, Th4, 20/11, source at 1200 m, GL = 5 m. Display similar to Figure 6-11..... 59

Figure 8-12: Enhanced visualisation of strain-rate of Figure 8-11. Display similar to Figure 6-12..... 59

Figure 8-13: Power spectral densities of Figure 8-11 strain-rate. Display similar to Figure 6-6. 60

Figure 8-14: Spatial cross-correlation of Figure 8-11 strain-rate. Display similar to Figure 6-14..... 60

Figure 8-15: Spatial and temporal cross-correlation of Figure 8-11 strain-rate. Display similar to Figure 6-15. 61

Figure 8-16: Stacked strain-rate, 1446 shots, Th4, 19-20/11, source at 1200 m, GL = 5 m. Display similar to Figure 6-11..... 62

Figure 8-17: Enhanced visualisation of strain-rate of Figure 8-16. Display similar to Figure 6-12..... 62

Figure 8-18: Power spectral densities of Figure 8-16 strain-rate. Display similar to Figure 6-6. 63

Figure 8-19: Spatial cross-correlation of Figure 8-16 strain-rate. Display similar to Figure 6-14..... 63

Figure 8-20: Spatial and temporal cross-correlation of Figure 8-16 strain-rate. Display similar to Figure 6-15. 64

Figure 8-21: Stacked strain-rate, 545 shots, Th3, 19/11, source at 920 m, GL = 5 m. Display similar to Figure 6-11. 65

Figure 8-22: Enhanced visualisation of strain-rate of Figure 8-21. Display similar to Figure 6-12..... 65

Figure 8-23: Power spectral densities of Figure 8-21 strain-rate. Display similar to Figure 6-6. 66

Figure 8-24: Spatial cross-correlation of Figure 8-21 strain-rate. Display similar to Figure 6-14..... 66

Figure 8-25: Spatial and temporal cross-correlation of Figure 8-21 strain-rate. Display similar to Figure 6-15. 67

Figure 8-26: Stacked strain-rate, 9 shots, Th3 and Th4, 17/11, source at 400 m, GL = 10 m. Display similar to Figure 6-11..... 68

Figure 8-27: Enhanced visualisation of strain-rate of Figure 8-26. Display similar to Figure 6-12..... 68

Figure 8-28: Power spectral densities of Figure 8-26 strain-rate. Display similar to Figure 6-6. 69

Figure 8-29: Parallel between the Welch spectrograms measured along the Th3 and Th4 FOCs put in series (top) and the OTDR report (bottom) (see “Appendix 1: OTDR measurements on the Th3 and Th4 fibres”). Each spectrogram is calculated with the Welch method to decrease the impact of noise at the cost of the frequency resolution. The depths at which the OTDR highlights strong energy losses are clearly identified on the spectrogram image by a widening of the excited frequency band, associated here with a deterioration of the measurement conditions due to strong reflexions at the connectors/splice/microbend..... 69

LIST OF TABLES

Table 1-1: Characteristics of the AST borehole source 11

Tables 5-1: Parameters of the stacking procedure 29

1 BACKGROUND

1.1 INTRODUCTION

In the frame of the INSIDE project, scientific investigations are carried out to assess the impact of geothermal exploitations on induced seismicity, focusing on several active and under-development plants in the Munich area (Germany, Molasse Basin). In that respect, the location of a seismic event is of major importance. It is well known that the seismic velocity model plays a major role to determine hypocentres with accuracy and high precision. To further constrain the seismic velocity model, an active cross-well survey has been acquired at the Schäftlarnstraße (SLS) geothermal plant (see Figure 1-1), which is one of the site of interest of the INSIDE project. The survey was held from 16-20/11/2020, before the six wells of the geothermal site go into production.

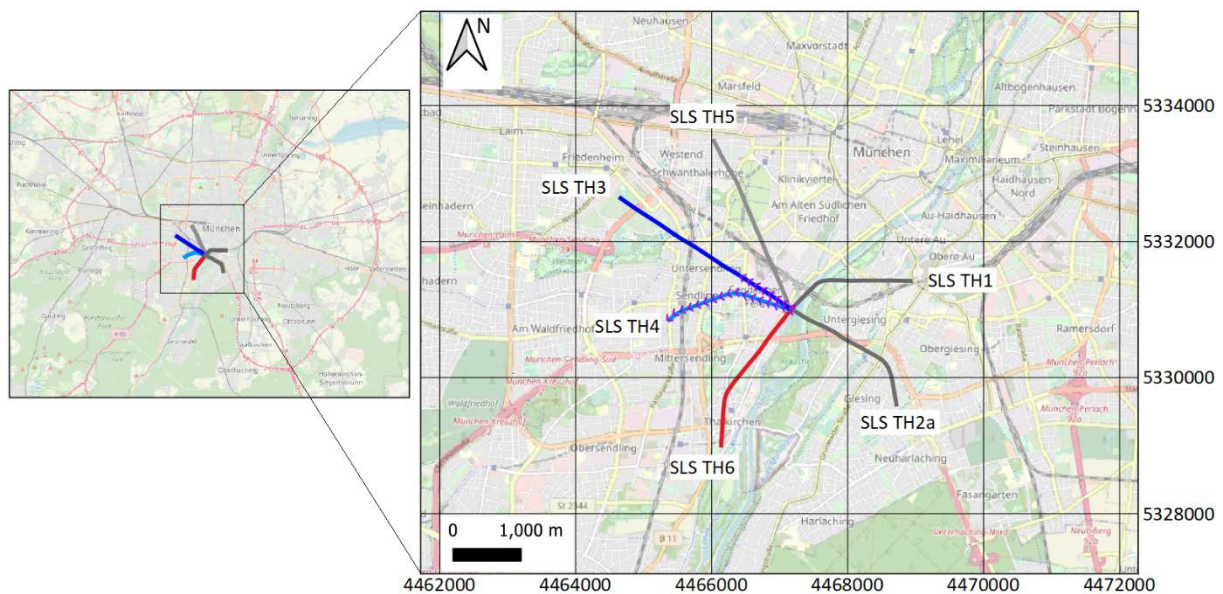


Figure 1-1: Location of the Schäftlarnstraße geothermal field, in the Munich area (Sendling) and trajectory of the six wells. The red curves shows the well, SLS Th6, in which the source was run. The blue curves show the wells, SLS Th3 and SLS Th4, which acquired the data using with fibre-optic cables deployed over the sections shown by the purple arrows.

Two fibre-optic cables (FOCs) have been deployed in the SLS geothermal field, thanks to the GAB (Geothermie-Allianz Bayern) project, the Technical University of Munich (TUM) and the field operator Stadtwerke München (SWM) (see Figure 1-1). One is cemented behind the tubing of the 1st section of the well Th3, and the other one is attached to a sucker rod deployed from top to bottom inside the well Th4. Distributed Acoustic Sensing (DAS) acquisitions and processing techniques can therefore be applied, which opens perspectives to measure acoustic signals along the cables, using distributed sensors. The combination of this recording method with a mobile seismic source allows, theoretically, sampling the multiple layers of the geothermal field, from surface down to reservoir (Figure 1-2).

The survey has been designed to further refine the velocity model, to gain knowledge on the less constrained S-wave velocity field, and to improve the imaging of the underground. Another important aspect was to mimic a seismic event that would occur at the reservoir level with a “calibration” shot positioned as deep as possible in the well Th6, where the source was deployed. Since real location and timing of the active source are controlled, calibration of the velocity model between the source and the FOCs should be possible. Another objective of the test is to perform a cross-well tomography to go beyond the calibration and to image the velocity model.

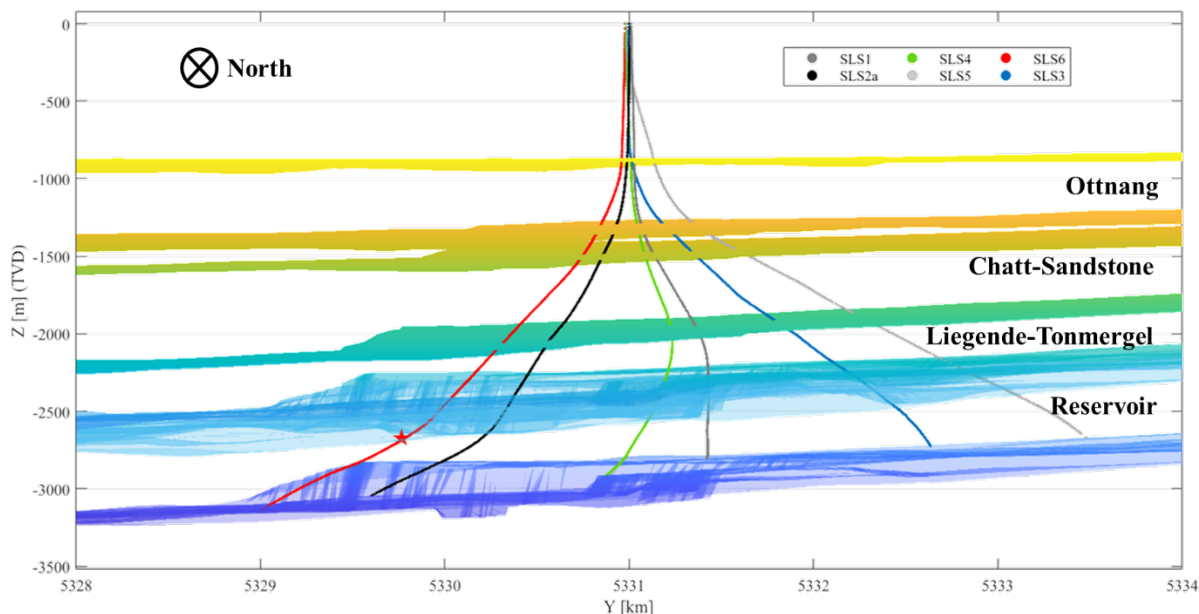


Figure 1-2: Overview of the subsurface of the SLS geothermal field. The main layers/horizons identified above the reservoir thanks to the 3D-seismic survey performed in the framework of the GRAME project (further information on mw.tum.de/es/forschung/projekte/abgeschlossene-projekte/grame/) are shown with the six well trajectories.

Several stakeholders were involved in the survey; they are listed below:

Service and supply	Company in charge
Field operator	Stadtwerke München (SWM)
Survey design	Karlsruher Institut für Technologie (KIT)
Survey design	Erdwerk (EW)
Wellhead services (WH)	Hartmann (HART)
Crane	BKL Crane Logistik GmbH
Wireline (WL)	Weatherford (WF)
Advanced Sparker Tool	Avalon Sciences Ltd (ASL)
Access to the fibre-optic cables	Technische Universität München (TUM)
Distributed Acoustic Sensing (DAS)	Febus-Optics (FO)

After introducing the flagship technologies of this survey (DAS technology and Sparker source), this document describes the design of the study, the data recording procedure, and the data processing.

1.2 DISTRIBUTED ACOUSTIC SENSING (DAS)

Distributed Acoustic Sensing (DAS) is used to interrogate a FOC by propagating a light pulse from an optical phase-based system (the DAS-interrogator). The DAS-unit is connected to one end of the cable and sends light pulses through the entire fibre. This technology enables to detect local acoustic stimulations by measuring the deformation undergone by the fibre.

The measurement principle of the DAS relies on the Rayleigh backscattering of the light pulse propagating through the fibre. When travelling into the fibre, a small fraction of the pulse is continuously sent back to the DAS interrogator from random heterogeneities located in the fibre (see sketch in Figure 1-3). This principle enables to record a 2D-data set, as represented in Figure 1-4, with the light pulse interrogating the fibre both in time and space.

An acoustic signal reaching the FOC locally perturbs the fibre that will modify the way the light is propagating through it. Detection / location of the perturbation is therefore possible from the flying time of the light. The optical dephasing between two positions on the optical fibre is directly related to the longitudinal constraint applied to the fibre, i.e. its elongation or compression. The strain (typically in nanostrain, i.e. 10^{-9} m/m) applied to the cable is therefore computed from the optical dephasing acquired along a distance called the gauge length (GL). Similarly, a derivation time (DT) is set to calculate the derivative of the strain in time, leading to a strain-rate (in nanostrain. s^{-1} or nm/m/s). The calculation of the strain-rate from the raw optical measurements allows correcting the data from temperature effects among others.

The interrogator used in the survey is the so-called Febus A1-R DAS-unit (provided by the Febus-Optics company, <http://www.febus-optics.com/en/>). It enables to acquire two distinct types of data:

1. The raw data, corresponding to the amplitude and phase of the optical signal, along the FOC, measured by the interrogator. After acquisition, these raw data can be used to generate strain and/or strain-rate data with variable gauge lengths and derivation times (to be defined according to purpose).
2. Strain-rate data, for which the gauge length and derivation time have been determined and fixed before acquisition.

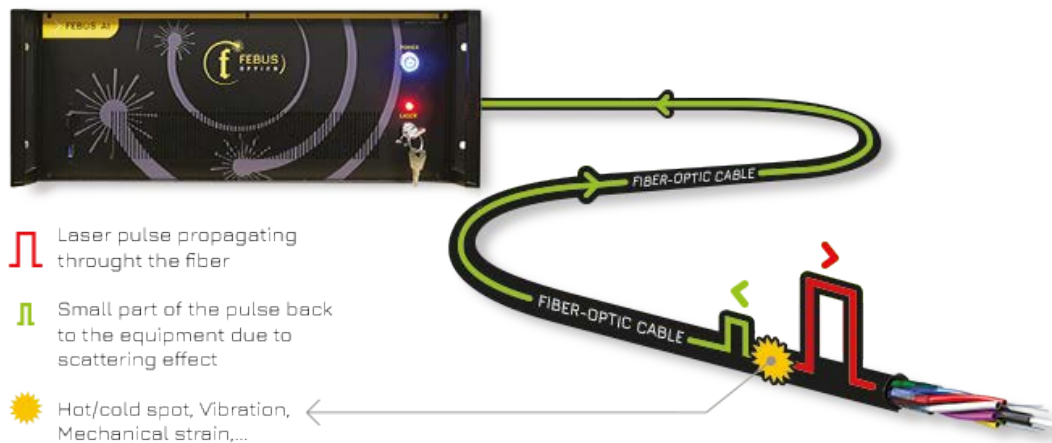


Figure 1-3: Principle of the Febus DAS-interrogator. Source: <http://www.febus-optics.com/en/>

The interrogator provides broadband measurements: the acoustic bandwidth can extend from less than 1 Hz to several tens of kHz. The interrogator offers sampling intervals (for the optical data) from 0.4 to 12.8 m, and wide gauge-length capabilities (from 1 to 50 m). Typically, the GL should be smaller than the wavelengths of the acoustic signal of interest. The Febus A1-R reaches a noise-floor of the order of 10 picostrain (10×10^{-12} m/m).

Several parameters are necessary to set-up an acquisition (Figure 1-4). They characterize the light pulse sent into the fibre as well as the temporal and spatial sampling of the raw data:

- Fibre distance to be interrogated;
- Optical power to optimize the optical signal;
- Pulse width to optimize the optical signal;
- Pulse rate frequency (number of pulses sent into the fibre per second);
- Spatial sampling resolution (distance between two consecutive samplings along the optical fibre).

As described above, the gauge length (signal integration distance along the optical fibre) and the derivation time (signal derivation time) have to be fixed in addition when acquiring in a dynamic way.

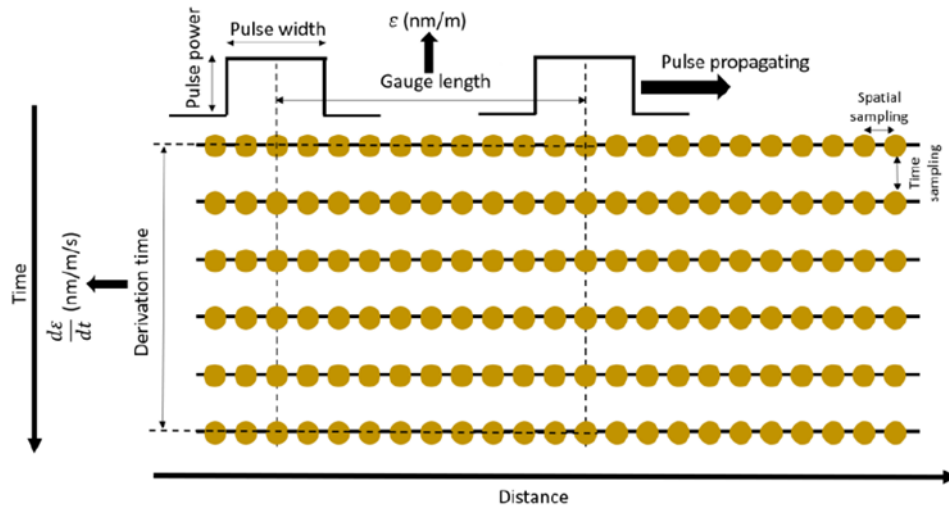


Figure 1-4: Schematic of the parameters used to set-up a DAS-acquisition. A pulse, with a given power and spatial width, is propagating through the interrogated fibre and is back-scattered by random heterogeneities. The temporal and spatial sampling of the raw optical data is distinguished from the discretization of the strain rate measurements, which are obtained by temporal and spatial differentiation. Source: Febus Optics.

1.3 SPARKER BOREHOLE SEISMIC SOURCE

The Advanced Sparker Tool (AST) of the Avalon Sciences Ltd. company (<https://avalonsciences.com/>) is a borehole source that provides a repeatable omni-directional energy pulse (Figure 1-5). To be operated, direct current needs to be supplied from surface to the High Voltage Power Supply Unit (HVPSU – see diagram below). The unit charges several capacitors until a critical voltage threshold is reached. Energy is then transmitted to the electrode, which generates a spark and provides a high-energy output pulse. Table 1-1 describes the main characteristics of the source.

Table 1-1: Characteristics of the AST borehole source

Output signal	10 – 4000 Hz omni-directional
Peak power	1000 Joules/shot
Firing interval	20 s
Environmental constraints	3" diameter Up to 150°C and 65 MPa Operation in any type of conductive well fluid

An important technical aspect is that the firing head needs to be recharged after approximately 1000 shots, which requires pulling the tool out of hole. A well inclination smaller than 60° is also necessary to run the tool in hole without the help of a tractor, which is the case in this survey.



Figure 1-5: Advanced Sparker Tool (AST) of Avalon Sciences Ltd. Source: <https://avalonsciences.com/>

2 SURVEY DESIGN

The measurement campaign at Schäftlarnstraße has been planned for four days, with the AST source providing multiple acoustic excitations at different depths in Th6. The acquisition is carried out using the FOCs installed in the Th3 and Th4 wells and three three-components seismometers installed at the surface at the site. To design the survey, the well trajectories and inter-well distances were analysed and simulations were conducted. The following paragraphs focusses on the main results of the survey design.

The source well has been pre-selected by analysing first the inclination of the six wells except Th4, in accordance with the well inclination limiting the movement of the source in the hole (see Figure 2-1). Th4 cannot be used to run the source since it already contains the FOC deployed on a sucker rod. In Th3 and Th5, the limiting inclination is reached at around 1300 m TVD; in Th1, it is around 2600 m TVD; and in Th6 and Th2a the limit is around 2755 m TVD, the closest to the reservoir. A second factor of importance is the inter-well distance which controls part of the attenuation of the source amplitude at the receivers. Hence, it is a priori better to select nearby source-receiver wells to increase the chance of recording a signal. Consequently, Th6 was pre-selected as the source well.

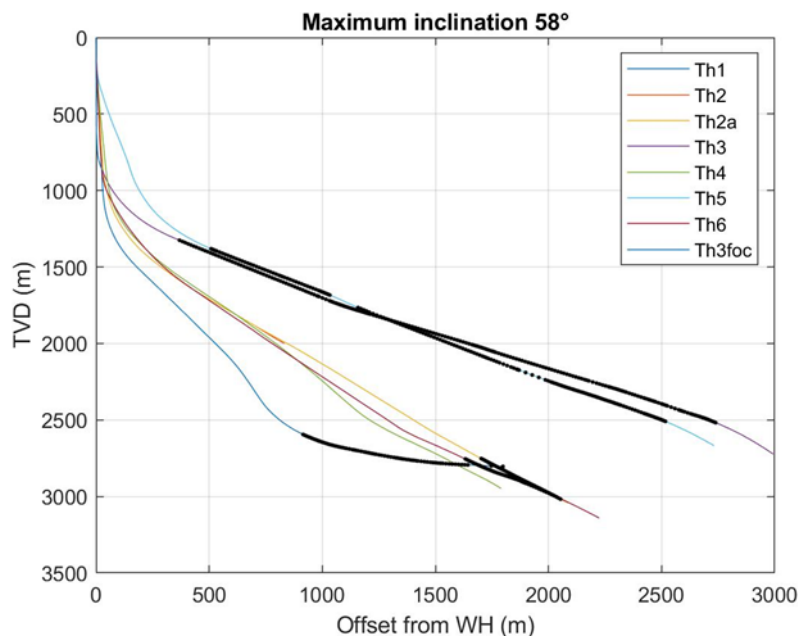


Figure 2-1: For the six wells, evolution of the offset from wellhead as a function of the true vertical depth (TVD). The black dots highlight the depth levels at which the well inclination reaches the 58° limit.

However, another aspect should be considered: one drawback of DAS measurements is their directional sensitivity. Indeed, only the deformation along the fibre can be measured, which implies that acoustic waves travelling along the FOC can be detected but acoustic waves propagating perpendicularly to the FOC cannot be detected. In other words, only the projection of the acoustic signal on the fibre, locally, can be detected. This effect brings complexity. Therefore, it was decided to simulate the cross-well survey to get an idea of the seismograms that could be expected in the field and to plan the survey, e.g. the firing/acquisition sequence. For this purpose, finite-differences based modelling has been performed. For a precise description of the principle and main outcomes of the simulations, please see “Appendix 2: Cross-well survey simulations”.

3 DATA ACQUISITION

3.1 OVERVIEW

Figure 3-1 gives an overview of the fieldwork context. In particular, it shows the location of the control room, used for the DAS acquisition, as well as the wireline truck, used to control the AST, and the crane at the Th6 wellhead.

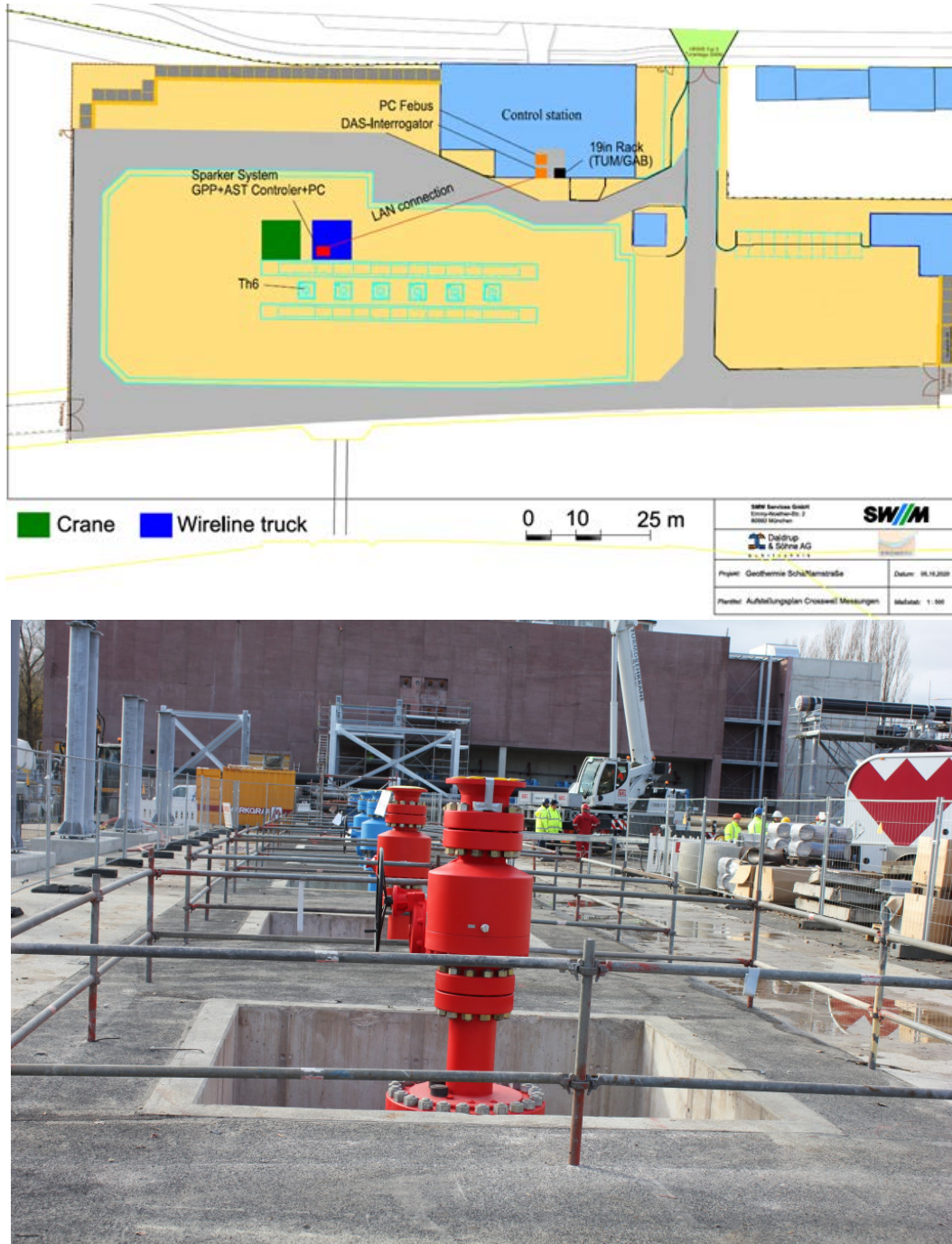


Figure 3-1: Top - Overview of the fieldwork context, at the Schäftlarnstraße geothermal site, with position of the control room, of the crane and of the wireline truck. Bottom - Illustrative picture, Th6 is the last well of the row.

The AST controller commands the firing of the borehole source. Time-break signals are transmitted from the AST downhole unit to the surface control panel. A LAN (Local Area Network) connection is setup between the wireline truck and the control room to transmit GPS-referenced time-break signals. The time stamps are used

to perform quasi-real time processing of the DAS measurements on the PC-Febus, when recording strain-rate data. The crane, next to the wireline truck, is necessary to move the AST assembly in the borehole (Figure 3-2).



Figure 3-2: Schematic (top) and pictures (bottom) showing the deployment and the routing of the AST assembly in the Th6 borehole.

3.1 RECEIVER CHARACTERISTICS

In addition to the FOCs in the wells Th3 and Th4, short-period seismometers have been deployed at the surface in case the borehole shots could be observable from there.

3.1.1 SURFACE SEISMOMETERS

Three autonomous stations have been installed during the survey, close to the wellheads, and were recording continuously, during the whole campaign (Figure 3-3).

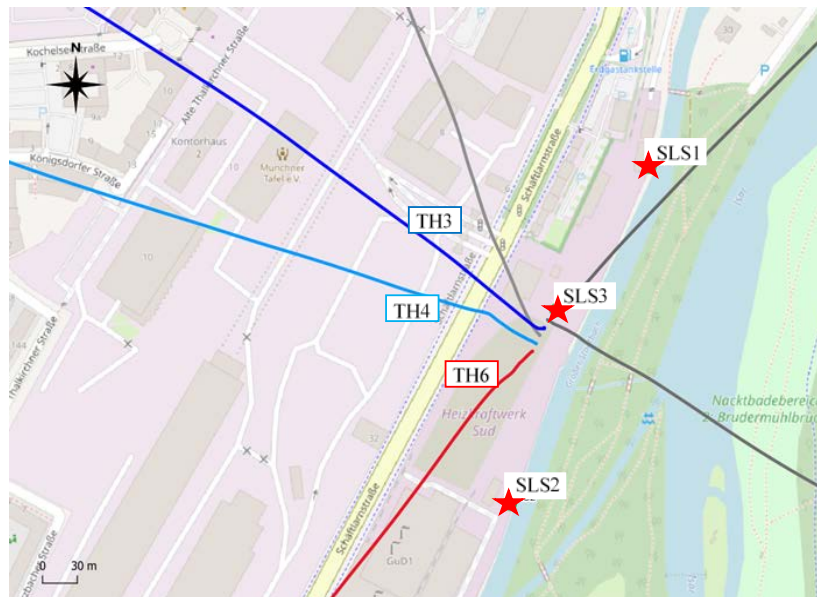


Figure 3-3: Position of the three seismometers at the Schäftlarnstraße geothermal site.

Each station was composed of a short-period L-4-3D seismometer (three-components), a Centaur datalogger, a GPS antenna and was powered by a 12 V battery (Figure 3-4). Sampling rate was set at 250 Hz. The positions of the seismometers, highlighted by a star in Figure 3-3, were the following:

- **SLS1:** 48.117419 N, 11.558782 E, 571 m a.s.l.
- **SLS2:** 48.114835 N, 11.557194 E, 567 m a.s.l.
- **SLS3:** 48.116317 N, 11.557735 E, 565 m a.s.l.





Figure 3-4: Top – Station SLS1. Bottom – Station SLS3, in the cellar of the well SLS-Th2a.

3.1.2 FIBRE-OPTIC CABLES AND DAS-ACQUISITION

Acquisition set-up

Figure 3-5 illustrates the setup, splices and connections of the fibre-optic cables in the Th3 and Th4 wells.

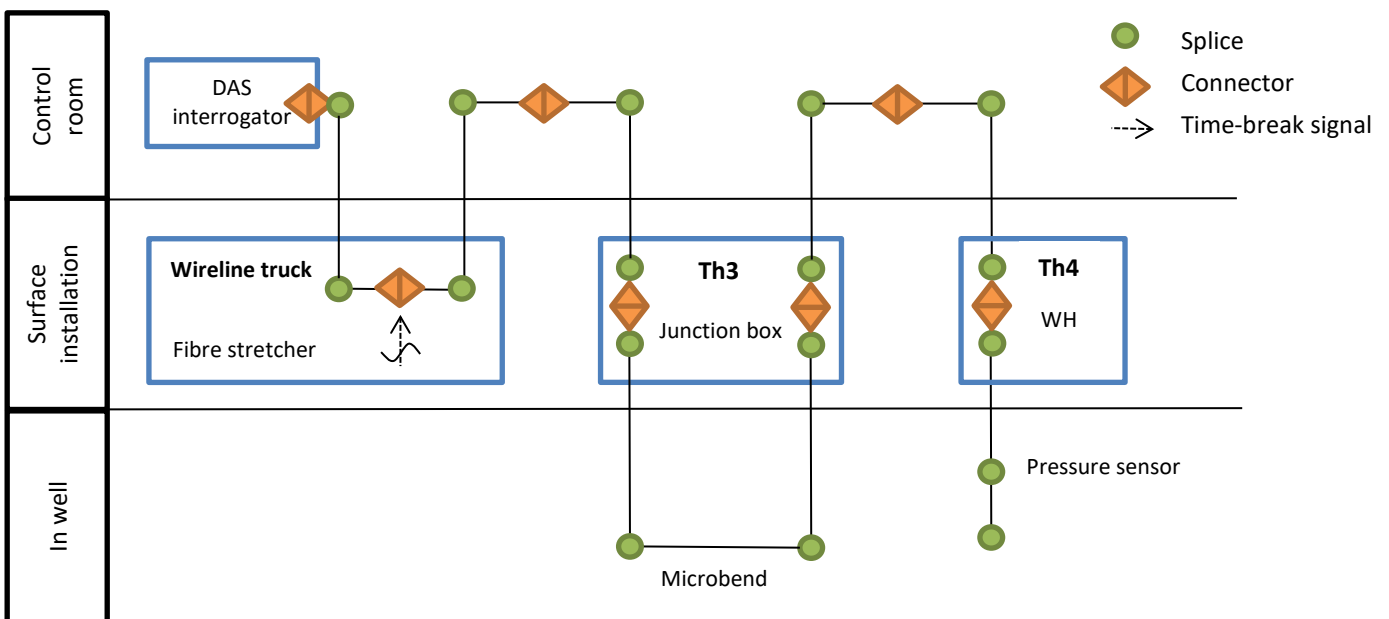


Figure 3-5: Schematic of the arrangement of the fibre-optic cables in the Th3 and Th4 wells. The schematic shows a configuration where the DAS interrogator, in the control room, acquires the signals along the Th3 and Th4 FOCs in series. The position of sensitive points (splices, microbend) where light pulses may suffer energy loss (which deteriorates the acquired data quality) are highlighted.

The deployment of the FOCs differs between wells Th3 and Th4:

- Th4 is designed to serve as a production well when the plant goes into production. The FOC in Th4 is clamped to a sucker rod that is deployed inside the well from top to bottom. It is a single-end deployment. The coupling of the FOC to the “ground” is controlled by the weight of the rod and the fact that the latter lays on the borehole wall. Consequently, the coupling is non-homogeneous along the well, probably better when the well is deviated and when the FOC is stuck to the wall, but it is likely that a large proportion of the FOC does not touch the borehole wall directly.

- In Th3, the two-end FOC is cemented behind the casing of the first well section that is from surface to 699.2 m TVD. Therefore, the coupling to the ground is controlled by the cementation quality and likely better than in Th4.

At surface, in the control room, one-end of the Th3 FOC can be connected to the single-end of the Th4 FOC. Hence, both FOCs can be acquired in series as illustrated in Figure 3-5. However, it is also possible to acquire only the signal along the Th3 FOC loop or only along the Th4 FOC.

As shown on Figure 3-5, before being connected to Th3 FOC or Th4 FOC, the A1-R interrogator is first connected, by an additional FOC, to a fibre stretcher located in the wireline truck. This connection is a back-up that can be used to assess the timing of the sparker shots. In addition to the SEG2 time-break files provided by Avalon (see next paragraph). Indeed, the sparker time-breaks are converted by the stretcher to sinusoids on the fibre, which can be identified on the records.

Figure 3-5 also shows the position of the different connectors and splices along the FOCs. The optical signal sent from the DAS interrogator into the fibre is naturally attenuated along the cable, but connections and splices are sensitive points where additional attenuations occur due to the reflections of the optical signal. This will influence the quality of the recordings. On 17/09/20, the losses along the fibres have been quantified using an Optical Time Domain Reflectometer (OTDR), for different DAS acquisition configurations (Th3 alone, Th4 alone, Th3 and Th4 in series). The results of these OTDR tests are presented in “Appendix 1: OTDR measurements on the Th3 and Th4 fibres”. They highlight the location of the defects that degrade the quality of the optical transmission (splices, connections) along the fibre(s). In particular, the splice made at the Th3 wellhead in difficult conditions deteriorates the signal in a more pronounced way than a normal splice, but much less than the microbend, at the return loop in Th3, which is the major cause of energy loss. (Consequently, it was decided to keep this wellhead junction as it is before the cross-well survey.)

Firing and DAS-acquisition procedure

Figure 3-5 illustrates the firing and acquisition procedure.

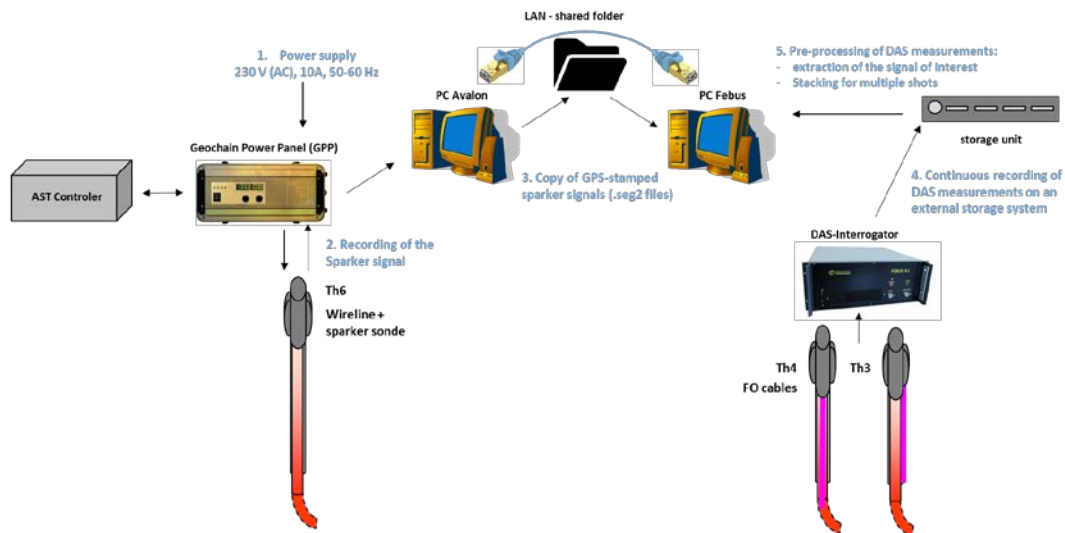


Figure 3-6: Firing and DAS acquisition / pre-processing procedure.

The AST surface panel, located in the wireline truck (Figure 3-7), consists in the AST controller and the Geochain Power Panel (GPP). Direct current is supplied to the GPP, which charges the AST. The surface panel also records the sparker signals that will be stored in SEG2 files in the form of GPS-stamped time breaks. These files are accessible by the PC-Febus, located in the control room, from a shared folder on a NAS, using a LAN.

The DAS-unit, located in the control room (Figure 3-7), interrogates the fibre-optic cable and is used to continuously acquire data on an external storage unit. Two types of data can be recorded by the A1-R DAS-unit:

- The raw data, corresponding to the amplitude and phase of the optical signal, along the FOC, measured by the interrogator. After acquisition, these raw data can be used to generate strain and/or strain-rate data with variable gauge lengths and derivation times (to be defined according to purpose). However, such acquisition type implies to store large amounts of data (~560 GB/hour, with the acquisition parameters of 20/11/20, see Table 3-1). In addition, data conversion from raw to strain-rate is a time-consuming process. Consequently, raw data acquisition prevents from processing in real-time and seeing the results after one or several shots.
- Strain-rate data, for which the gauge length and derivation time must be determined and fixed before acquisition. The amount of data stored is much smaller than the raw data. Calculations give a rate of ~279 GB/hour and 93 GB/hour, when acquiring in Th4 with a gauge length of 5 m and of 10 m respectively, with the parameters of the 20/11/20. This type of acquisition is suitable for quasi-real time processing. This processing consists of stacking the data acquired for multiple shots, which provides important results for the guidance of the survey. After firing a given number of shots from the AST, extraction of the corresponding data subsets is performed on the PC-Febus, thanks to the time break signals contained in the SEG2 files. Then, all data subsets are stacked (added). In theory, the signal to noise ratio (SNR) of the stacked datasets is improved by a factor of \sqrt{n} compared to the SNR achieved with a single shot, where n is the number of shots.



Figure 3-7: AST control panel in the wireline truck, with fibre stretcher used for the recording of time-break signals on the top (left). DAS-unit, data-storage device and Pc-Febus in the control room (right).

3.2 SHOOTING AND ACQUISITION PROCEDURE

3.2.1 SOURCE CHARACTERISTICS

The main characteristics of the AST sparker source can be found in Section 1.3.

3.2.2 SHOOTING SEQUENCE AND ACQUISITION PARAMETERS

Figure 3-8 gives a chronology of the source position in well Th6 and of the number of shots. In the survey, three firing heads were used. After about 1000 shots, one firing head of the AST had to be replaced by another one.

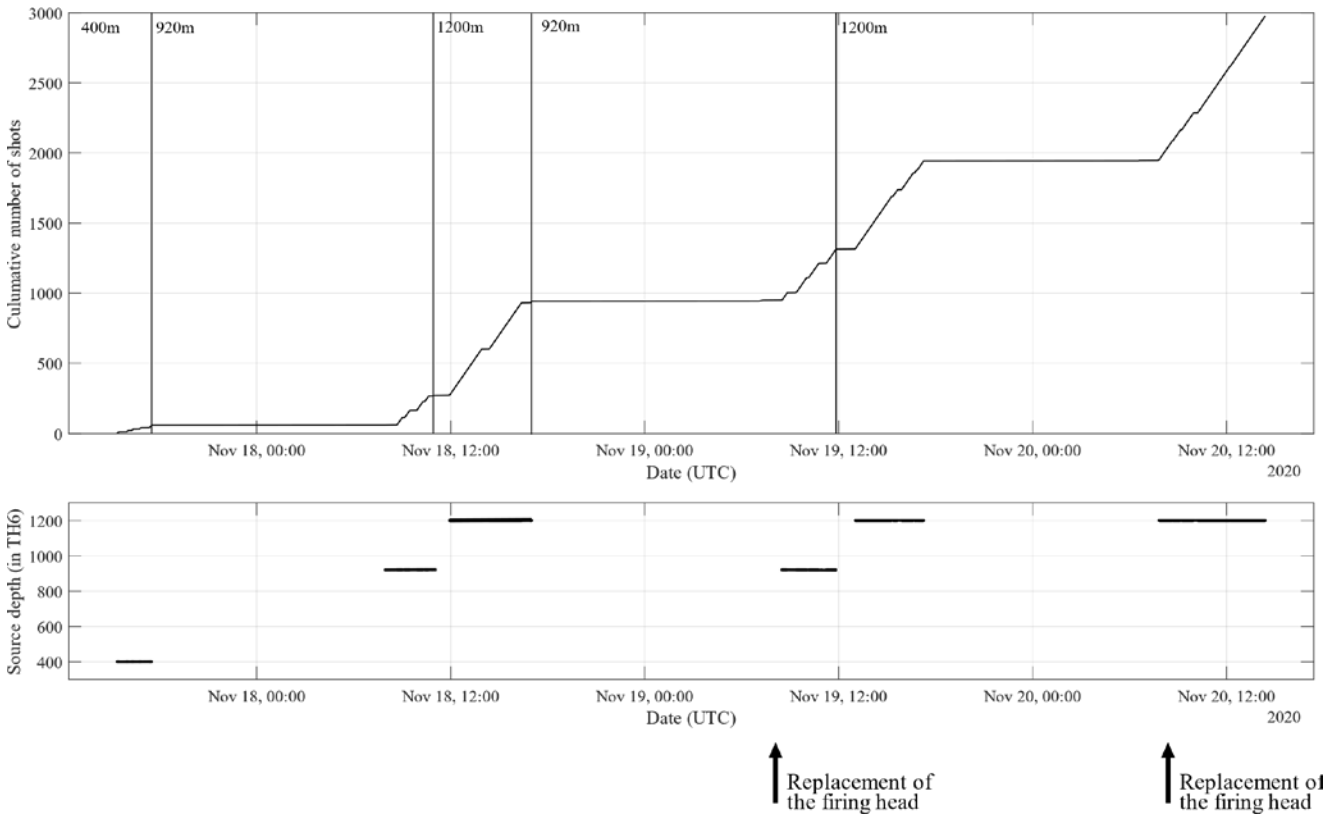


Figure 3-8: Chronology of the number of shots (top) and source position (bottom). The source position in Th6 is given in m MD and the dates are in UTC time (local time = UTC+01). The vertical lines in the upper subplot indicate changes in the source position. The replacement of the firing head occurred at the dates indicated by the arrows at the bottom of the figure.

For each firing sequence, Table 3-1 reports the characteristics of the shots and the associated acquisition parameters of the DAS-interrogator. In addition to the parameters represented schematically in the Figure 1-4 (temporal and spatial sampling, characteristics of the light pulse), the table specifies the recording well (Th3 or/and Th4) and the type of acquired data (raw data – RAW – or strain-rate data – SR).

Table 3-1 shows that three source positions in Th6 have been investigated during the survey: 400, 920 and 1200 m MD. The choice of these positions is explained in the section 3.2.3.

Table 3-1: Characteristics of the shots and acquisition parameters.

17.11	Recording well	Source depth [m - MD]	Start of shot sequence (UTC, on file names)	Start of shot sequence (local hour, UTC+1)	Nb of shots	Type of recorded data	Raw data spatial sampling [m]	Raw data temporal sampling [Hz]	Source optical power [dBm]	Pulse width [m]	Gauge Length (GL) [m]	Derivation Time (DT) [ms]	Nb pts /GL	Nb pts /DT
	Th3+Th4	Tap-test	14:20:00	15:20:00	-	Strain Rate (SR)	0.4	10000	30	5	10	5	4	4
	Th3+Th4	400	15:21:13	16:21:13	5	Raw data (RAW)	0.8	5000	33	3	-	-	-	-
	Th3+Th4	400	15:25:29	16:25:29	5	SR	0.8	10000	33	3	5	5	4	4
	Th3+Th4	400	15:57:17	16:57:17	10	SR	0.8	10000	33	3	10	5	4	4
	Th3+Th4	400	16:17:22	17:17:22	20	SR	0.8	10000	33	3	10	1	4	4
	Th3+Th4	400	17:20:06	18:20:06	18	SR	0.8	10000	30	5	5	2	4	4

18.11	Recording well	Source depth [m - MD]	Start of shot sequence (UTC, on file names)	Start of shot sequence (local hour, UTC+1)	Nb of shots	Type of recorded data	Raw data spatial sampling [m]	Raw data temporal sampling [Hz]	Source optical power [dBm]	Pulse width [m]	Gauge Length (GL) [m]	Derivation Time (DT) [ms]	Nb pts /GL	Nb pts /DT
	Th3+Th4	Descent --> 920m	06:32:00	07:32:00	-	SR	0.8	10000	30	5	10	5	4	4
	Th4	920	07:31:26	08:31:26	200	SR	0.8	10000	30	5	5	2	4	4
	Th4	920	10:51:12	11:51:12	2	RAW	0.8	5000	30	5	-	-	-	-
	Th3	920	11:00:53	12:00:53	2	RAW	0.8	10000	30	5	-	-	-	-
	Th4	Descent --> 1200m	11:24:30	12:24:30	-	SR	0.8	10000	30	5	10	5	-	-
	Th4	1200	11:54:25	12:54:25	330	RAW	0.8	5000	30	5	-	-	-	-
	Th4	1200	14:18:24	15:18:24	340	SR	0.4	10000	33	3	5	1	4	4

19.11	Recording well	Source depth [m - MD]	Start of shot sequence (UTC, on file names)	Start of shot sequence (local hour, UTC+1)	Nb of shots	Type of recorded data	Raw data spatial sampling [m]	Raw data temporal sampling [Hz]	Source optical power [dBm]	Pulse width [m]	Gauge Length (GL) [m]	Derivation Time (DT) [ms]	Nb pts /GL	Nb pts /DT
	Th3	920	08:25:27	09:25:27	369	SR	0.4	10000	33	3	5	1	4	4
	Th4	1200	12:58:58	13:58:58	629	RAW	0.8	5000	33	2	-	-	-	-

20.11	Recording well	Source depth [m - MD]	Start of shot sequence (UTC, on file names)	Start of shot sequence (local hour, UTC+1)	Nb of shots	Type of recorded data	Raw data spatial sampling [m]	Raw data temporal sampling [Hz]	Source optical power [dBm]	Pulse width [m]	Gauge Length (GL) [m]	Derivation Time (DT) [ms]	Nb pts /GL	Nb pts /DT
	Th4	Tap-test	07:23:56	08:23:56	-	SR	0.8	5000	33	2	5	2	-	-
	Th4	1200	07:49:15	08:49:15	1028	RAW	0.8	5000	33	2	-	-	-	-

Figure 3-9 represents the evolution, in the receiver well, of the source-receiver distance, which has been computed using the well trajectories.

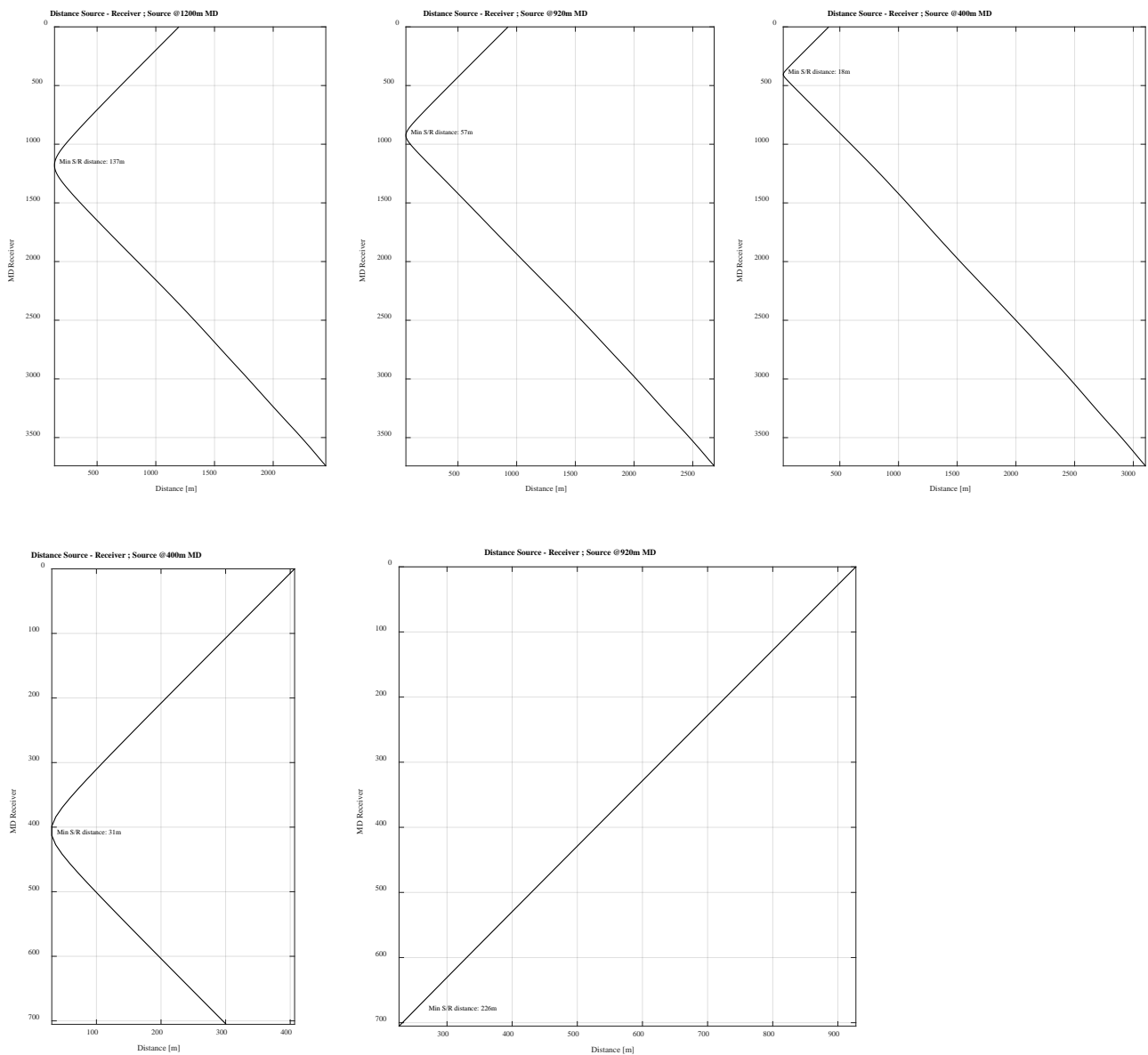


Figure 3-9: Evolution with depth (m MD) of the source-receiver distance, in Th4 (top panels) and Th3 (bottom panels). Source positions: 400, 920 or 1200 m MD in Th6.

3.2.3 EXPLANATION OF THE SHOOTING AND ACQUISITION PROCEDURE

The characteristics of the shooting and acquisition procedure (position of the source, number of shots, receiver well, parameters of the DAS-unit) have been adapted during the operation as the field results were acquired. This section explains the choices that have been made.

Tuesday 17/11/2020

Objective - After finalizing the installation, the objective is to perform test-shots to check the acquisition chain and to adjust the shooting process with the help of the survey modelling (see Appendix 2: Cross-well survey simulations) that is determining the number of shots needed to record the associated signal in the fibre. These test-shots are performed at shallow depth (400 m MD in Th6). The acquisitions are pre-processed (stacked) in quasi-real time and analysed before deciding what to do next. Previous experience from Febus, with similar

source and inter-well distances, is that a minimum of 5 shots are required for a source-receiver distance of around 25 m.

Operation - The source is lowered at 400 m MD (Th6-Th4 min distance is about 7.5 m, Th6-Th3 minimum distance is around 22.5 m). The acquisition is performed in both wells in series, Th3 and Th4, and the parameters of the DAS interrogator are optimized to acquire on both fibres, despite the losses highlighted in Th3 during the OTDR tests of 17/09/20 (especially at the microbend in Th3, see results in “Appendix 1: OTDR measurements on the Th3 and Th4 fibres”). In this design, the light pulse energy needs to be increased in order to ensure acquisition after the microbend. However, this increase could also saturate the signal and deteriorate the acquisition in the first section, down to the microbend. Several couple of parameters have been tested and the acquired strain rate data have been stacked for each set of parameters.

Result - No visible signal on the strain-rate measurements after stacking for multiple shots (up to 20) when source is at 400 m MD. For this specific source depth, this is interpreted as the effect of the tie-back (see Figure 3-10) of the well Th6 that could behave as a wave-guide in the annular and strongly attenuate the source amplitude before it reaches the formation.

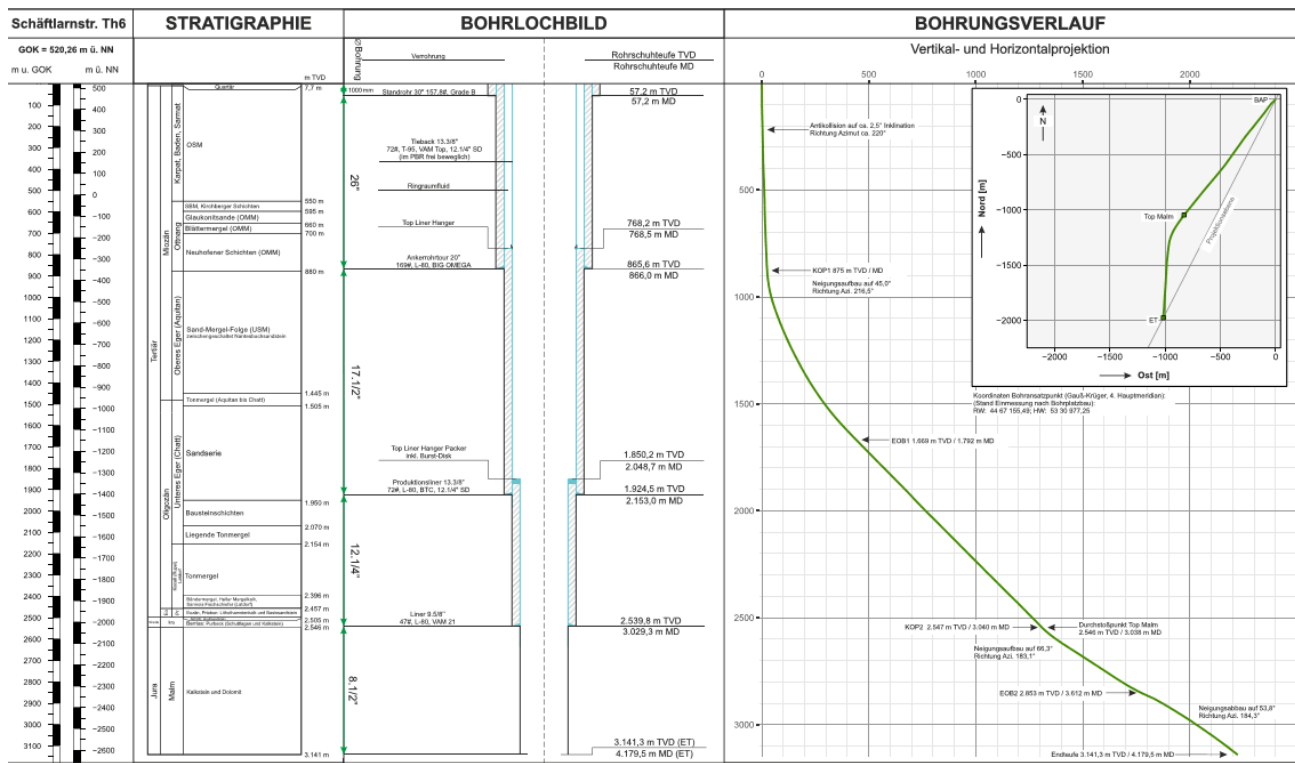


Figure 3-10: Th6 borehole stratigraphy (left), completion (middle) and trajectory (right). The completion highlights the presence of a tie-back, down to 768 m (the end of the first section of the well), which could behave as a wave guide for the seismic signal generated by the AST. The well trajectory enables to identify depths at which the AST could lay against the well, which could improve the coupling to the ground.

Wednesday 18/11/2020

Objective - The main objective is to see signal to constrain the shooting process. To go below the tie-back of Th6, the source is lowered to 920 m MD, at the top of the second section of the well. Other arguments are in favour of this firing depth: the Th4 well starts to be deviated (inclination is of ~5°), which should possibly improve the coupling of the FOC compared to purely vertical section. The minimal distance between the source and Th4 is 60 m, between the source and Th3 it is 120 m. Because of the distance to Th3 and to avoid the energy losses along the Th3 fibre, the acquisition is made only with the Th4 fibre. The DAS-unit parameters are optimized accordingly.

Operation - The source is lowered at 920 m MD. At this depth, Th6 inclination is around 8°. The strain rate data from 250 shots are stacked in quasi-real time. No signal can be seen on the strain-rate stacked datasets. For two shots, we switch the acquisition to RAW data, and one data file is sent to the Febus facilities to assess the strength of the noise on the fibre. Their analysis confirm that the optical noise recorded on the fibre is low and that the parameters of the acquisition are appropriate for the recording conditions.

Decision is to lower the source at 1200 m MD. Th6-Th4 minimal distance is ~140 m, 420 m for Th6-Th3). At this depth, inclination is around 24° for both Th6 and Th4. Theoretically, this should provide a better coupling with the ground both for the source and the FOC. The data related to 330 shots are recorded in RAW, for later processing. In addition, strain-rate data is acquired for 330 supplementary shots and processed, but no seismic signal is visible on the stacked datasets, still. The first set of 1000 shots has been used at this point. The source is pulled out of hole. Before pulling out of hole to change the firing head, 12 additional shots are fired at 400 m and recorded RAW. The shooting process is checked by hearing distinctively, at the wellhead, the sound of the bubble generated by the Sparker.

Conclusion - Signal can still not be seen from the stacked data, but the operations have led to check that the AST, as well as the acquisition and processing chain, were working properly (sound of the source at the wellhead, acceptable optical noise on the Th4 fibre used for the recording). We identified potential causes preventing us from recording any seismic signal, despite the relatively short source-receiver distances and the important number of stacked shots:

- the AST provides a source energy which is too weak, and we need more shots for such distances;
- the coupling of the fibre-optic cable is not good enough, and we need to go deeper to force the cable to stick to the well. We could also preferably use the Th3 fibre-optic cable, which is cemented (but source/receiver distances are even larger);
- the completion of the source-well Th6 prevents the transmission of a sufficient amount of energy into the formation. At 1200 m, the well diameter is 13 3/8", the AST diameter is 3", so a relatively large amount of the released energy is lost in the well.

Thursday 19/11/2020

Objective – Even if the purpose of the survey is not to validate the proposed design, the main goal remains to see any seismic signal for “interesting” depths, i.e. depths where the analysis of the seismic signal could bring valuable knowledge on the velocity model. Hence, the objective is to stack the data acquired for a larger number of shots and strive for a better coupling between the fibre-optic cable and the ground (by switching for example the acquisition to the Th3 well). Regarding the source position, the objective is to find the best compromise: it should not be too deep to prevent large source-receiver distances, but deep enough to reach deviated sections of the well(s) and to obtain satisfactory information on the velocity model.

Operation - After changing the firing head, the AST is first set at 334 m MD in Th6 and three test shots are fired at this depth, all of them are heard distinctively at the wellhead. Then, the source is positioned at 920 m MD below Th6 tie-back. The recording is performed in Th3 only, to ensure a better coupling to the ground (by cementation) and also a good alignment of the FOC with regards to the position of the source 120 m below. The strain-rate data from 250 shots are stacked in quasi-real time, but there is still no signal visible on the stack. Therefore, decision is taken to move the source down to 1200 m MD and acquire RAW data for a large number of shots. Th3 fibre is disconnected to optimize the acquisition parameters. One main reason for this choice is that there is no scientific interest in using the remaining shots for Th3 at such depth. The rest of the day is dedicated to finish the second set of 1000 shots.

Conclusion – At this point of the survey, no seismic signal has been observed from the data stacked in quasi real-time, using either the fibre installed in Th3 or Th4. The recording of the raw data, however, allows applying different types of processing to obtain strain-rate values that could be adapted and optimized a posteriori. In other words, the acquisition of raw data can prevent from any unsuitable acquisition parameters that could be made when acquiring strain-rate data.

Friday 20/11/2020

Objective - After changing the firing head, the AST is positioned at the same depth as for the experiments conducted in the afternoon of the 19/11/20. The objective is to shoot and record in the same way as the 19th (and the 18th) when the AST was positioned at 1200 m MD in Th6, in order to complete the dataset acquired previous days and to stack the data for as many shots as possible, while applying different gauge lengths during the conversion from raw to strain-rate data (during post-processing).

Operation - The source is positioned at 1200 m MD in Th6. Raw data are acquired in Th4 with the same parameters as on the 19/11/20. All 1000 shots of the third firing head are recorded with unchanged source position and acquisition parameters.

Conclusion - No real-time processing has been performed on the data recorded on the 20/11/20. The processing of the raw data is conducted afterwards.

Chapter 5 and 6 focus on the (pre-)processing of the dataset acquired in the period 17-20/11/20.

4 SEISMOMETERS DATA

Using the time-break signals from the AST, the recordings of the three stations have been stacked for two shooting depths: 920 m (576 stacked traces) and 1200 m (2327 stacked traces). Taking into account the excavation and surface work that took place intermittently on site, the SLS3 station was probably the most likely to record signal from the Th6 source. Therefore, we focus here on SLS3 measurements.

For each shot, the signal of interest starts at the shooting time ($t = 0$ s in the figures) and two seconds of data are extracted after the shot. The stacked data (Figure 4-1) have been analysed in the spectral domain by computing the power spectral densities (PSD) (Figure 4-2). PSDs highlight a strong 50 Hz electrical noise. Data have been finally filtered in two frequency bands (with third order Butterworth passband filters): from 5 to 20 Hz, and from 60 to 100 Hz (Figure 4-3).

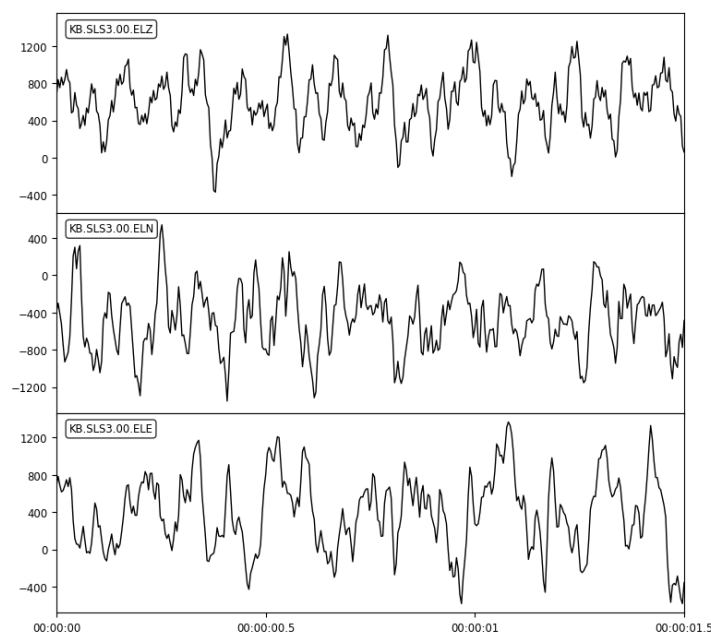


Figure 4-1: Stacked traces (non-filtered) obtained from the recordings of the three channels of the SLS3 seismometer. Position of the source: 1200 m MD in Th6.

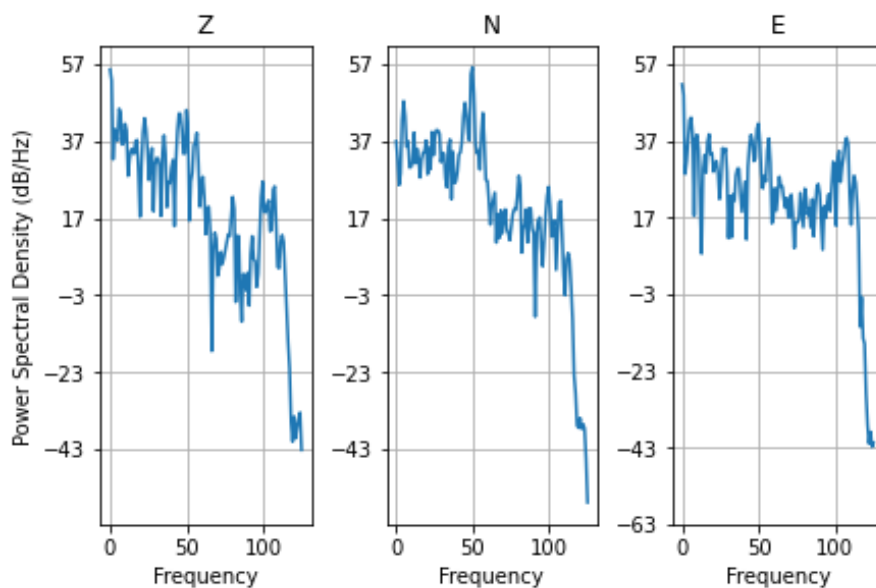


Figure 4-2: Power spectral densities of the stacked traces of the three components of SLS3.

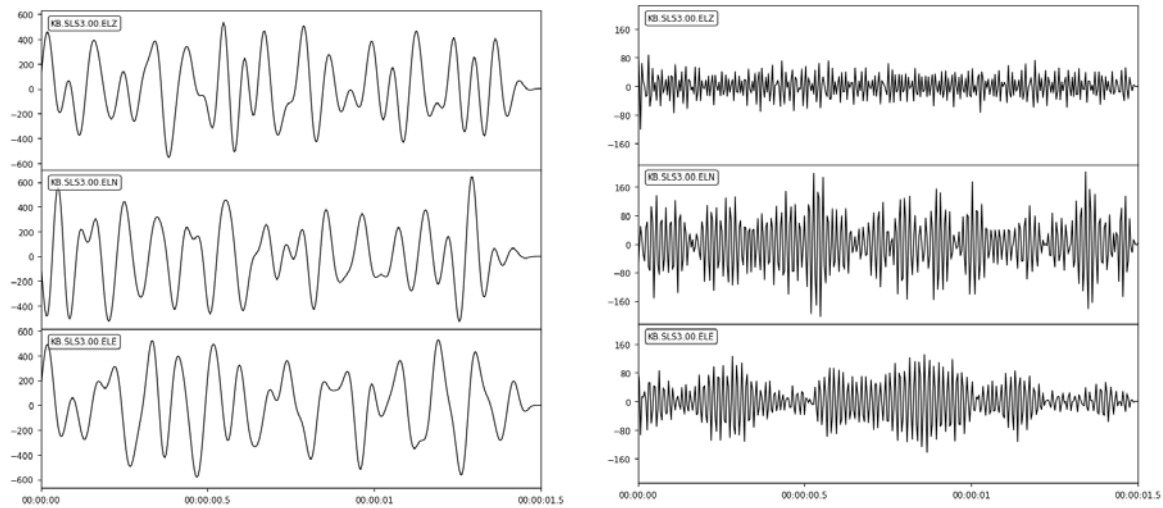


Figure 4-3: Stacked and filtered traces of the three components of SLS3. A third order Butterworth bandpass filter has been applied in the frequency range 5-20Hz (left) and 60-100Hz (right).

No seismic signal can be identified from the stacked data, on SLS3 but also on the other seismometers. This may be expected because i) anthropogenic noise was strong at surface ii) attenuation of the seismic waves at shallow surface is stronger than at depth and 3) no signal was recorded on Th3 nor Th4 FOCs.

5 PRE-PROCESSING OF THE DAS RAW DATA

5.1 PRINCIPLE

For a given position of the source, the data pre-processing consists of extracting data-windows of interest, around each shooting time break and of stacking (summing) all these data-windows. This stacking procedure applies to strain-rate data. A preliminary task is therefore the conversion of the raw data into strain-rate. As described in section 3.2.3, two days were dedicated to the acquisition of raw data, enabling to process the acquisitions with different gauge lengths (GL) and to investigate the content of the records for various wavelengths. The light-pulse width corresponds to the smallest GL (2 m for the acquisitions on 19-20/11/20, see Tables 5-1). The wavelength of the acoustic signal of interest defines the largest GL. In most applications, GL of 10 or 20 m are used. We decided to investigate GL from 2 to 50 m. Theoretically, the signal to noise ratio should improve with higher GL.

Tables 5-1 reports the characteristics of the pre-processing applied for the three available source positions (400, 920 and 1200 m MD in Th6):

- The well in which the measurements have been acquired,
- The gauge lengths that have been tested,
- The date at which the stacked shots have been acquired,
- The number of shots that have been stacked together.

Tables 5-1: Parameters of the stacking procedure

Source @ 1200 m MD	18/11/2020	19/11/2020	20/11/2020	19+20/11/2020	18+19+20/11/2020
Recording well	Th4	Th4	Th4	Th4	Th4
Nb of stacked shots	334	545	901	1446	1780
Gauge lengths [m]	5	2, 5, 10, 20, 50	2, 5, 10, 20, 50	2, 5, 10, 20, 50	5

Source @ 920 m MD	19/11/2020	18/11/2020
Recording well	Th3	Th4
Nb of stacked shots	304	200
Gauge lengths [m]	5	5

Source @ 400 m MD	19/11/2020	19/11/2020
Recording well	Th3+Th4	Th3+Th4
Nb of stacked shots	6	9
Gauge lengths [m]	5	10

The stacks obtained when merging the data acquired on 18, 19 and 20/11/20 must be analysed carefully because the source was not left at the firing-depth from one day to another (Figure 3-8). The imperfect repositioning of the source at the same depth (due to cable elongation) can potentially lead to a seismic signal distortion, while still decreasing the amplitude of incoherent noise. Consequently, after analysing the effect of the number of stacked shots on the recorded amplitudes, we will focus on the analysis of the stacks obtained from unmoved source positions.

5.2 PRE-PROCESSING RESULTS

Figure 5-1 shows the result of the stacking procedure for the data acquired on the 20/11 (source at 1200 m MD, Th4 FOC) for variable GLs. The procedure leads to 2D-datasets, showing the strain-rate amplitude as a function

of depth (i.e. along the FOC, vertical axis) and time (horizontal axis). The black vertical line indicates the time at which all shots were aligned. 901 shots have been stacked.

Figure 5-2 presents, for the source at 1200 m MD, Th4 and a GL = 10 m, a single shot (top) and the stack of 1446 shots (19+20/11). For each 2D-plot, the colour map range corresponds to the inter-quartile range (IQR) of the dataset. Each box-plot shows basic statistics on the dataset: Q1 and Q3 (blue limits), Q2 (red segment) and the outliers above and below the upper inner fence and the lower inner fence respectively¹.

No seismic signal generated by the AST is visible on the figures and stacks. If signal would be there, it should look like the modelling results shown Figure 8-8: starting at ~0.2 s at a depth close to 1200 m and having a “<” shape. However, we can see that:

- For a fixed GL, e.g. 10 m, Figure 5-1 (middle) and Figure 5-2, the increasing the number of stacked shots lowers the values of the first and third quartiles (Q1 and Q3) of the corresponding datasets. This means that the stacking procedure decreases the incoherent noise constituting most of the signal, as expected.
- On the contrary, increasing the number of stacked shots improves the visibility of the coherent noise caused by the surface installations. This is clearly visible in Figure 5-2 for depths close to 0. This is also expected and the seismic signal generated by the AST should behave similarly.
- The stack of the 1446 shots (Figure 5-2, bottom) leads to an inter-quartile range limited to absolute strain-rate amplitudes below $90 \text{ nm}\cdot\text{m}^{-1}\cdot\text{s}^{-1}$. These values are extremely low and will be latter compared to the response to a tap-test (see section 6.3). If the dataset includes a seismic signal from the AST, its amplitude is below this threshold.

¹

Q1 = first quartile (25%)

Inter-quartile range = IQR = Q3 – Q1

Q2 = median (50%)

Upper inner fence = Q3 + 1.5×IQR

Q3 = third quartile (75%)

Lower inner fence = Q1 – 1.5×IQR

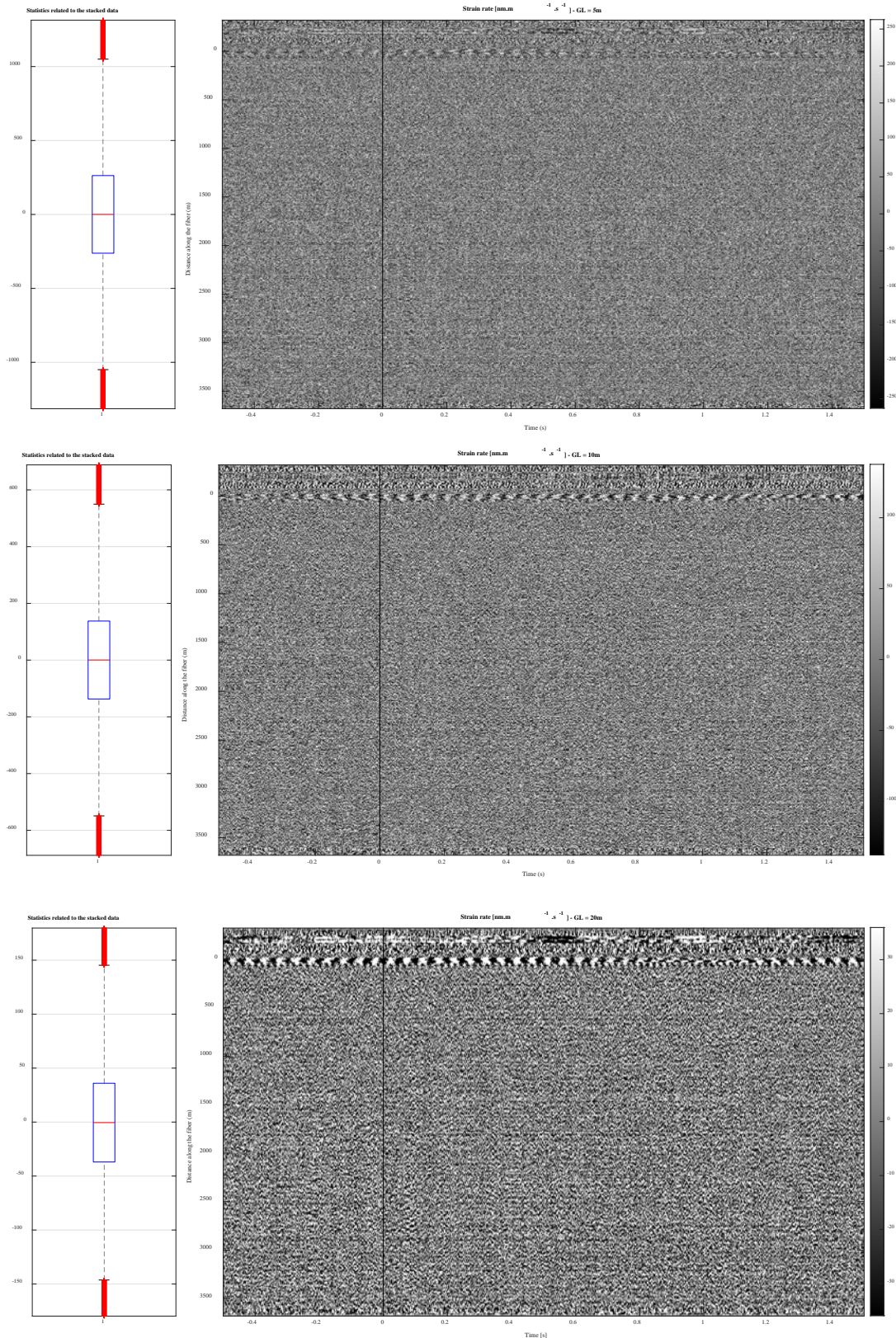
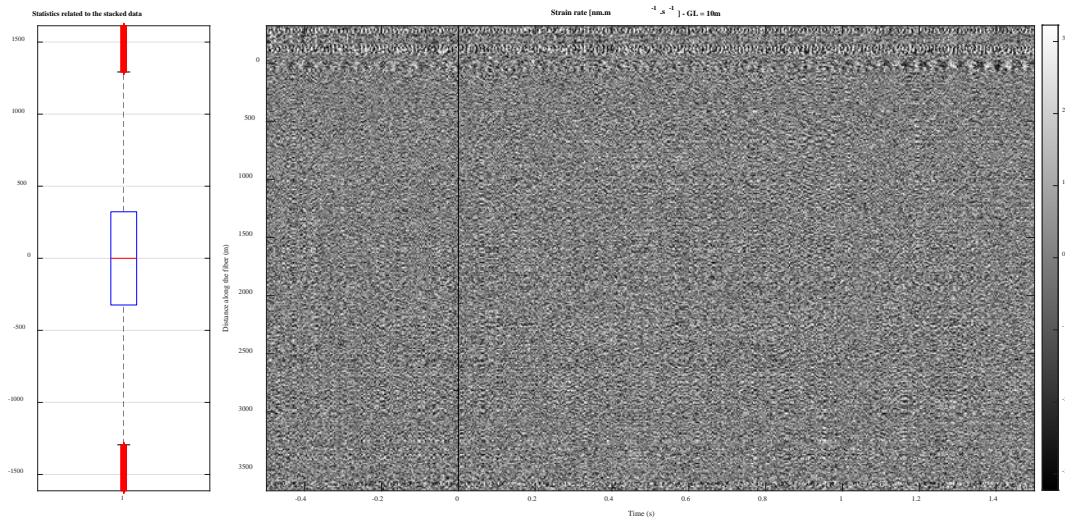


Figure 5-1: Source at 1200 m MD. Strain-rate stacks of 901 shots (20/11). GL equals 5 m (top), 10 m (middle) and 20 m (bottom), DT = 2 s. The origin of the Y-axis is positioned at the wellhead. $t = 0$ s is the firing time break. The grey-scale shows the strain-rate amplitude, which covers, for each subplot, the inter-quartile range of the strain-rate amplitudes (i.e. the [Q1, Q3] range, where Q1 and Q3 are the first and third quartiles respectively). The box-plots on the left show basic statistics on the amplitudes shown on the right: the blue box is limited by Q1 and Q3, the red segment shows the median (Q2) and the red points below and above the whiskers show the outliers above and below the upper inner fence and the lower inner fence respectively¹.

1 shot



1446 shots

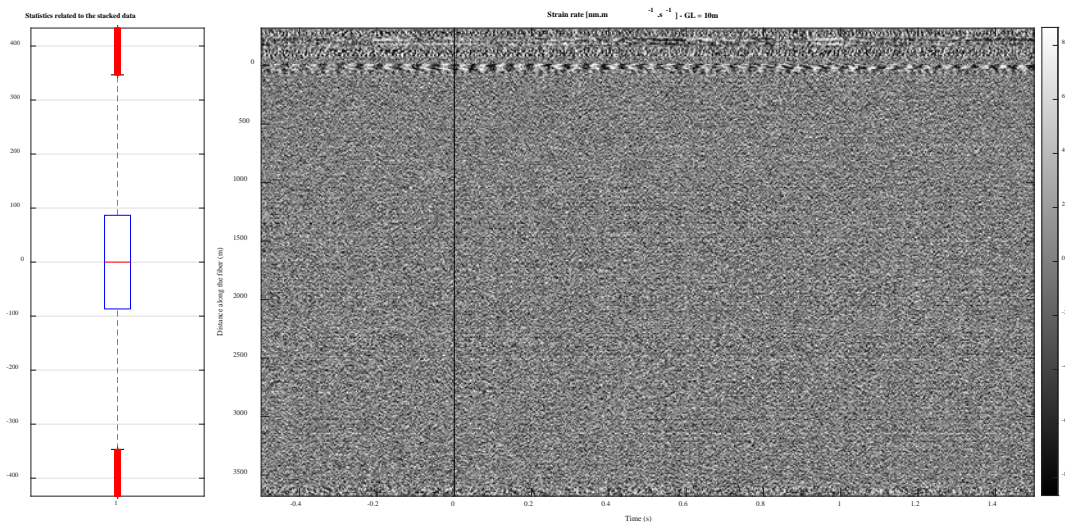


Figure 5-2: Source at 1200 m MD. Top – Strain-rate for one shot (20/11). Bottom – Strain-rate after stack of 1446 shots (19+20/11). The grey-scale shows the strain-rate amplitude, the range varies for both datasets.

5.3 STACKING PROCEDURE QUALITY-CONTROL

We can verify that the stacking is properly done by looking at the correct alignment of the stacked data-windows. This is confirmed by the emergence in the upper part of the stacked datasets (i.e. for negative distances in Figure 5-1) of strongly resolved permanent features related to the noise generated at key points in the surface setup. This coherent noise is not removed when stacking the records, unlike the incoherent noise, which was decreasing and can be observed in both stacked and unstacked datasets.

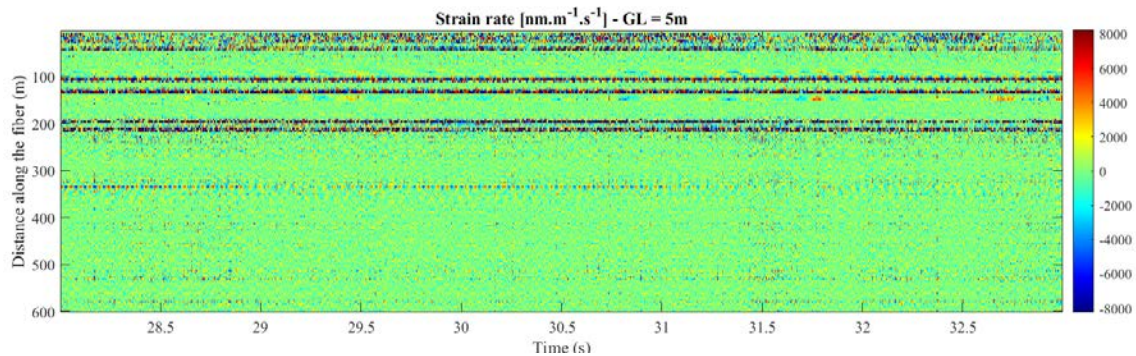


Figure 5-3: Two seconds strain-rate data-window (unstacked), from the connector plugged to the DAS-interrogator to 600 m downstream. The Th4 wellhead is located at 320 m. GL = 5 m.

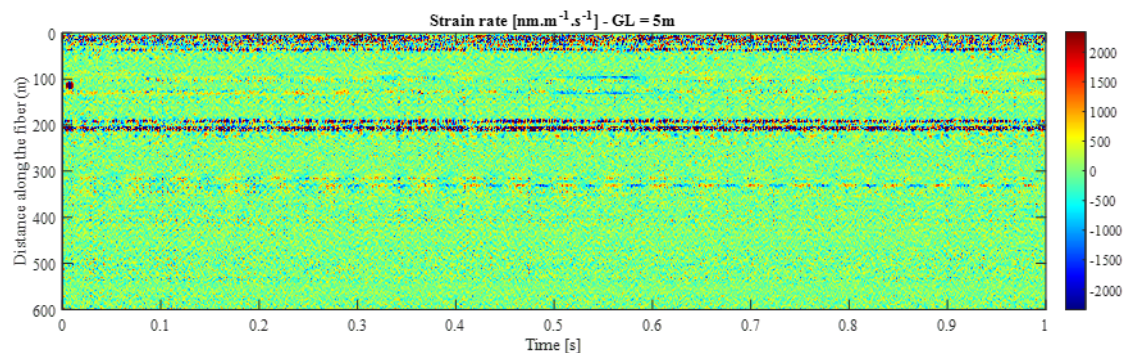


Figure 5-4: Same as Figure 5-3 but stack of 901 shots.

The unstacked strain-rate data of Figure 5-3 clearly show three permanent signals (horizontal lines on the figure):

- Strong amplitudes around 110 m and 130 m mark the limits of the fibre stretcher (see Figure 3-5) located in the wireline truck.
- Two strong amplitudes around 200 m mark the entrance and exit of the distribution box, in the control room. The optical noise at the origin of these two strong horizontal lines is produced by the connectors and the strong reflexion of the optical signal at these sensitive points.
- The strong line around 320 m is related to noise generated by the environment of the fibre, at the wellhead of the Th4 well. It is a distinct permanent sinusoidal signal, with a frequency of 20 Hz, that is slightly moving in space and is weakly attenuated by stacking (coherent noise). The origin of this periodic noise is not identified.

The stacked strain-rate displayed in Figure 5-4 shows that the signal at the fibre stretcher is decreased strongly whereas the time-break is perfectly added (see red dot close to 0 s at 120 m). The periodic noise around 300 m remains clearly visible but is also blurred due to its moving position.

6 PROCESSING AND ANALYSIS OF THE STRAIN-RATE DATA

6.1 PURPOSE AND MEANS

The goal of the strain-rate data processing is to identify any seismic-signal related to the sparker source in the (stacked) recordings.

The first processing sequence seeks to refine the visualization of the data in the temporal and spectral domain. In both cases, we start by focusing on a restricted data window, in which the seismic signal is expected. The results of the survey simulations are therefore used (see “Appendix 2: Cross-well survey simulations”). In this time-depth range, we compute basic statistical parameters to characterize the dataset and to adapt the visualization accordingly. This assumes that the sparker amplitudes on the FOC are stronger than the noise-level and that most of the data range still contains mainly noise. In the spectral domain, a similar procedure is applied but spectral normalization in order to account for an acquisition noise related to the DAS-unit is added.

A second processing sequence is applied to account for the coherency of the sparker signal along the FOC, over time and space. This approach aims at highlighting even weak acoustic signal by cross-correlation and relies on the results of the survey simulations (see “Appendix 2: Cross-well survey simulations”).

6.2 CONTRIBUTIONS OF THE SURVEY SIMULATIONS

Two distinct physical processes are acting on the strain-rate amplitudes recorded by the DAS-unit: the geometrical spreading, leading to a decrease of the signal amplitude as the source/receiver distance increases, and the directional sensitivity, because the fibre is poorly sensitive to longitudinal waves propagating perpendicularly to it. Hence, the points along the fibre where the source/receiver distance is minimal are not necessarily those with the highest strain-rate amplitudes. For a given position of the source, the simulations described in “Appendix 2: Cross-well survey simulations” helped to quantify these combined effects and to estimate the relative evolution with time and depth of the amplitude of the strain-rate recorded along the fibre (Figure 6-1).

The amplitude variation displayed on the right-hand side of Figure 6-1 highlights the effect on the DAS-measurements of the two physical processes mentioned above. In particular, the strong decay of the amplitudes in Th4 at the depth very close to the source depth in Th6 illustrates the consequences of the directional sensitivity. The left-hand side of Figure 6-1 gives an estimate of the apparent velocity of the seismic signal on the records.

The simulations performed for a given shot point are therefore used to define where the signal of interest should be expected and led to the following constraints on the strain-rate 2D-plots:

- a time-window, which is fixed from 0 s (time-break) to 0.5 s after the shot;
- a spatial-extent, which is fixed to the depth range where amplitudes larger than 70% the maximum estimated value are observed, i.e. a roughly $\pm 300\text{m}$ range around the source position.

We will later see that the simulation results are also used for coherency analysis (section 0)

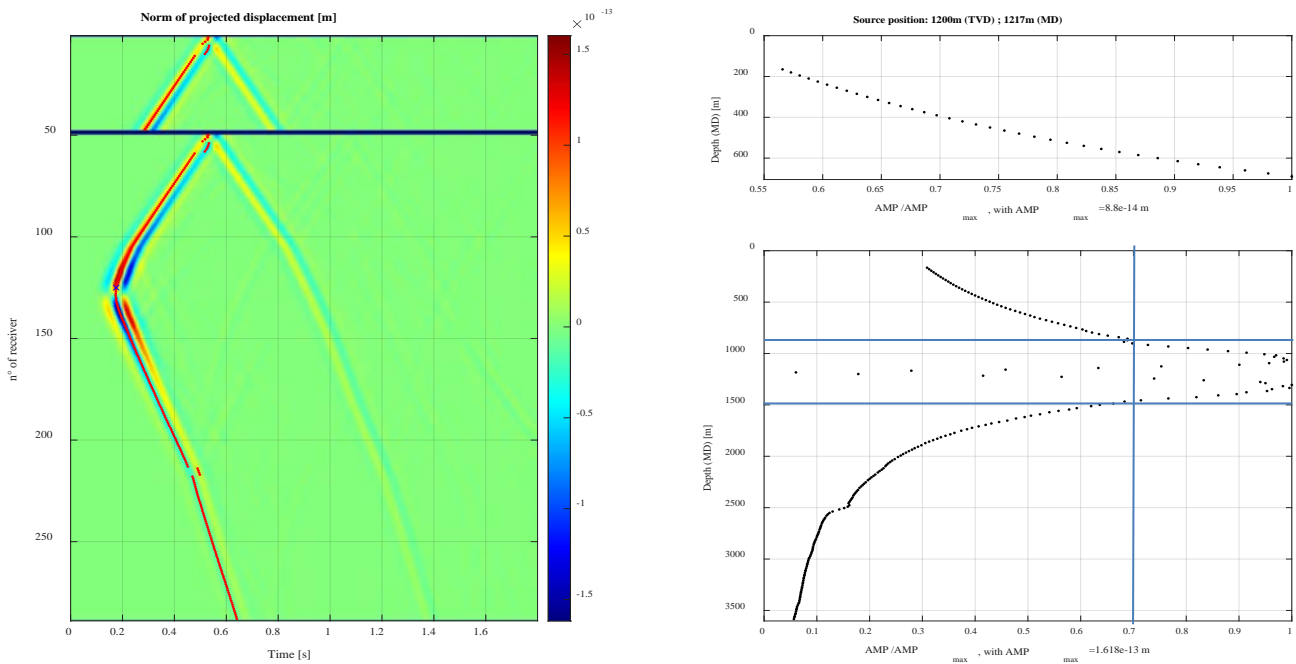


Figure 6-1: Simulation of a source at 1200 m TVD in Th6. Left - dynamic displacements (meters) computed from the simulations in both receiver-wells (Th3, downward on top slice – Th4, downward, on bottom slice). The red dots indicate the maximum amplitude of the first arrivals. Right - evolution with depth of the maximal amplitude of the first arrivals, normalized by the absolute maximum over the whole dataset, in Th3 (top) and Th4 (bottom).

6.3 TAP-TEST ANALYSIS (TH4)

By applying the data processing procedure to a case where a known signal has been recorded (i.e. the tap-tests performed on 20/11/20) our objective is to check the relevance of the applied processing while describing its content.

During the tap-test, the wellhead was repeatedly hit with a hammer (Figure 6-2) while strain-rate data were recorded on the fibre with GL = 5 m.

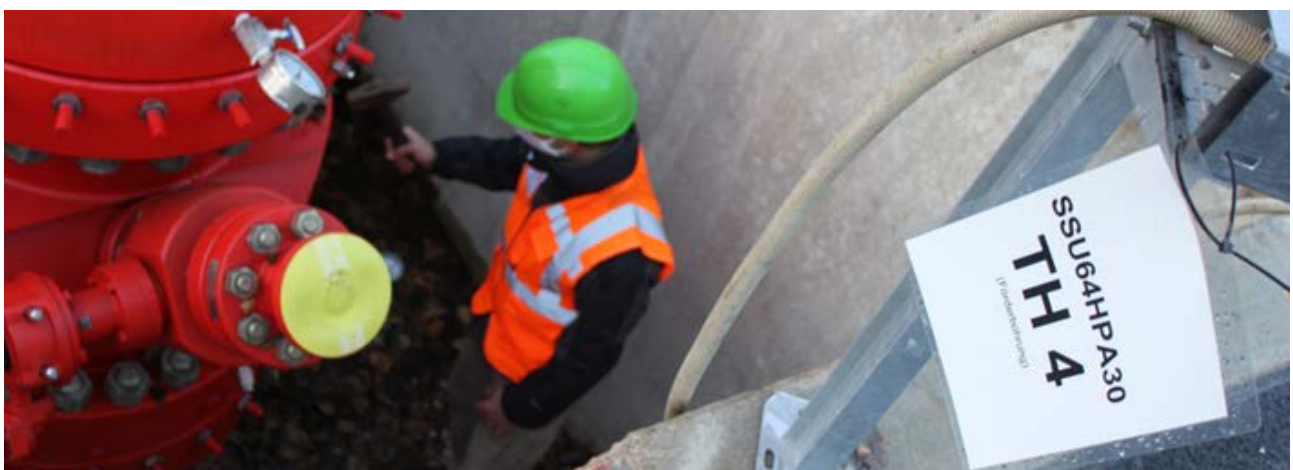


Figure 6-2: Picture of the tap-test performed on the Th4 wellhead.

In section 1.3, we mentioned that one sparker shot emits around 1000 Joules. For one hammer strike, we can suppose that the kinetic energy, E_c , in joules, of the hammer is transmitted to the wellhead while hitting. Considering that we use a 0.5 kg hammer and strike the wellhead with a velocity of about $10 \text{ m}\cdot\text{s}^{-1}$, we can infer that around $E_c = \frac{1}{2} \times 0.5 \times (10^2) = 25 \text{ J}$, are transmitted to the wellhead.

6.3.1 TIME DOMAIN

The first step in the processing consists in extracting the data of interest and presenting them as a time-depth image of the strain-rate combined with the corresponding box-plot (see section 5.2 and Figure 5-1 for a detailed description) (Figure 6-3, top). From the time-depth image, we extracted four distinct traces that are also shown (Figure 6-3, bottom).

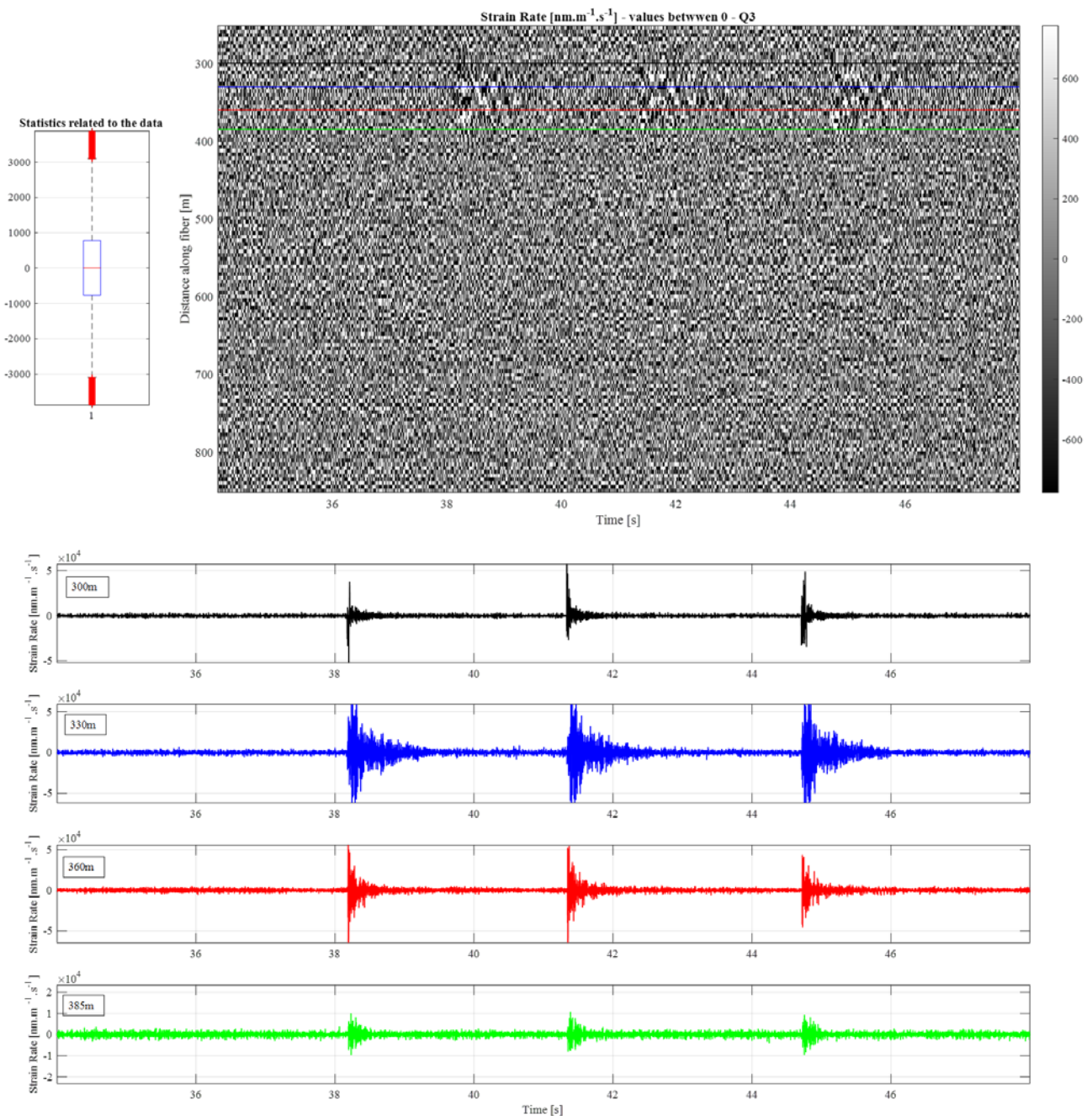


Figure 6-3: Top: Strain-rate data produced during the tap-test (left) and corresponding box-plot (right, see Figure 5-1 for details). The 600-m depth range excludes the strong noise recorded at the surface due to the environment of the fibre. Bottom: strain-rate traces extracted at the depths of 300, 330, 360 and 385 m after the control room respectively. Horizontal lines in the top plot highlight these depths. Note the change of strain-rate scale for the trace at 385 m.

We observe that the amplitudes related to the tap test are:

- much stronger than the background noise and therefore most of the strain-rate values belong to the “outliers” in the boxplot;
- much stronger than what was observed on the sparker test stacks: for the tap-test, Q3 is ~ 1000 nanostrain. s^{-1} and it was ~ 100 nanostrain. s^{-1} for the 901-shot stack;
- visible on the fibre-optic cable down to 85 m.

To enhance the visualisation of the signal of interest, the statistical parameters summarizing the extracted data are used to hide incoherent noise and adapt the colour map. Indeed, if the dataset includes some seismic-signal of interest, the associated amplitudes should be higher than the noise that constitutes most of the dataset. Therefore, we choose to whiten all strain-rate values within the inter-quartile range¹ (Figure 6-3, top). Figure 6-4 shows that such a whitening has a positive effect by increasing the contrast between the incoherent noise and the signal of interest.

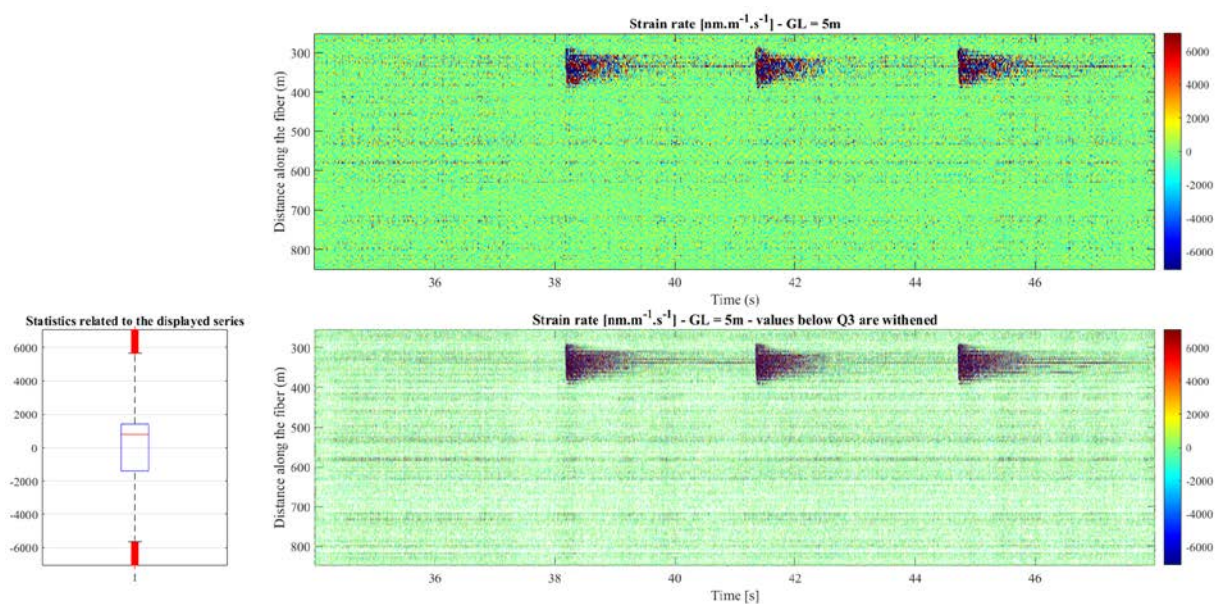


Figure 6-4: Enhanced visualization of strain-rate by data whitening. Top-right: original dataset. Bottom-right: dataset after whitening all strain-rate values within the inter-quartile range. The colour map for both plots are set according to the boxplot of the dataset after removal of the whitened values (bottom-left).

Moreover, it is possible to follow the apparent velocity of the tap-test along the FOC by zooming on the first arrivals. We computed an apparent velocity of 5000 m. s^{-1} . This value is consistent with acoustic wave velocity propagating within a metallic material (wellhead and casing). For L80 steel², which is the material used for the Th4 wellhead, velocity of the order of 5900 m. s^{-1} is expected.

To assess the noise-level in an unstacked dataset, we use the strain-rate amplitudes recorded in a 0.5 s data-window just before the hammer-strike. In the spatial domain, we focus here on the traces from 300 to 350 m. In this window, it is therefore expected to record only uncoherent noise. In order to quantify the noise-level, we retain the third quartile Q3 value, which is in this case of about 800 nanostrain. s^{-1} .

² e.g. Wiskel et al., ‘Ultrasonic Velocity and Attenuation Measurements in L80 Steel and their Correlation with Tensile Propertie’, in 19thWorld Conference on Non-Destructive Testing, 2016.

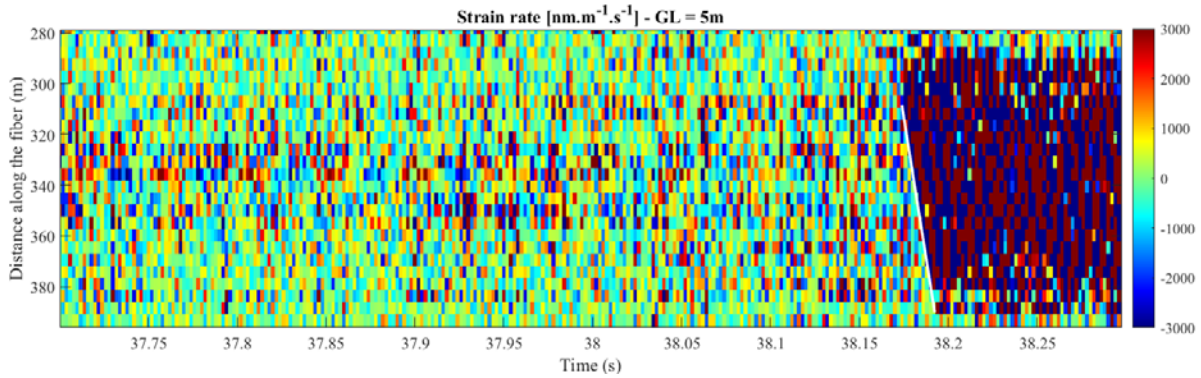


Figure 6-5: Zoom on the first hit displayed Figure 6-4. The white line, with a slope of 5000 m/s, highlights the propagation velocity of the acoustic signal along the FOC and is consistent with propagation in steel material.

6.3.2 FREQUENCY DOMAIN

An additional step in the data analysis consists in looking at the dataset in the spectral domain. Hence, power spectral densities (PSDs) of the strain-rate time-series recorded at each depth are computed. To enhance the visualization of the signal, whitening is also performed for PSD values smaller than Q3 (Figure 6-6).

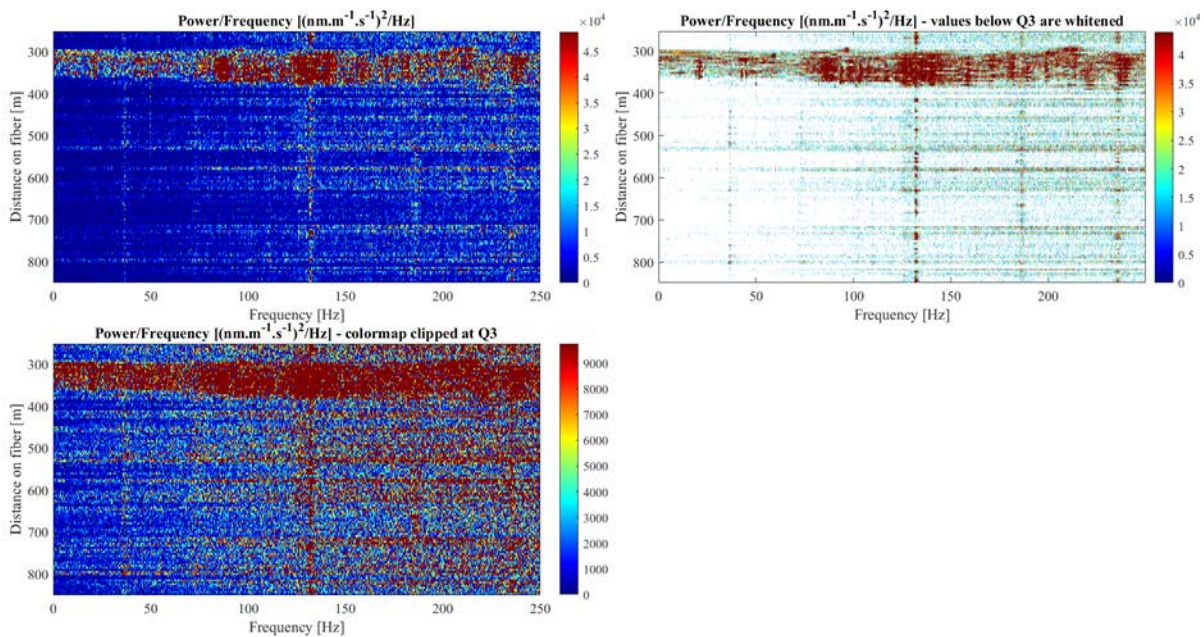


Figure 6-6: Power spectral densities of the strain-rate along depth recorded during the tap-test. Left: PSDs represented with different colour-scale limits. Top-right: Spectrogram after whitening the amplitudes smaller than Q3.

We can observe on all spectrograms of Figure 6-6 strong vertical features. This means that specific frequencies are excited over the whole fibre length, from the control room to final depth. These patterns are generated during acquisition by the DAS-unit. To remove this artefact, which can potentially pollute our signal of interest, we apply a spectral normalization to the spectrogram, before returning to the temporal domain by inverse Fourier transform. Considering the spectrogram $S(z, f)$ (Figure 6-7 – top left), we first normalize the values at a given frequency, $S(z, f_i)$ by their median, $Q2(S(z, f_i))$ (Figure 6-7 – bottom left) and then apply a Hamming taper window (Figure 6-7 – top right) before applying the inverse Fourier transform to obtain the normalized strain-rate (Figure 6-7 – bottom right). Note that this procedure is, however, doing more than just removing the acquisition artefact.

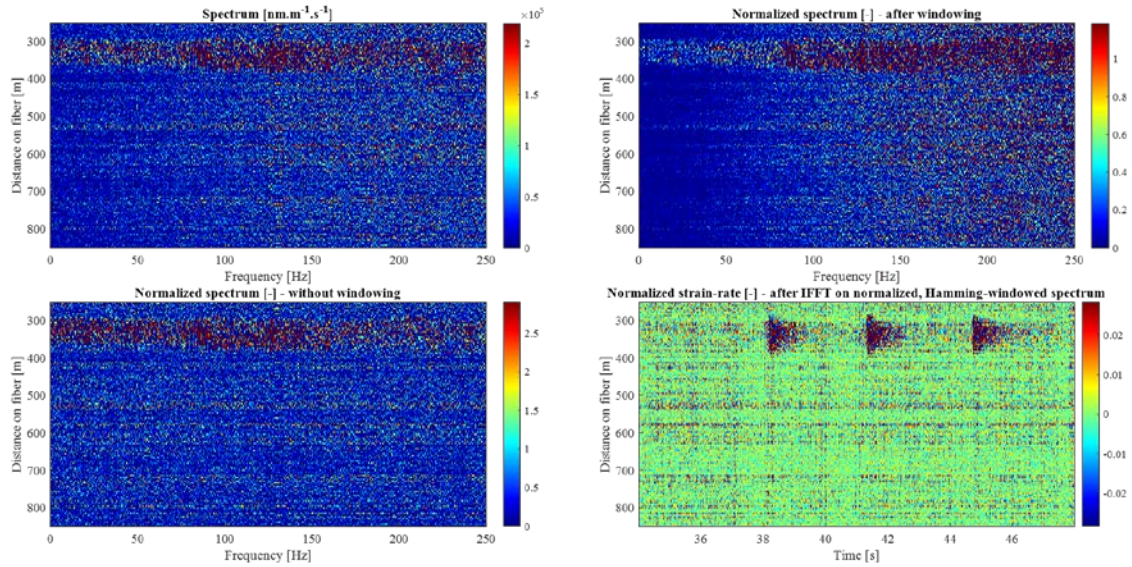


Figure 6-7: Illustration of the normalization procedure to remove acquisition-related noise. The spectra computed from the strain-rate data (top-left) are normalized (top-bottom) and tapered using a Hamming window centred on the requested frequency band – here 150 – 250 Hz – (top-right). A normalized strain-rate is obtained after inverse Fourier transform of the tapered normalized spectrum (bottom-right).

The normalized spectra in Figure 6-7 – bottom left look like the spectra in Figure 6-6 – left, but the strong vertical lines have been removed (especially that around 140 Hz). Applying this procedure shows that the signal previously identified in the strain-rate data is recovered in the normalized traces (Figure 6-8). Figure 6-9 shows that the signal is preserved after normalization (black curve).

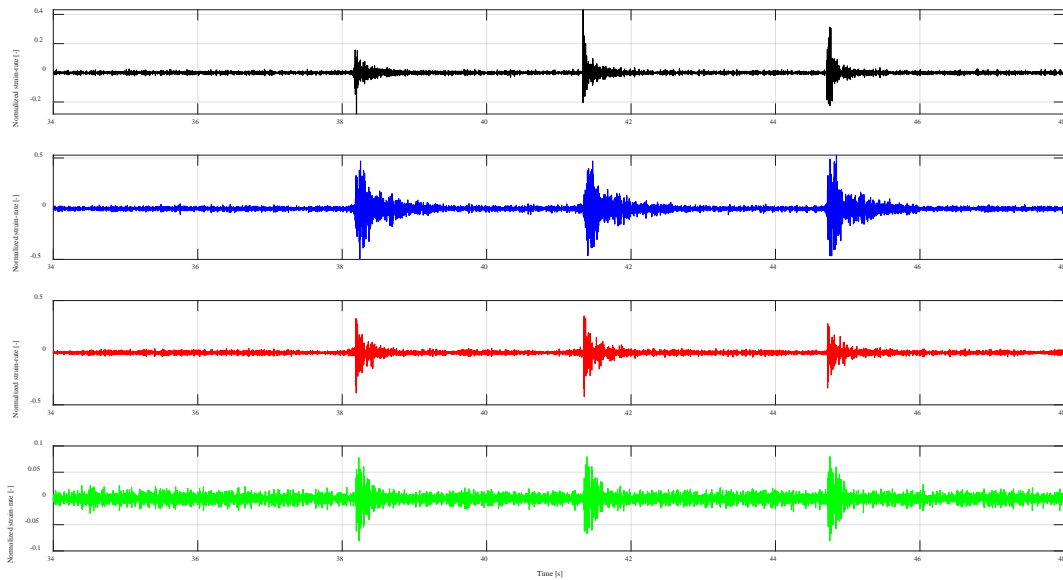


Figure 6-8: The four traces of Figure 6-3 after spectral normalization.

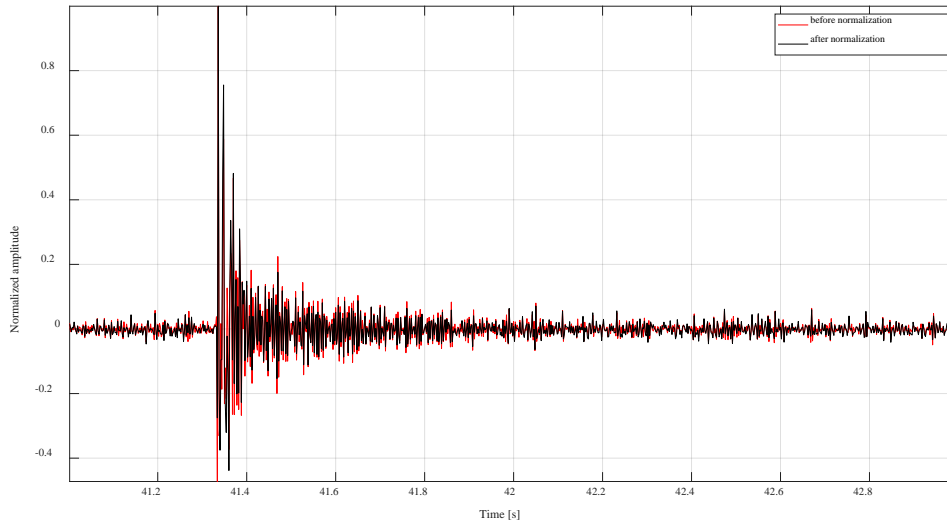


Figure 6-9: Strain-rate generated by the second hammer strike at 300 m (see Figure 6-8) before spectral normalization (red) and after spectral normalization (black). For comparison, both signals are normalized by their respective maximum value.

The spectral analysis enables to evaluate the frequencies that are excited by the signal of interest and help to define a filter that would be appropriate to enhance the later. In Figure 6-10, the tap-test data are filtered between [50, 150] Hz with a third-order Butterworth band-pass filter.

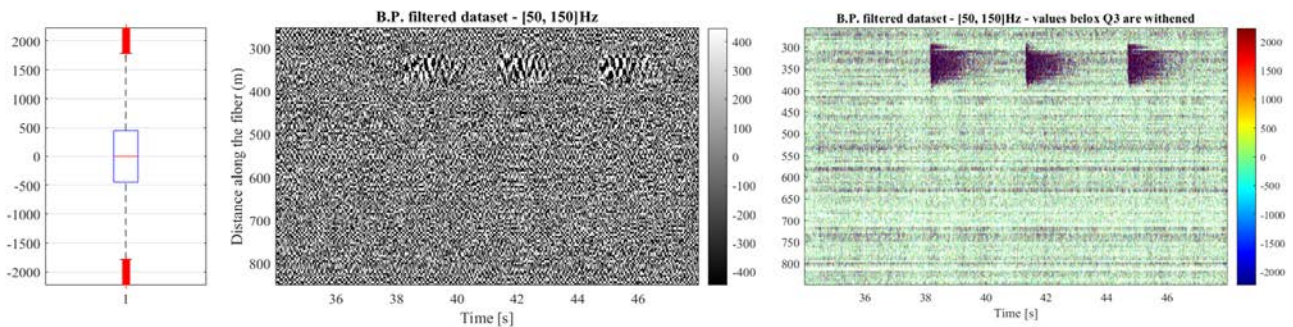


Figure 6-10: Tap-test data of Figure 6-3 after [50, 150] Hz band-pass filtering using a third-order Butterworth filter. Left: grey scale corresponds to the inter-quartile range. Right: full colour scale but values below Q3 were whitened.

Applying the described processing steps to the tap-test measurements showed that a toolbox to improve the data visualization is now available. The tap-tests could be identified in the temporal domain or in the spectral domain, with or without filtering and several ways to enhance the signal were discussed. This will be applied to the records of the sparker survey. However, it is important to recall that the strain-rate corresponding to the tap-tests is much larger than to the strain-rate amplitudes achieved when stacking 901 shots (compare Figure 5-1 top and Figure 6-3 top).

6.4 SPARKER SHOT-POINT RESULTS AND INTERPRETATION

The processing flow is applied to the stacked datasets resulting from the pre-processing of the DAS raw data (see section 5.2 “Pre-processing results”). As an illustration, we show here the results obtained with the recordings of 20/11/20, in Th4, source at 1200 m MD, and the stack of the 901 shots (Table 3-1). A gauge length of 10 m is applied.

6.4.1 TIME DOMAIN

Figure 6-11 shows the strain-rate for the arrival-time and depth ranges in which the signal is likely to be observed (according to the simulation results, see section 6.2). The minimal distance between the source and the receivers is 137 m; the depth range covers a source-receiver distance up to ~ 310 m (top of image) and ~ 350 m (bottom of image).

In order to assess the noise-level in this data excerpt, the third quartile Q3 value of all samples recorded 0.5 seconds before the firing time (black line on the right-hand side plot of Figure 6-11) and ± 25 m around the shot depth (i.e. from 1175 to 1225 m). This Q3 value is ~ 100 nanostrain. s^{-1} for the 901-shot stack. It is consistent with the third quartile computed with the datasets showed in Figure 6-11, or with the Q3 value computed with the entire dataset (displayed in Figure 5-1, middle figure for $GL = 10$ m). This shows that the amplitudes observed in the area of interest are statistically of the same level as those recorded in an area where we expect to record only noise. In addition, this third quartile value was ~ 800 nanostrain. s^{-1} when we considered a noise data-window of same size within the records related to the tap-test, and without stack.

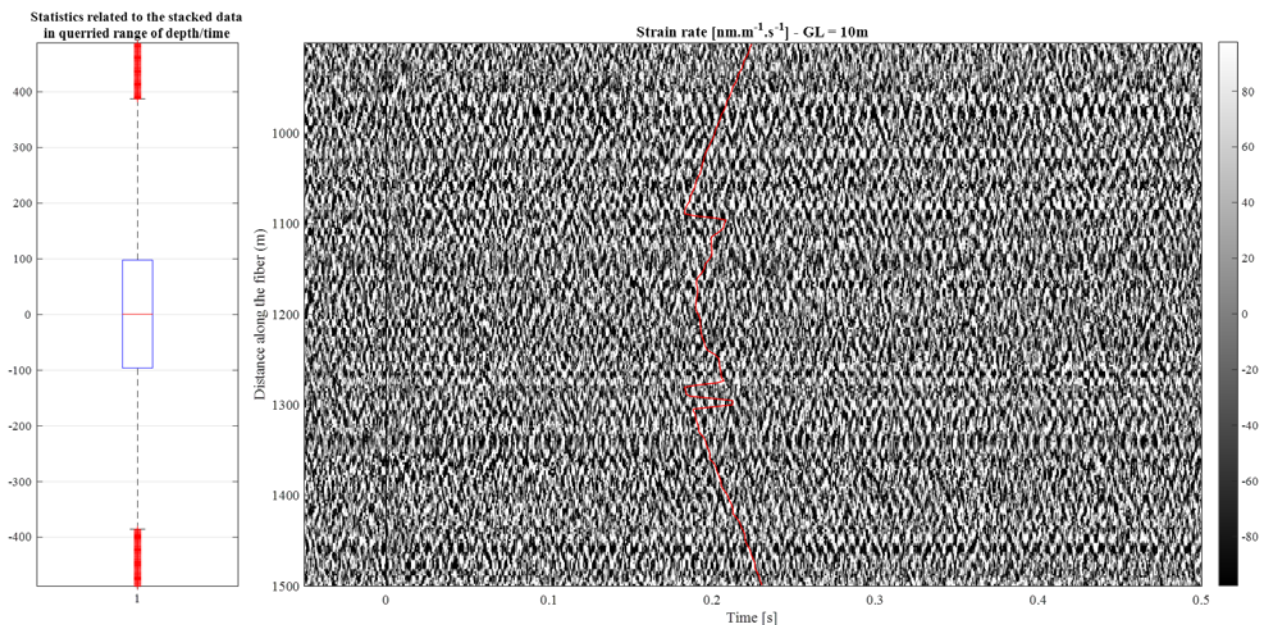


Figure 6-11: Strain-rate, $GL = 10$ m, stack of 901 shots recorded in Th4 on 20/11/20, source at 1200 m MD in Th6. Right: The black vertical line, at $t = 0$ s, indicates the firing time; the red line shows the expected time of arrival of the P-wave as calculated by the simulations; the grey colour scale ranges between Q1 and Q3 of the strain-rate. Left: box-plot of the strain rate values shown on the right-hand side.

In the bottom panel of Figure 6-12, strain-rate values within the inter-quartile range are whitened. The objective is to emphasize, in the time domain, uncommon strain-rate values within the dataset, as expected from the arrival of seismic waves that would originate from the sparker shot. However, no specific feature can be observed in the likely zone of the wave arrivals.

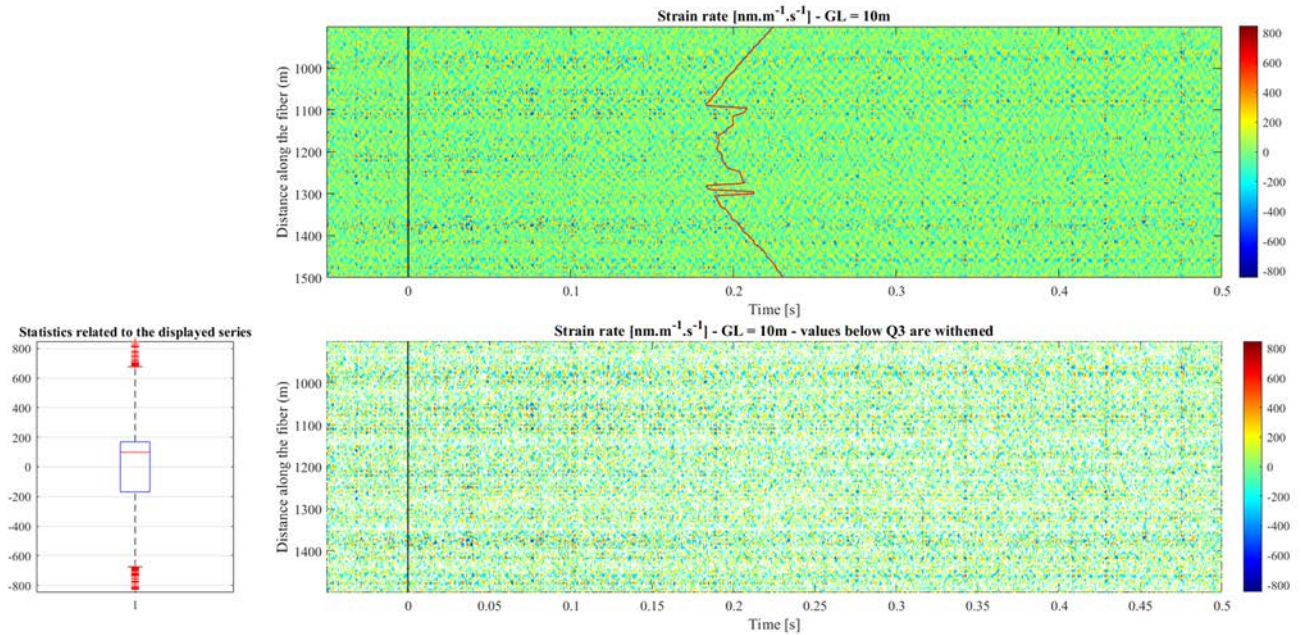


Figure 6-12: Enhanced visualisation of strain-rate data of Figure 6-11. Top-right: strain-rate amplitudes; the red line indicates the simulated P-wave arrival times. Bottom-right: same as top-right but the strain-rate amplitude within the inter-quartile range are whitened. In both images, the colour map covers the full range of strain-rate amplitudes. Bottom-left: box-plot of the strain-rate amplitude after removal of the whitened values.

6.4.2 FREQUENCY DOMAIN

Figure 6-13 presents spectrograms of the studied signal. The objective is to emphasize, in the frequency domain, unusual signal.

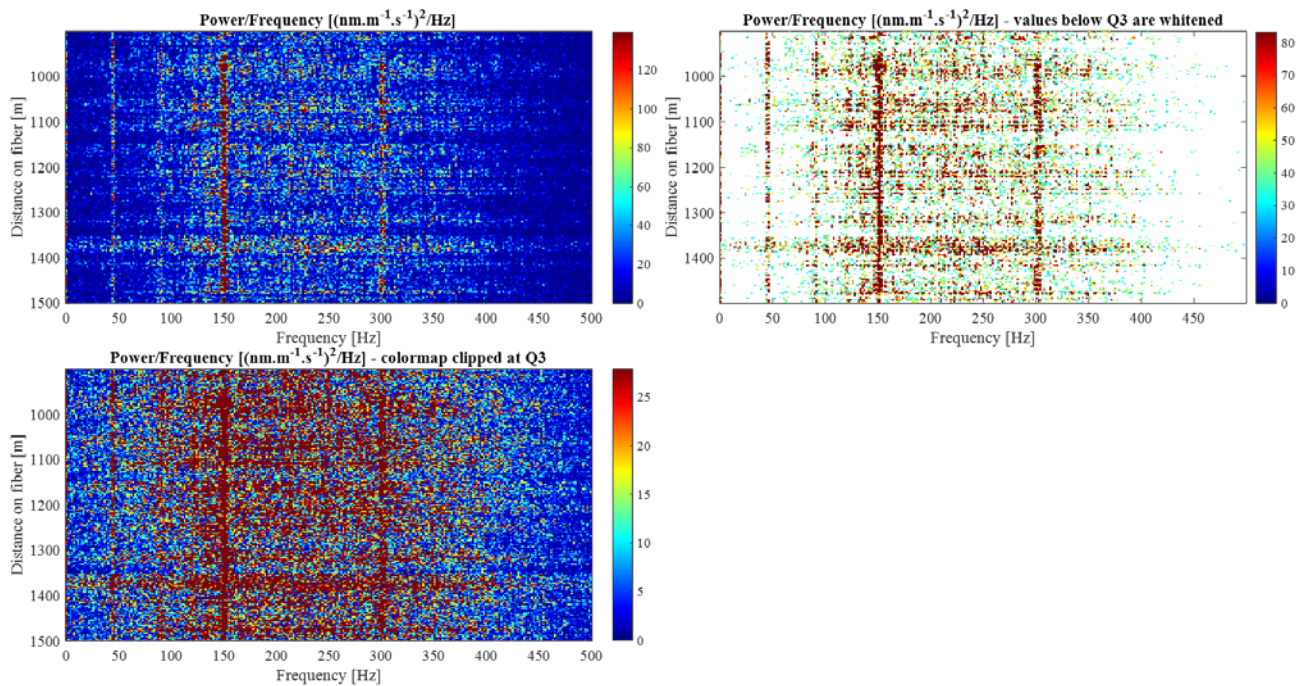


Figure 6-13: Three representations of the spectrograms of the strain-rate shown in Figure 6-11. Top left: the colour scale is bounded by the upper-inner-fence of the samples. Bottom left: the colour scale is bounded by the Q3 of the samples. Top right: – Data with amplitudes below Q3 are whitened and the colour scale adapted accordingly.

Various colour limits and whitening have been applied in relation with the statistical distribution of the power spectral densities (PSD), as explained in section 6.3. The PSD are shown over the depth interval and, as described in section 6.3, the PSD have been normalized to reduce the impact of acquisition noise. In addition to the vertical features already observed and discussed with the measurements of the tap-test, the spectrograms show reddish horizontal bands (e.g. close to 1300 – 1400 m) that correspond to larger amplitudes and wider range of excited frequencies. These features are typical of incoherent noise along the fibre.

The above-described processing-procedure was applied extensively to all data recorded during the sparker survey (see Table 3-1), i.e. the data acquired at other dates, for other source depths and with other acquisition parameters:

- In “Appendix 3: GL = 5 m, data acquired in Th4 on 20/11, source at 1200 m”, we show the results obtained with a different gauge length, GL = 5 m.
- In “Appendix 4: GL = 5 m, data acquired in Th4 on 19-20/11, source at 1200 m”, we increase the number of stacks and process the data from 19/11 and 20/11/20.
- In “Appendix 5: GL = 5 m, data acquired in Th3 on 19/11, source at 920 m”, we consider the measurements acquired in Th3, the source being at 920 m MD in Th6.
- In “Appendix 6: GL = 10 m, data acquired in Th3 and Th4 on 17/11, source at 400 m”, we show the measurements of the test-shots performed with a source at 400m.

6.4.3 COHERENCY ANALYSIS

If the sparker signal is recorded along the FOC, it should exhibit some coherency in space and time. To emphasize such characteristics, even for a weak acoustic signal, spatial and time cross-correlation are performed. To some extent, they both rely on the results of the survey simulations (see “Appendix 2: Cross-well survey simulations”).

Spatial cross-correlation

If a coherent signal reaches the FOC, then it should not be too different from one position along the FOC to the next one(s). This should apply close to the simulated arrival time of the P-wave along the fibre. Hence, a 0.2 s time window centred on the P-wave arrival time for each depth level along the fibre is taken as a reference and cross-correlated with all other windows. If the signal is consistent between two levels, then the cross-correlation coefficient should be close to 1 for that pair of level. The cross-correlation also takes into account incorrect prediction of the P-wave arrival time (from the simulation) by up to ± 0.1 s. The similarity of the signal content between two levels is quantified by the maximum correlation coefficient computed between the corresponding time windows (Figure 6-14).

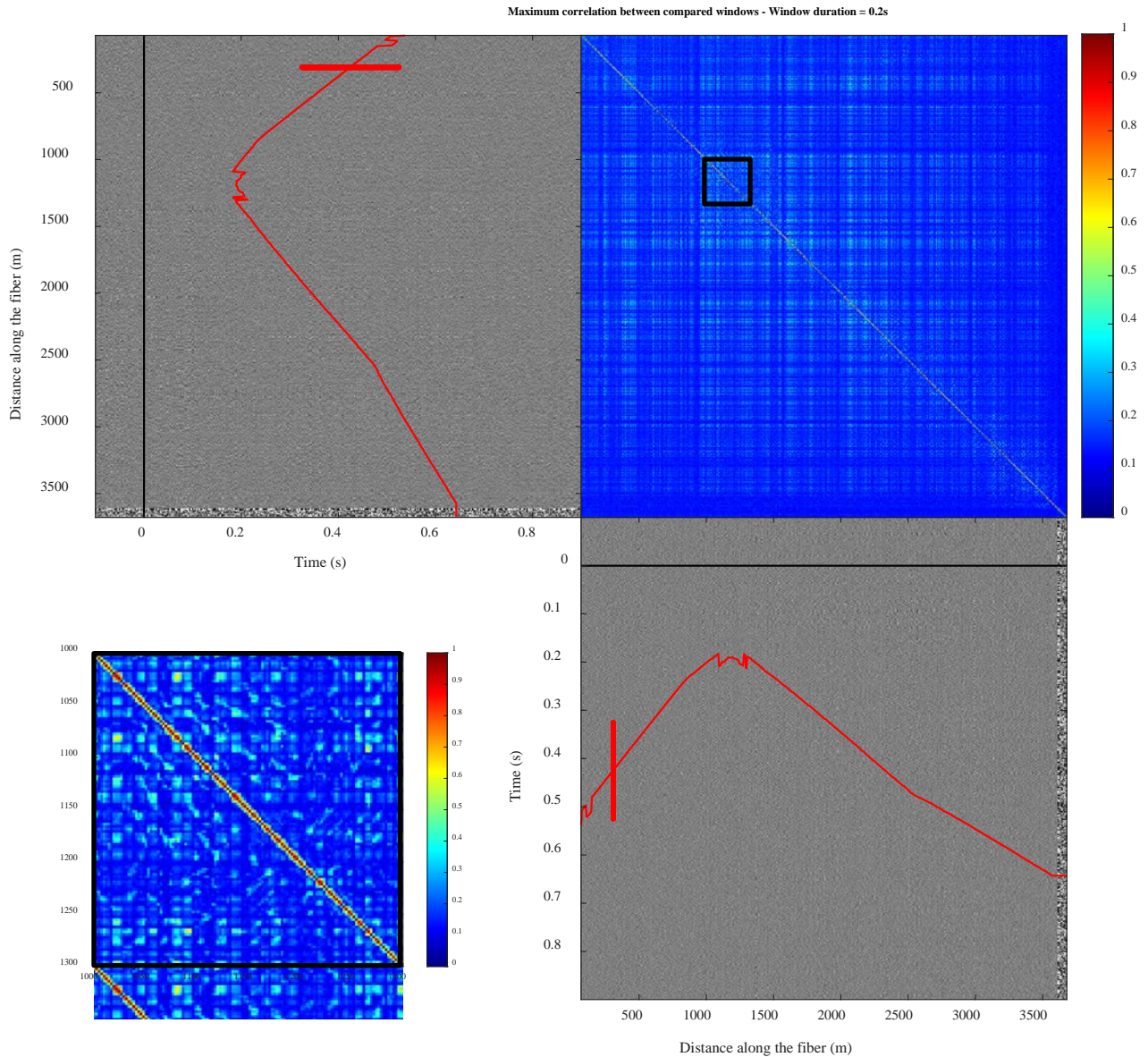


Figure 6-14: Strain-rate, GL = 10 m, stack of 901 shots recorded in Th4 on 20/11/20, source at 1200 m MD in Th6. The top-left and bottom-right panels show the dataset and the central position (simulated P-wave arrival time) of each window. They are shown to ease the understanding of the correlation matrix, which is displayed on the top-right. The correlation matrix gives the maximum cross-correlation coefficient between two windows at given depths. Consequently, it is symmetric and the diagonal elements equal one because this corresponds to the auto-correlation of the trace. The plot on the bottom-left is a zoom of the correlation matrix in the black square.

As shown in Figure 6-14, each time window correlates perfectly with itself; consequently, the maximum correlation value is one along the diagonal of the correlation matrix. Each window also correlates with the next or the next two depth levels, however, less perfectly. This observation is interpreted as the effect of the spatial oversampling set in the acquisition parameters of the DAS-interrogator. Otherwise, all other window pairs correlate weakly together, as shown by the poor correlation values. Moreover, the correlation increases only in a discontinuous way, which is not expected if the signal would propagate continuously in depth. From Figure 6-14, we see that distinct windows close to the source depth do not share any coherent content, which would be related to the same seismic source. On the contrary, the highlighted patterns rather suggest that the selected windows share similar noise, with comparable level of fading with depth and time.

Spatial and temporal cross-correlation

A second approach is applied and consists in selecting one reference window (in red in Figure 6-15), still 0.2 s long, centred on the simulated P-wave arrival time, at the 1000 m depth level. Then, cross-correlation is computed with similar length windows taken between 900 m and 1500 m depth (the blue horizontal lines in Figure 6-15) over a period of 0.9 s after the sparker shot time (black vertical line in Figure 6-15). These depth and time ranges are the most likely to contain signal (see also Figure 6-1 for example). We use a 95% overlap between successive comparison-windows.

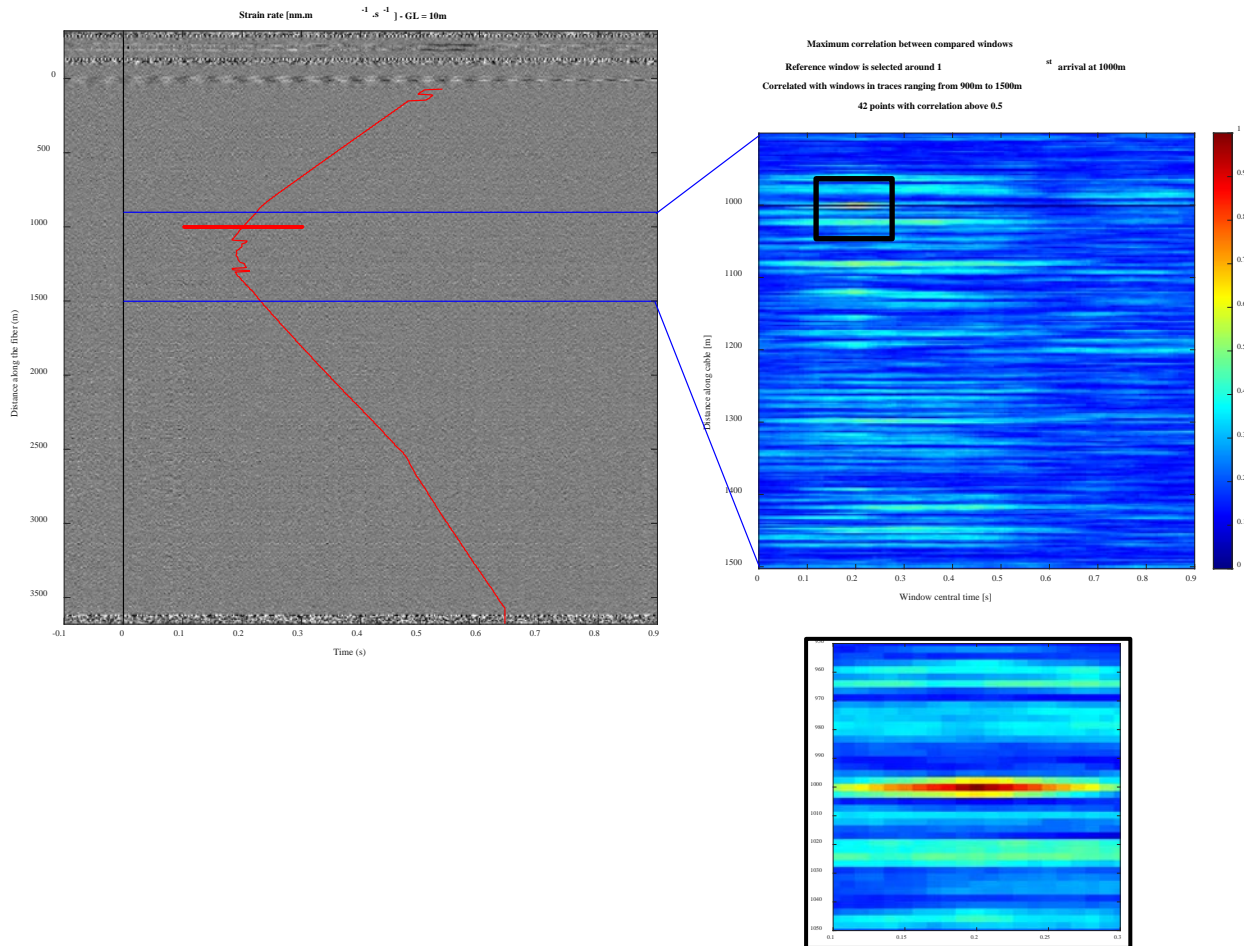


Figure 6-15: Strain-rate, GL = 10 m, stack of 901 shots recorded in Th4 on 20/11/20, source at 1200 m MD in Th6. Top-left: the blue horizontal lines, at 900 m and 1500 m respectively, and the black vertical line, at 0 s time, limit the zone of interest. The 0.2 s reference window (in red) is centred on the simulated P-wave arrival time at 1000 m depth. Top-right: correlation coefficients computed over the zone of interest, which is computed for each window comparison, in the queried area. The plot on the bottom-right is a zoom of the correlation coefficients around the reference trace (black square).

If coherent signal associated with the sparker shot exists in the recording, the cross-correlation values should be large at the signal arrival on the fibre. This is not observed. In Figure 6-15, the reference window only correlates strongly with itself and surrounding windows, which is again the effect of the depth oversampling set during the data acquisition. We observe that only 0.1% of the correlation coefficients in the window of interest (i.e. 42 values) are larger than 0.5. The variation over time and depth of the – low – correlation coefficients are interpreted as resulting from noise with same level of fading.

For comparison, we applied the same processing to tap-test data. The reference window encompasses the tap-test signal observed at 330 m (see the green trace in Figure 6-3) between $t = 41.2$ s and 42.0 s. Then, it is correlated with time windows in the 300 to 400 m depth range. The three narrow vertical features identified on the correlation coefficient plot (Figure 6-16) show, first, that the signal coherency is maintained over time.

The reference signal correlates very well with the signal of the previous and next hits, observed around $t = 38$ s and $t = 45$ s in the trace. We also observe that the coherency is maintained over depth, until around 50 m below the reference window. On the other hand, the rest of the record that consists of noise correlates very poorly with the reference window. Figure 6-16 also shows that the reference window correlates better with the signal at regularly spaced positions along the fibre, approximately every 20 m. This could be the results of a tighter coupling between the fibre-optic cable and the ground, happening at specific depths, but could not be related to any specific feature of the sucker rod at the moment.

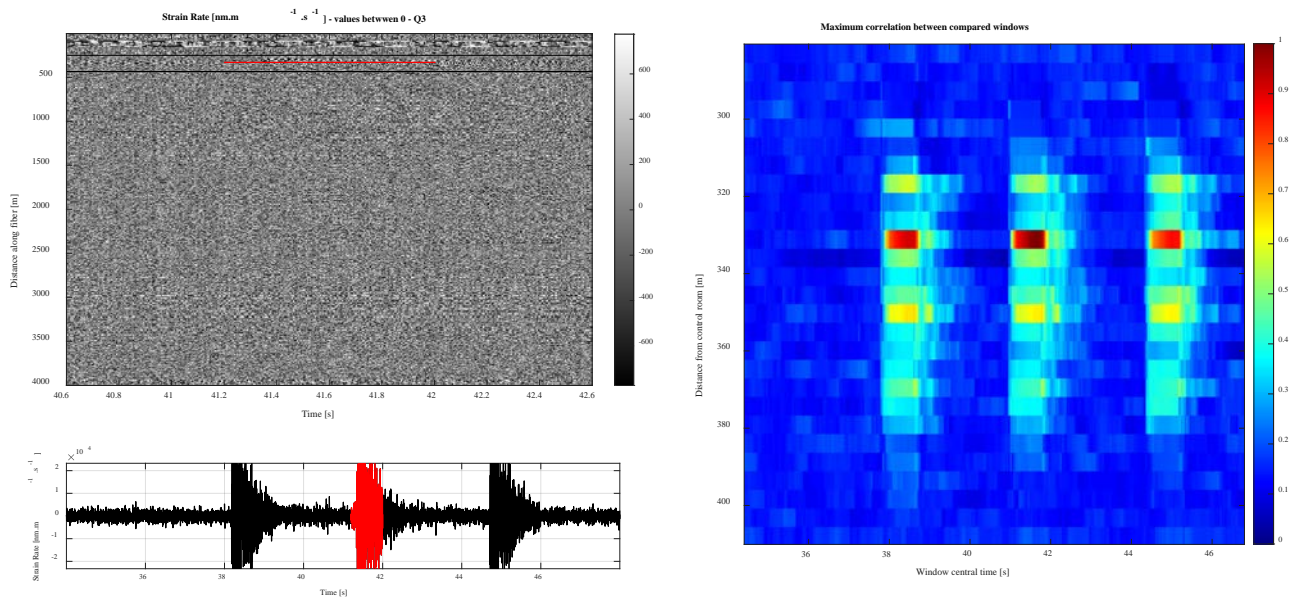


Figure 6-16: Tap-test. Top-left: a 0.8 s window is selected in the dataset (red segment) and compared by correlation to successive windows selected within the depth interval ranging from 280 to 400 m (black horizontal lines). Bottom-left: strain-rate trace of the tap-test at 330m; the reference window is highlighted in red. Right: maximum correlation coefficient between the reference trace and the rest of the signal over depth and time.

7 FINAL DISCUSSION AND CONCLUSION

No seismic signal associated with the sparker shots has been identified on the records acquired either by Th3 or by Th4 or both fibre-optic cables. The stack of up to thousand records associated with shots performed at the same depth level did not provide signal either. Despite the application of various pre-processing and processing flows the expected signal could not be observed. Among the pre-processing sequences, several gauge lengths were applied (2, 5, 10, 20 and 50 m) as well as different stacks, in quantity, source position, and recording fibre(s). Among the processing sequence, temporal and spectral inspections of the signal with enhanced visualizing procedures were done. Coherency of the recorded signal on the fibre was also analysed in time and space.

On the other hand, the signal related to hammer strikes made at the Th4 wellhead during a tap-test could be clearly distinguished and analysed. This tap-test was used to validate the pre-processing sequences including the raw data conversion to strain-rate data and the stacking procedure. The further processing sequences could also be evaluated on this dataset.

Our results show that, if the seismic signal associated with the sparker shots exist in the records, the corresponding strain-rate amplitudes are very small, smaller than $100 \text{ nanostrain} \cdot \text{s}^{-1}$, below the noise level. Moreover, the third-quartile of strain-rate amplitudes, Q3, recorded over fibre lengths and periods where the seismic signal was expected and where it was not are equivalent. This further supports that the seismic signal if it exists cannot be distinguished from the background noise.

Beside the effect of source to receiver distance and of the directional sensitivity of the fibre that have been accounted for the survey design (thanks to the simulations), other factors could explain why the sparker shot energy is not larger than the noise recorded on the fibre-optic cables:

- The energy of the source could be too weak and never compensated by repeating the shots at the same depth (and then stacking the records). However, previous experience of Febus-Optics, the provider of the DAS-interrogator, under similar conditions concerning the source type, the inter-well distances and the acquisition parameters, tells that the sparker signal could be visible after a few tens of shots. The observations at Schäftlarnstraße are not similar and therefore could result from differences between both experiments. Apparent differences involve the source well completion, the signal attenuation in the geological formations, or the coupling of the fibre-optic cables or a combination of them.
- The Th6 well completion could have an impact (Figure 3-10). In the shooting interval, between 400 m and 1200 m, the well diameter is 13.3/8" and the sparker source is 3" diameter. The dimension ratio being relatively large, most of the energy released by the sparker source would remain in the well. It is known that the well can act as a seismic-wave guide due to the large impedance contrast between the fluid in the well (low impedance) and the steel casing (high impedance). Hence, the energy transmitted to the formation through the casing is low compared to the reflected energy and it applies only for a small solid angle at the source. This effect is squared for the first 770 m of Th6 well due to the tie-back: before cementation to the formation, two steel casings are set, with 13.3/8" and 20" diameters respectively, and separated by an annulus filled with fluid. Although this phenomenon is frequency dependent, it would eventually decrease the effective amount of energy transmitted into the formation up to the FOC that would not be compensated by the ~ 1500 or ~ 1800 shots that would increase the signal to noise ratio by about 40.
- Finally, the coupling of the Th4 FOC to the ground could be weak. In fact, the coupling exists through the weight of the sucker-rod that supports the FOC and which is lying on the Th4 casing. However, active VSP data have been successfully recorded by Th4 FOC. Besides, coupling of the Th3 FOC should be better because the FOC is cemented behind the casing. Consequently, the coupling of Th3 or Th4 FOCs may not be the major issue.

The main goal of the sparker survey was to gain knowledge on the velocity model, to better constrain the S-waves velocity field and to better locate possible induced seismicity. This guided our choices during the field

work. Unfortunately, the DAS recordings did not allow us fulfilling these scientific objectives, nevertheless experience and lessons have been learned. In particular, a series of pre- and post-processing procedures dedicated to the analysis of DAS data were developed. This toolbox will be used when passive DAS monitoring will take place. Furthermore, it is likely that the characteristics of the well in which the sparker source is used play a major role in the transmission of the source energy into the formation. So far, such aspects have not been considered as they should.

In the frame of the INSIDE project, to reach part of the goals set for the sparker survey, it will be necessary to further analyse part of the existing data (e.g. active VSP data).

8 APPENDICES

8.1 APPENDIX 1: OTDR MEASUREMENTS ON THE Th3 AND Th4 FIBRES

Objective – In order to optimize the acquisition parameters of the DAS-interrogator – especially the characteristics of the light pulse interrogating the fibre – the energy losses within the fibre installed in the SLS wells have been quantified, in September 2020, using an Optical Time Domain Reflectometer (OTDR).

Operations – The device injects a series of optical pulses into the fibre and records the (Rayleigh) back-scattered or back-reflected light, which is analyzed to characterize the optical fibre. The strength of the return pulses is measured and integrated as a function of time. On this occasion, all possible configurations were tested separately:

- connection to the Th3 fibres,
- connection to the Th4 fibres,
- connection to Th3 and Th4 fibres set in series.

Two wavelengths have been used with the OTDR: 1310 nm and 1550 nm. The wavelength used by the Febus A1-R interrogator is 1550 nm. The results produced by the OTDR device are presented from Figure 8-1 to Figure 8-3.

Conclusions – The conclusions are similar for the different configurations tested. Two large attenuations exist:

1. at the U-loop of Th3, with a loss of around 1.3 dB,
2. at the splice at the wellhead of Th3, with a loss of around 0.4 dB. (This splicing was conducted under difficult conditions by Baker Hughes).








These two attenuations lead to a cumulative loss of more than 2 dB at the return point of Th3. As a consequence, the acquisition of Th3 and Th4 FOCs in series provide a much lower signal quality on Th4 section than acquiring Th4 alone. To acquire Th3 and Th4 FOCs in series, the DAS-interrogator will have to compensate the energy losses by sending higher optical amplitudes and larger pulse widths.

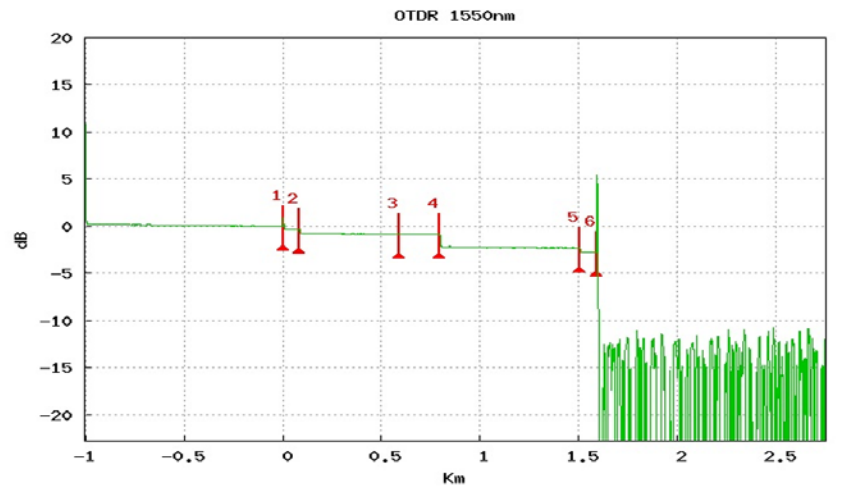
We also observe that losses occur at the connectors due to the strong reflection caused by the presence of dirt. These connectors have been cleaned before being connected to the DAS-interrogator during the cross-well survey.

Print date : 17/09/2020 09:57

Fichier : inside-th3-sm1-1550nm.sor.pdf

VIavi	Nom Câble : Cable Origine : Loc A Réf Intervention :	Nom Fibre : Fiber 4 Extrémité : Loc B Opérateur :
--------------	---	--

MTS 2000 (S/N 36597)	4126 LA (S/N 14635)	Date : 17/09/2020 09:55				
Setup	1550nm 30ns 5km 64cm 60.0s 1.46500(USER 1) -81.0 dB					
OTDR EXPERT						
Alarmes	None					
Seuils						
Résumé						
Nom Fichier	Laser nm	Bilan dB	ORL Liaison dB	Fin de fibre Km	Sens	Evt Alarmes
inside-th3-sm1-1550nm.sor	1550	0.844	44.76	0.589	Loc A -> Loc B	6
						
	-0.000	0.086	0.589	0.793	1.507	1.589 Km



Evt	Distance Km	Affaib. dB	Réfléct. dB	Pente dB/km	Section Km	Bilan dB
1	0.000	0.301	-68.89	0.206	1.005	
2	0.086	0.417		0.316	0.086	0.329
3	0.589	-0.001		0.198	0.503	0.844
4	0.793	1.323		0.137	0.204	
5	1.507	0.416		0.137	0.714	
6	1.589		-49.87	0.750	0.082	

Figure 8-1: Results of the OTDR test: fibre Th3 – SM1, downward and upward. Used wavelength: 1550 nm. The table highlights the main losses identified along the fibre. The 1.3 dB loss #4 is positioned at the microbend (i.e. the turning point of the fibre behind the casing).

Print date : 17/09/2020 09:17

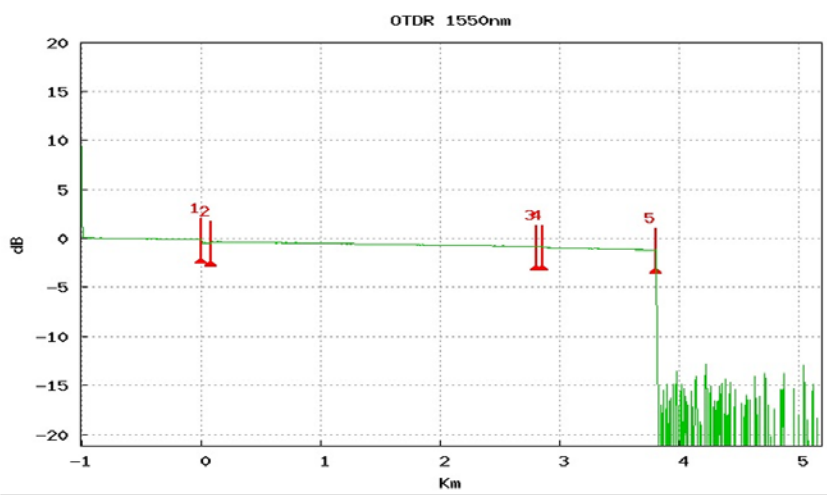
Fichier : inside-th4-sm1-1550nm.sor.pdf

Nom Câble : Cable
Nom Fibre : Fiber 4
Origine : Loc A
Extrémité : Loc B
Réf Intervention :
Opérateur :

MTS 2000 (S/N 36597) 4126 LA (S/N 14635) Date : 17/09/2020 09:15

Setup
OTDR EXPERT 1550nm 60ns 10km 64cm 60.0s 1.46500(USER 1) -81.0 dB
 Alarmes
 Seuils None
 Résumé

Nom Fichier	Laser nm	Bilan dB	ORL Liaison dB	Fin de fibre Km	Sens	Evt Alarmes
inside-th4-sm1-1550nm.sor	1550	0.688	37.65	2.802	Loc A -> Loc B	5



Evt	Distance Km	Affaib. dB	Réfléct. dB	Pente dB/km	Section Km	Bilan dB
1	0.000	0.328		0.206	1.010	
2	0.081	-0.121		0.089	0.081	0.335
3	2.802	-0.006		0.176	2.721	0.688
4	2.858	0.093		0.496	0.056	
5	3.802			0.274	0.944	

Figure 8-2: Results of the OTDR test: fibre Th4 – SM1. Used wavelength: 1550 nm. The table highlights the main losses identified along the fibre. The trace highlights the energy loss along the fibre, with a cumulative loss of about 0.69 dB at the end of the fibre.

Print date : 17/09/2020 10:49

Fichier : inside-th3-sm1-th3-sm2-th4-sm1-1550nm.sor.pdf

Nom Câble : Cable
Nom Fibre : Fiber 4
Origine : Loc A
Extrémité : Loc B
Réf Intervention :
Opérateur :

MTS 2000 (S/N 36597)		4126 LA (S/N 14635)				Date : 17/09/2020 10:46	
Setup							
OTDR EXPERT	1550nm	30ns	10km	64cm	60.1s	1.46500(USER 1)	-81.0 dB
Alarmes	None						
Seuils							
Résumé							
Nom Fichier	Laser nm	Bilan dB	ORL Liaison dB	Fin de fibre Km	Sens	Evt Alarmes	
inside-th3-sm1-th3-sm2-th4-sm1-1550nm.sor	1550	3.772	39.12	4.396	Loc A -> Loc B	7	

	-0.000		0.084		0.797		1.505		1.589		4.396		5.396 Km
--	--------	--	-------	--	-------	--	-------	--	-------	--	-------	--	----------

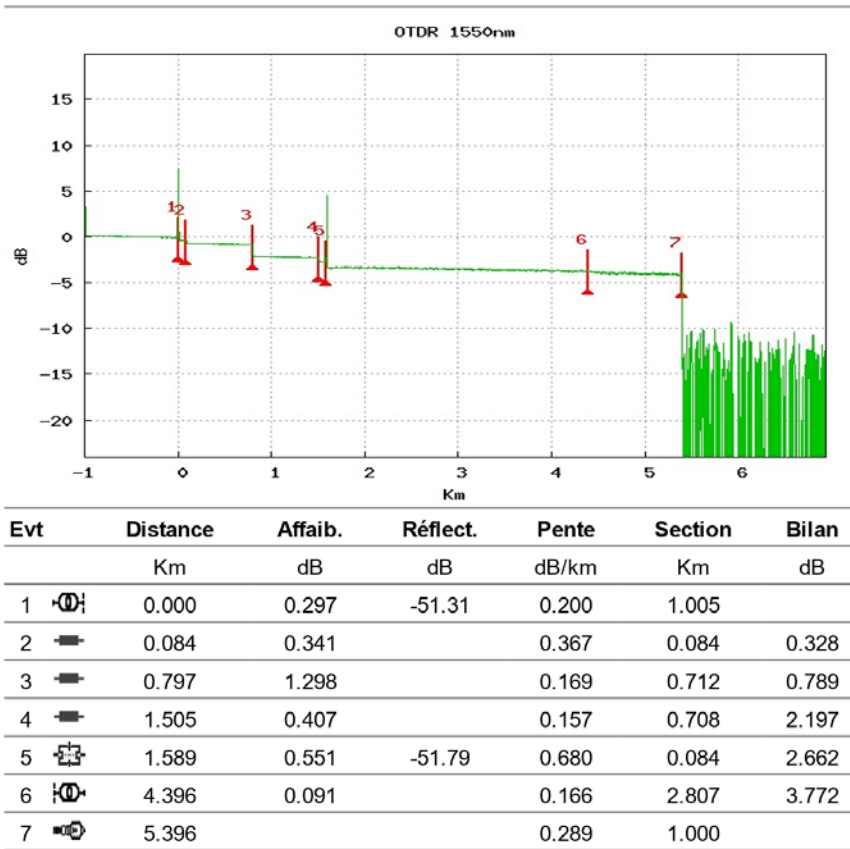


Figure 8-3: Results of the OTDR test: fibre Th3 – SM1 downward + upward connected to fibre Th4 – SM1. Used wavelength: 1550 nm. The table highlights the main losses identified along the fibre. The 1.3 dB loss #3 is positioned at the microbend located in Th3. The connection of Th3 and Th4 fibres brings an additional 0.55 dB loss (#5). The cumulative loss at the end of the fibre reaches 3.7 dB.

8.2 APPENDIX 2: CROSS-WELL SURVEY SIMULATIONS

Purpose and principles

The synthetic modelling enables to assess the impact of two factors on the observed strain rate amplitudes (Figure 8-4):

- the source/receiver distances on the strain-rate amplitudes, because of the geometrical spreading of the source energy,
- wavefront incident angle, or more precisely its relative angle to the well-trajectory, on the strain-rate amplitudes, because of the broadband insensitivity of the DAS measurements.

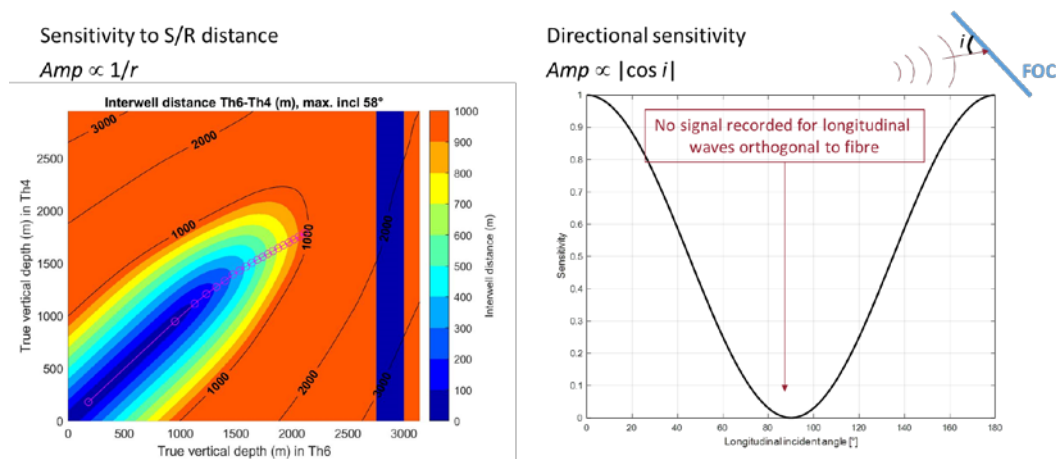


Figure 8-4: Schematic of the impact of two physical processes on the amplitude of DAS-measurements.

SOFI3D, a 3D finite-difference seismic wave simulator developed at KIT³, is applied to compute the X, Y and Z particle velocities along the Th3 and Th4 wells.

To model the source, the characteristics of the AST employed during the survey are used (see section 1.3): each shot is a 1000 J omni-directional source. We use here a central frequency of 10 Hz. According to the AST datasheet, 10 Hz corresponds to the lowest frequency excited by the Sparker. This source frequency is well-adapted to a node-to-node distance of about 10 m. Increasing the central frequency of the source would require decreasing the node-to-node distance and would therefore necessitate additional computation capabilities.

The seismic wave propagation medium was modelled with a blocky velocity model. The seismic horizons of the GRAME project provide the interfaces between the major layers and the layer-velocities are computed from the well sonic logs and geological logs (Figure 8-5). A homogeneous intrinsic attenuation factor, $Q = 50$, was also defined.

Finally, the receivers are modelled along the fibres deployed in Th3 and Th4 and follow the well trajectories. As we consider a regular grid with inter-node spacing of 10 m, the distance between two receivers is about 14 m.

Intermediate results and computation of DAS-measurements

An important aspect of the modelling is to convert the computed particle velocities to DAS-observations. For this purpose, particle displacements were computed and projected along the fibre trajectory. Then, strain-rate is calculated by differentiating the dynamic displacement spatially (over a given gauge length) and temporally (over a given derivation time). The evolution with depth, in Th3 and Th4, of the particle velocities (e.g. Figure 8-6) and of the difference angle between wave-front and well-trajectories (e.g. Figure 8-7) are intermediate results necessary to compute the final strain-rate.

³ Bohlen, Thomas: Parallel 3-D viscoelastic finite difference seismic modelling. Computers & Geosciences 28 (2002)

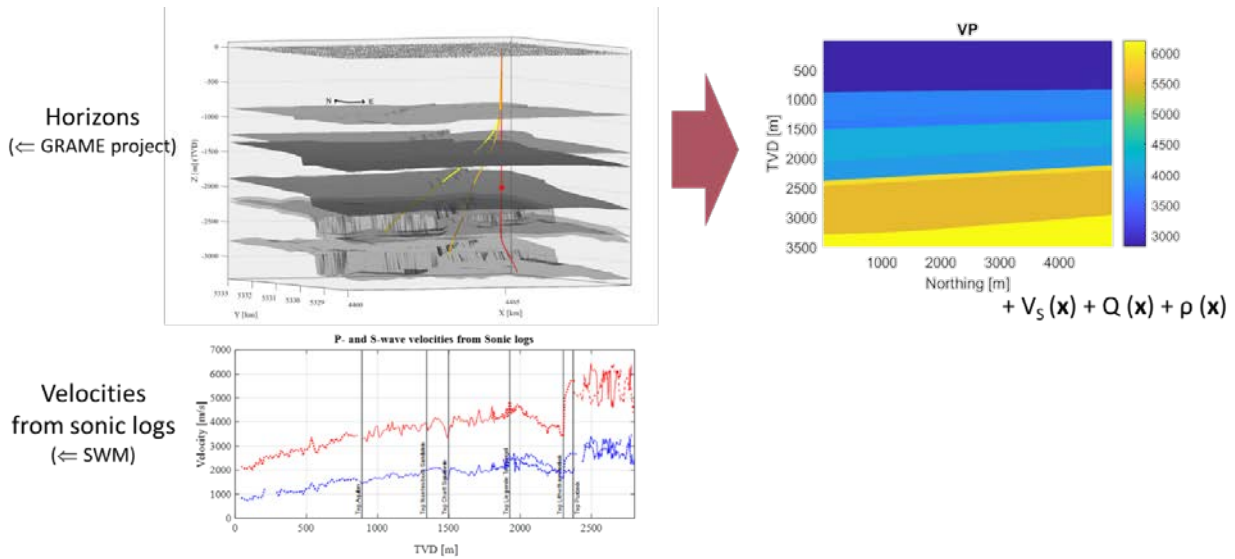


Figure 8-5: The horizons of the GRAME project are used with the trajectories and sonic-logs of the SLS wells to setup a 3D-blocky velocity model.

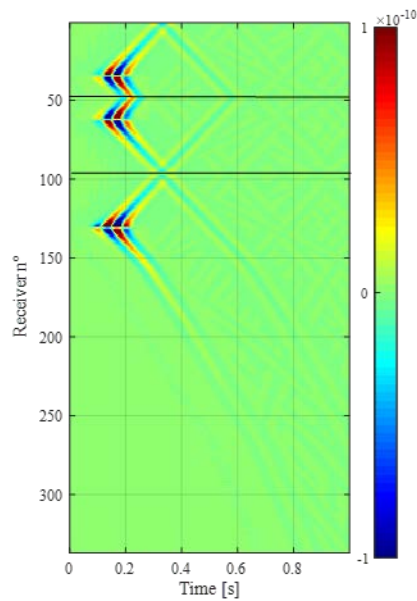


Figure 8-6: Evolution of the horizontal particle velocity (in $m \cdot s^{-1}$) with depth (here represented as the receiver #) in both Th3 (downward and upward, for the top and middle sections respectively) and Th4 (lower section) wells. The source is located at 400 m TVD in Th6.

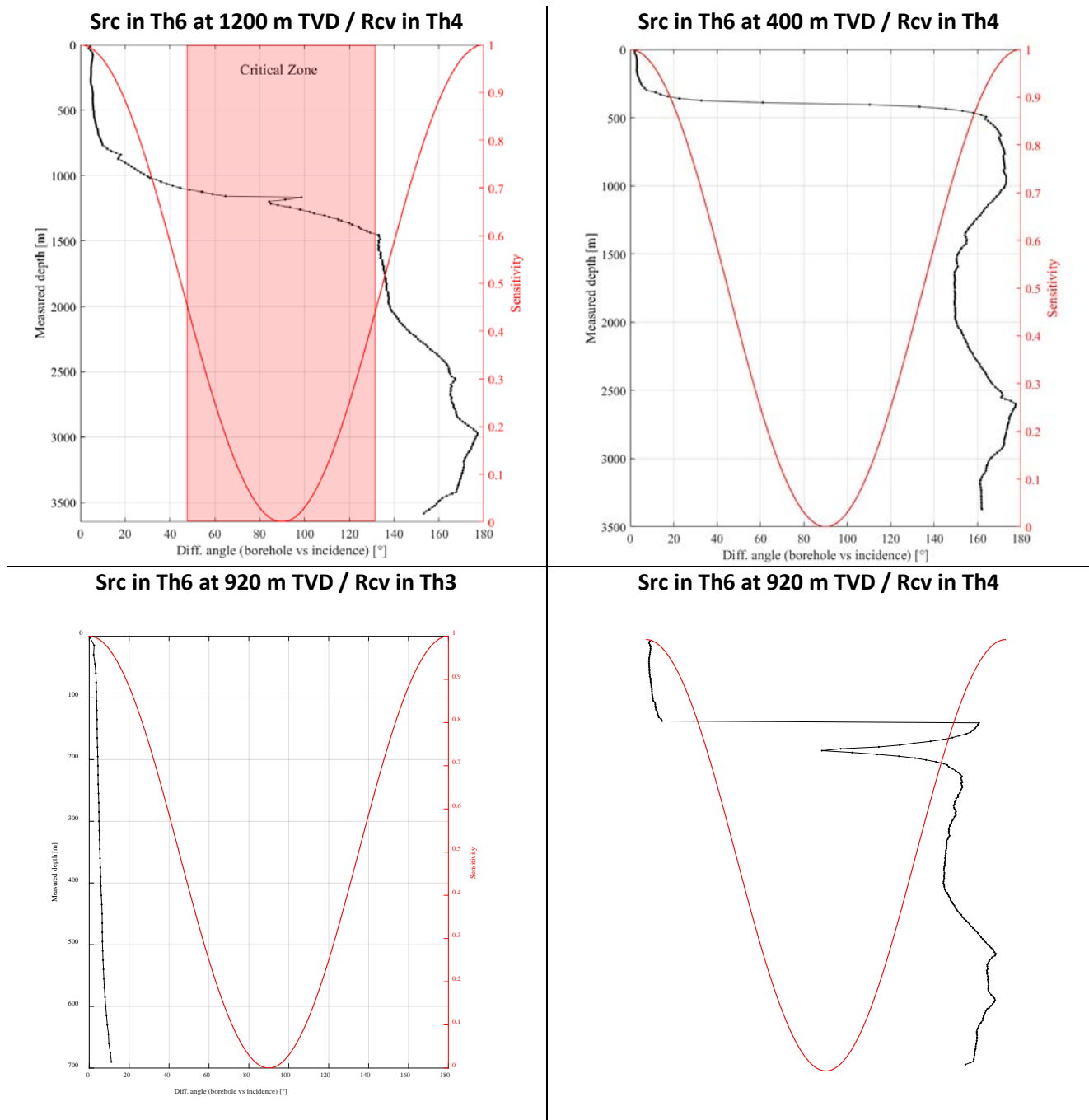


Figure 8-7: Evolution, with measured depth, of the angle between the wavefront and the well-trajectory (in black). The source is positioned in Th6 at 1200 m TVD (top-left), 400 m (top-right) or 920 m (bottom panels – in Th3 on the left, in Th4 on the right). The red curve indicates the theoretical sensitivity of DAS measurements toward longitudinal waves: sensitivity is null for longitudinal waves propagating orthogonally to the fibre.

Consequently, the modelled DAS-observations, which are computed from these preliminary results, encompass the effect of source amplitude attenuation due to geometrical spreading and directional sensitivity of the receiving fibres. In order to evaluate the ability to record signal in a given source/receiver configuration, the modelled observations are analysed in terms of amplitude by computing the evolution with measured depth of the maximal amplitude of the first arrivals (e.g. Figure 8-8).

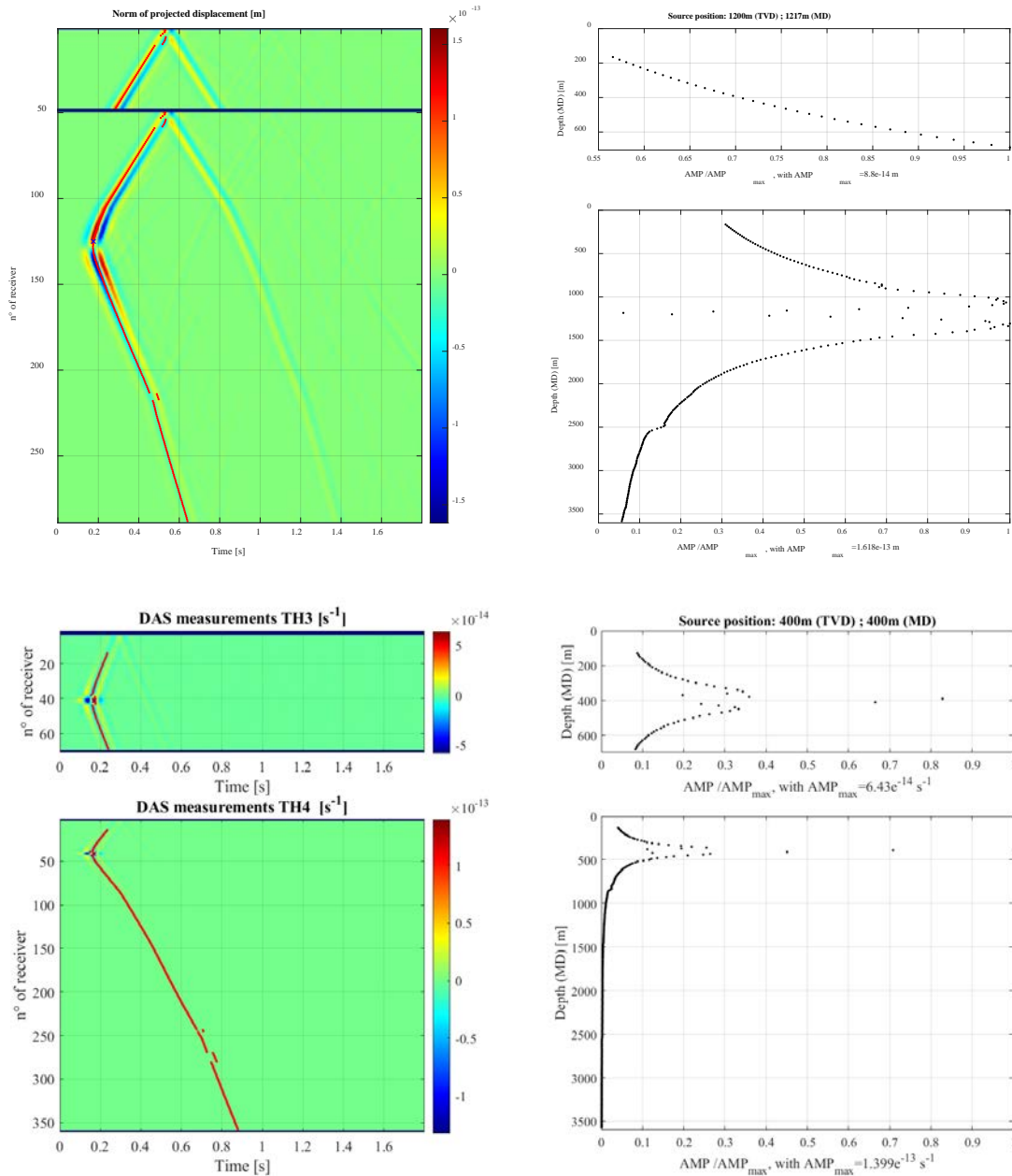


Figure 8-8: Left– Evolution with depth (here with # of receiver) of the dynamic displacement (in m – top panel) or of the strain rate (in $m \cdot m^{-1} \cdot s^{-1}$ – bottom panel), in Th3 and Th4. The source is located at a depth of 1200 m TVD in Th6 (top panel) or at 400 m (bottom panel). The time at which the amplitude of the first arrivals is maximal is highlighted for each trace by a red point. Right – Evolution with measured depth, in both Th3 and Th4, of the maximal amplitude, divided by the absolute maximal amplitude (observed for all the traces). These measurements are representative of the attenuation of the DAS-measurements, caused by the source energy geometrical spreading and the directional sensitivity of the receiving fibres.

Toward forecasting the number of shots required for a given source/receivers configuration

To estimate the number of shots necessary to visualize a signal in the stacked datasets is a major aspect of the survey design, especially because the number of shots is limited to 1000 for one firing head. The correct determination of this minimum amplitude should be confirmed or adapted from real observations made in the field, in particular from the recordings of test-shots planned at the beginning of the survey. Indeed, this amplitude threshold is strongly linked to the real efficiency of one source shot in terms of energy release inside the formation and to the real coupling of the FOCs to the formation that are difficult to assess from theoretical modelling.

However, before going to the field and to be prepared, several scenarios were modelled and are based on the following assumptions:

1. the minimal visible amplitude corresponds to 20% of the maximum amplitude recorded along the considered FOC with one shot located at 400 m MD/TVD in Th6.
2. the background noise on the FOCs is constant over time and distance along the fibre,
3. the signal to noise amplitude ratio improves by a factor \sqrt{n} when stacking the data related to n shots,

The first two assumptions define a minimal signal to noise ratio amplitude, SNR_Q , necessary to identify the source signal on the strain-rate trace. Combined with the third assumption, we can determine, for any shot position, ZS , and any receiver position, ZR , the number of shots, $n(ZR, ZS)$, necessary to identify the source signal on the strain-rate trace using the equation:

$$SNR_Q = \sqrt{n(ZR, ZS)} \times SNR_{sim}(ZR, ZS)$$

with $SNR_{sim}(ZR, ZS)$ the signal to noise ratio modelled at the receiver position, ZR , for a single shot at the position ZS .

This equation combined with the assumed minimum visible amplitude allows investigating the minimum number of shots that would be necessary to identify the source signal on the strain-rate trace as a function of the source position in Th6 and the receiver position in Th3 and Th4 (Figure 8-9).

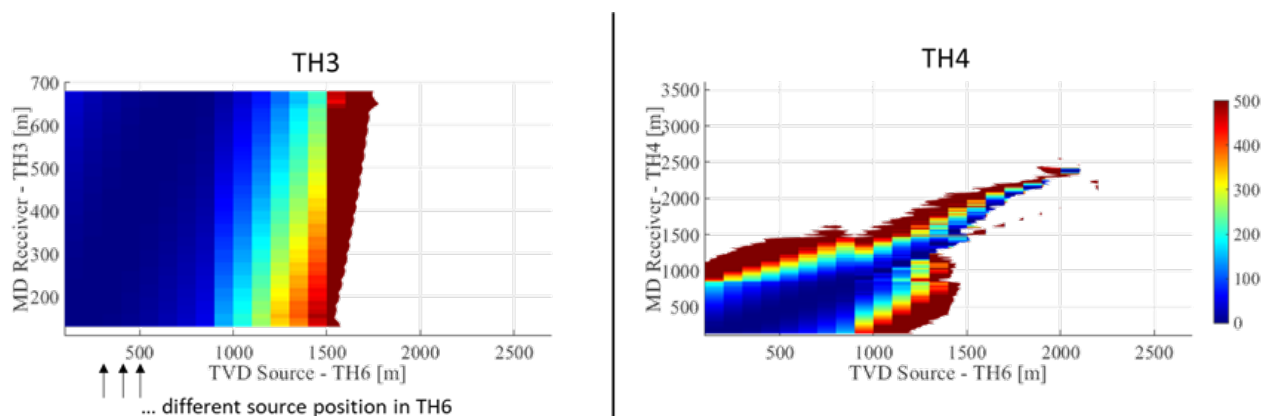


Figure 8-9: Minimum number of shots (represented by the colours) necessary to identify the source signal positioned along Th6 (horizontal axis) on the fibres (vertical axis) in Th3 (left subplot) and Th4 (right subplot). The colour map is saturated between 500 and 1000 shots and limited to 1000 shots. See text for the assumptions.

Another way to present the results is to plot, for a given position of the source in Th6, the range of receivers in Th3 or Th4 that would detect the source signal on the strain-rate trace as a function of the number of shots. Figure 8-10 illustrates this for well Th4.

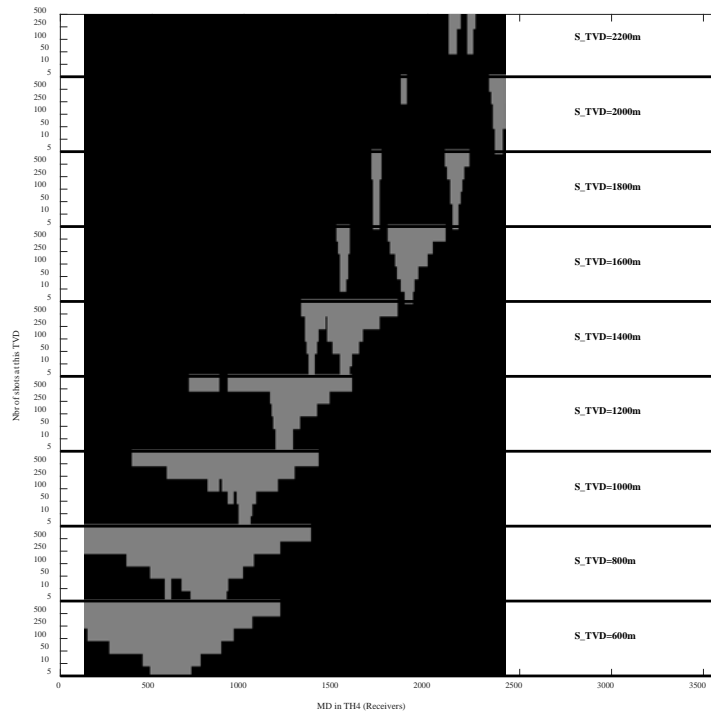


Figure 8-10: Prediction of the range of receivers in Th4 (horizontal axis in m MD) that can detect the signal of a source positioned in Th6 at different depths, S_TVD (horizontal subplots), as a function of the number of shots (Y axis of each subplot). See text for the assumptions.

Conclusions

The modelling of the DAS measurements accounting for the effect of the directional sensitivity and of the source/receiver distances on the strain-rate amplitudes have been used to design the survey. However, it could not answer the question of the minimum number of shots that are necessary to observe the sparker signal on the FOCs in Th3 or Th4. Only relative behaviour was simulated and was intended to prepare the correct scaling of the survey, in the field, as soon as initial real observations would be available. Hence, the survey was designed with an initial test phase that unfortunately was not successful.

However, the outcomes of the simulations have been useful to prepare the processing of the strain-rate data. In particular, the most relevant spatial and temporal zones to identify the seismic signal in the different recordings can be determined. This will be extensively applied to look for any signal in the recordings made in field during the survey.

8.3 APPENDIX 3: GL = 5 m, DATA ACQUIRED IN TH4 ON 20/11, SOURCE AT 1200 M

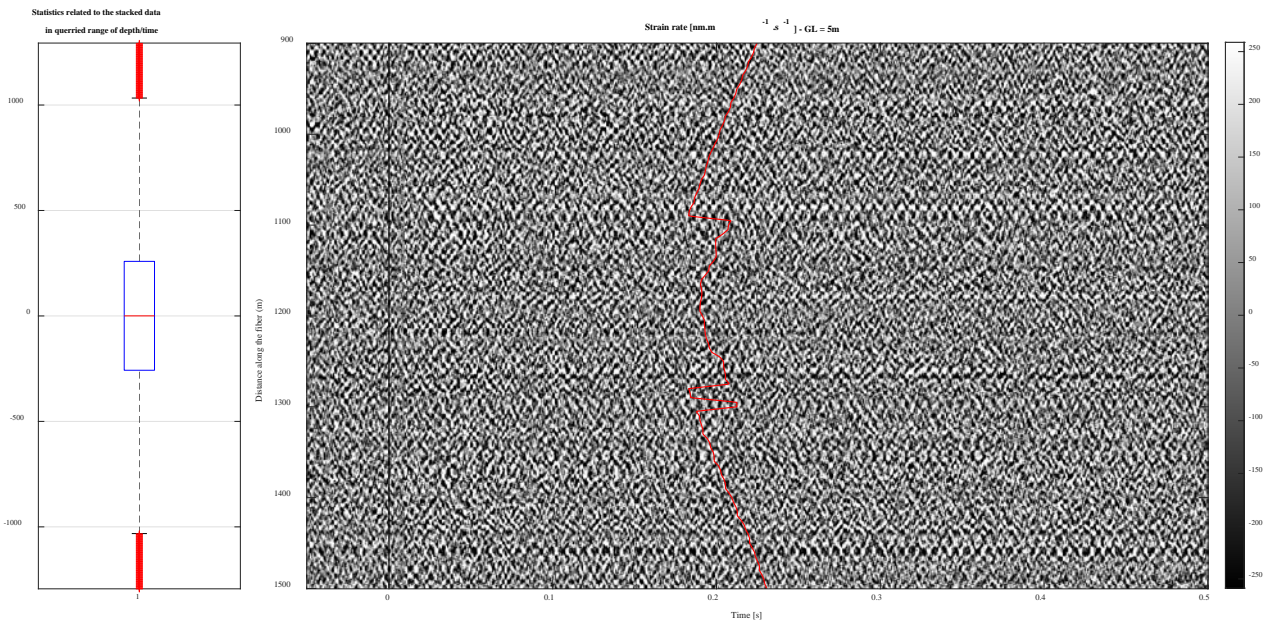


Figure 8-11: Stacked strain-rate, 901 shots, Th4, 20/11, source at 1200 m, GL = 5 m. Display similar to Figure 6-11.

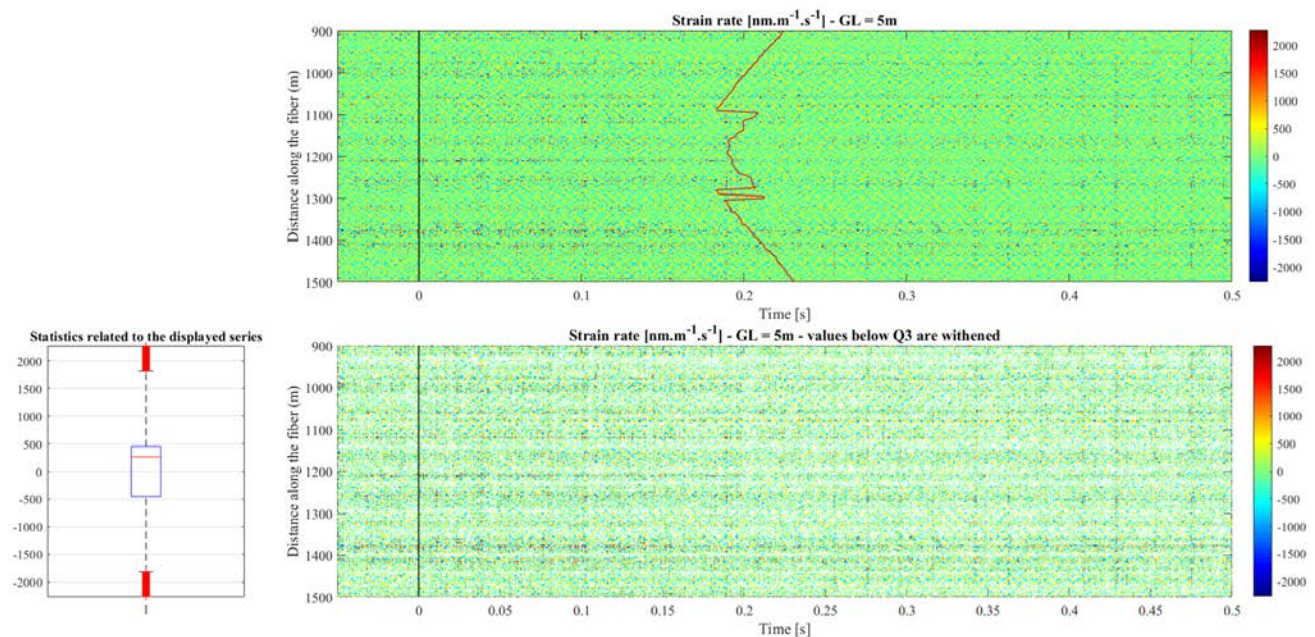


Figure 8-12: Enhanced visualisation of strain-rate of Figure 8-11. Display similar to Figure 6-12.

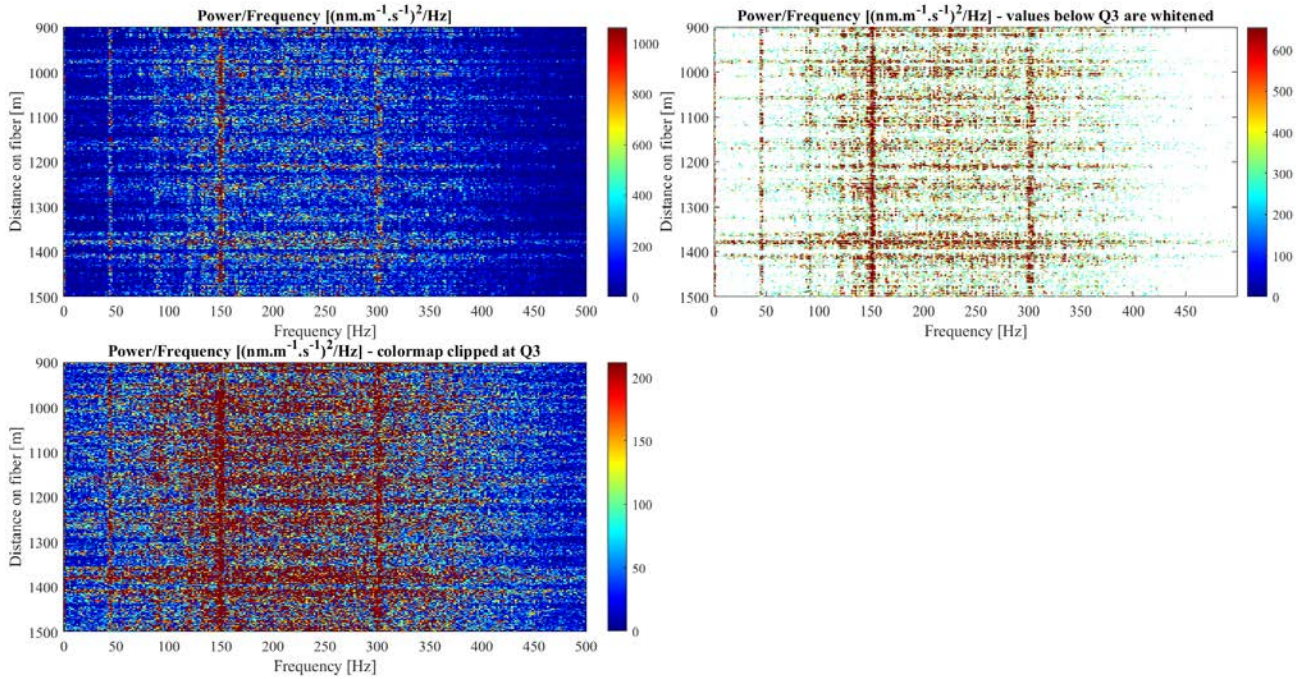


Figure 8-13: Power spectral densities of Figure 8-11 strain-rate. Display similar to Figure 6-6.

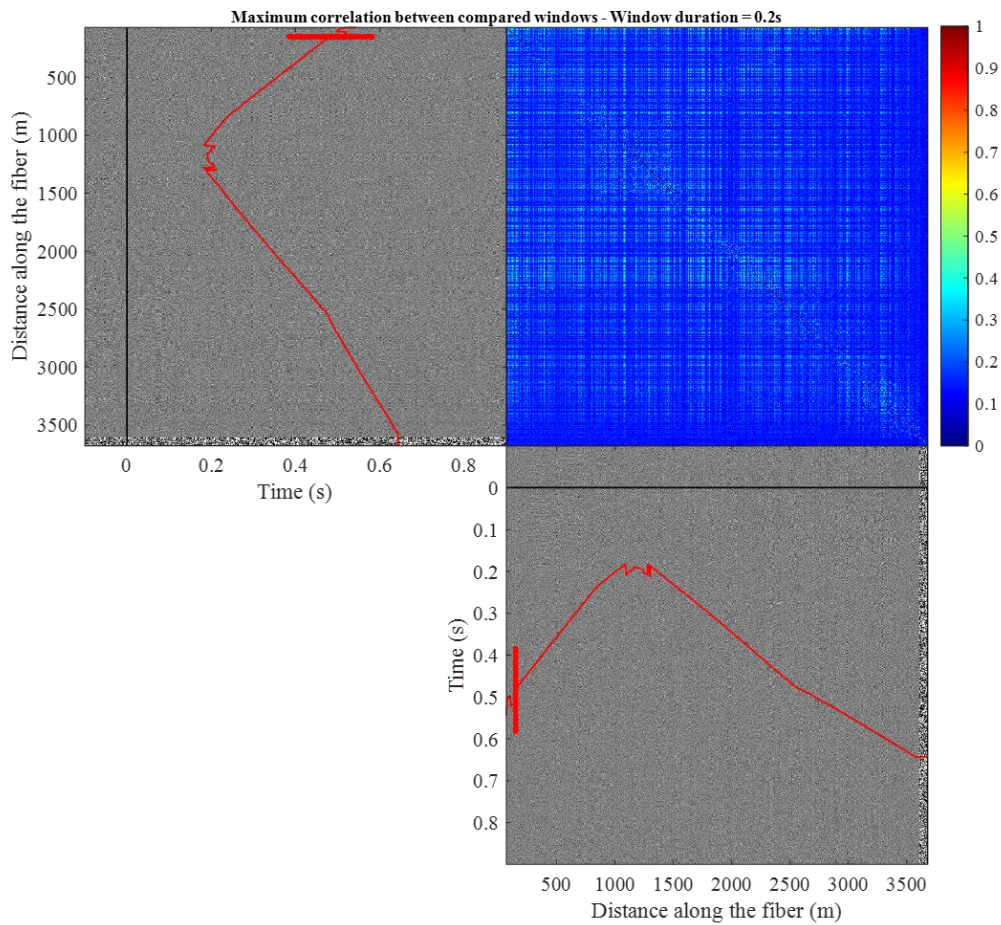


Figure 8-14: Spatial cross-correlation of Figure 8-11 strain-rate. Display similar to Figure 6-14.

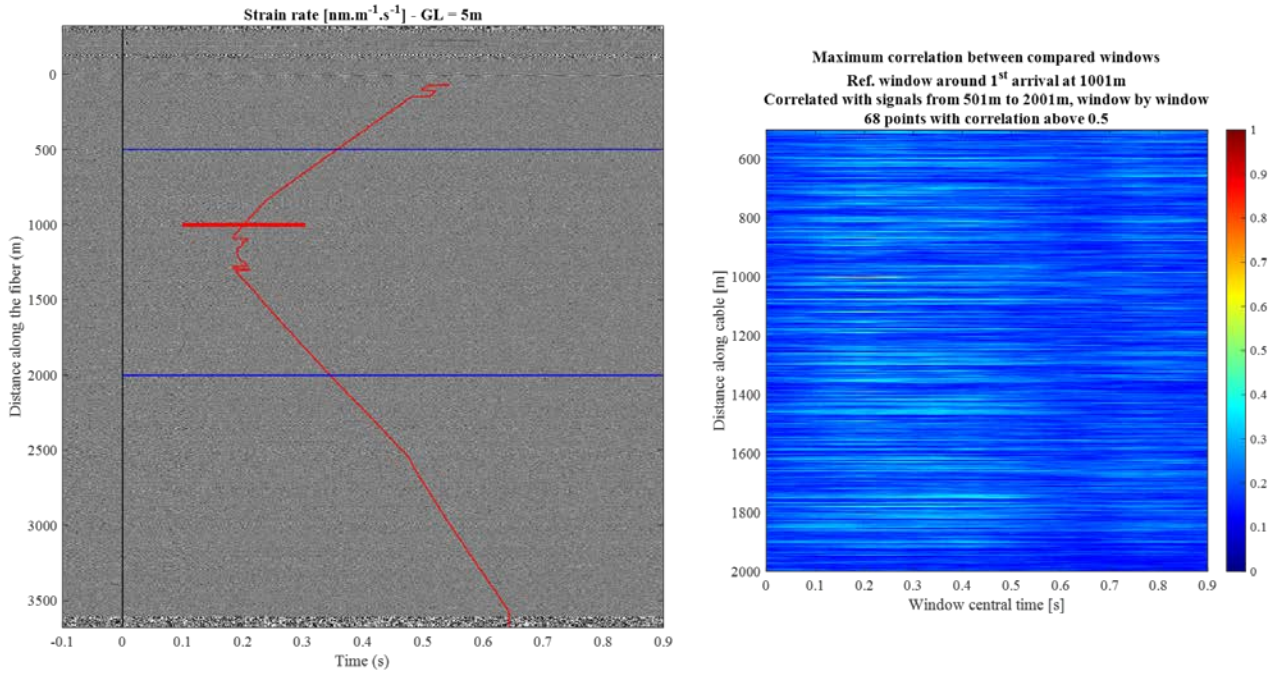


Figure 8-15: Spatial and temporal cross-correlation of Figure 8-11 strain-rate. Display similar to Figure 6-15.

8.4 APPENDIX 4: GL = 5 m, DATA ACQUIRED IN TH4 ON 19-20/11, SOURCE AT 1200 M

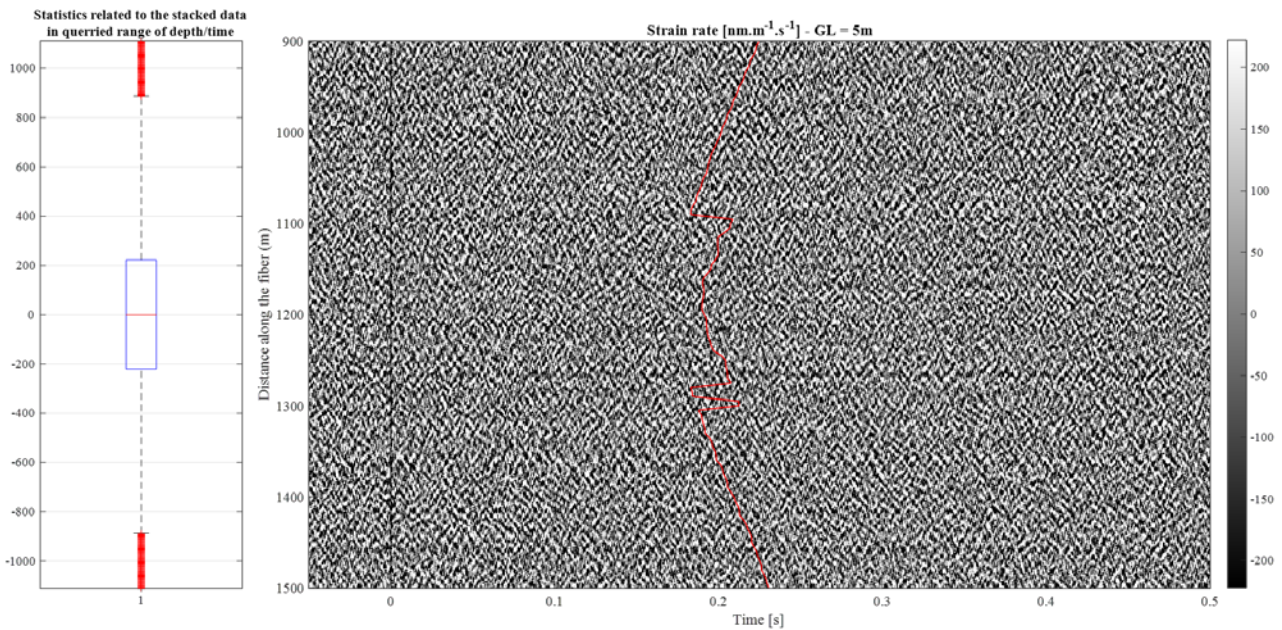


Figure 8-16: Stacked strain-rate, 1446 shots, Th4, 19-20/11, source at 1200 m, GL = 5 m. Display similar to Figure 6-11.

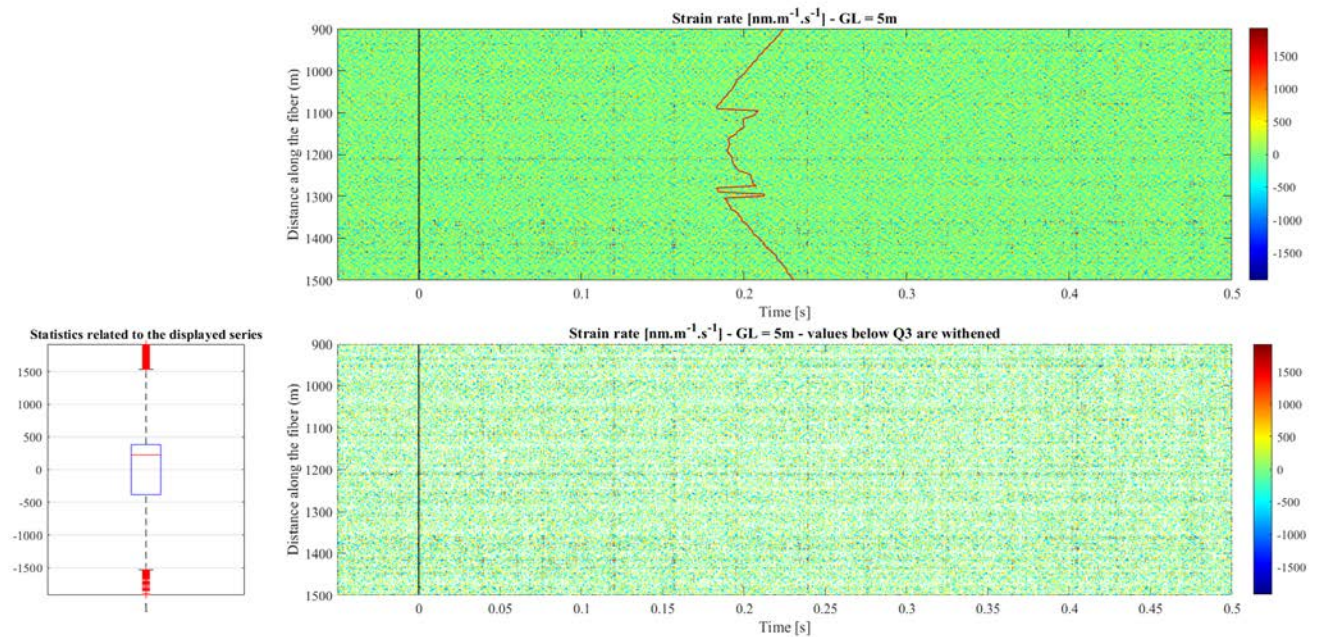


Figure 8-17: Enhanced visualisation of strain-rate of Figure 8-16. Display similar to Figure 6-12.

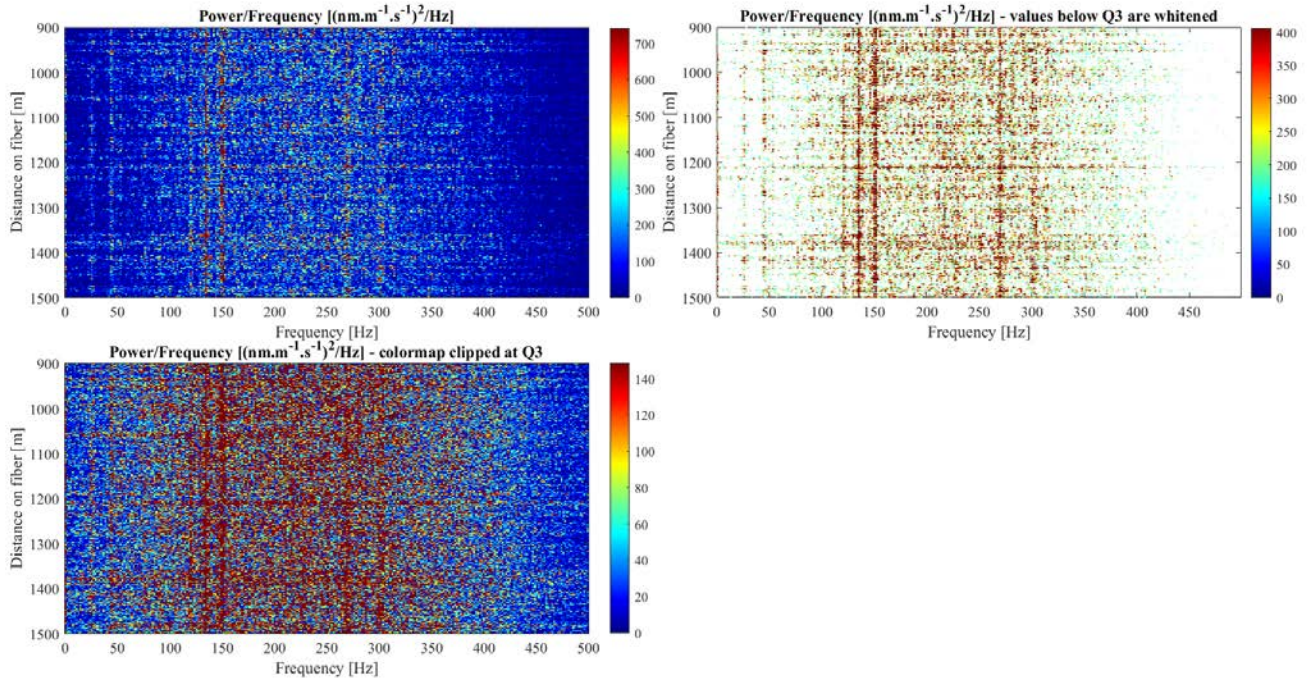


Figure 8-18: Power spectral densities of Figure 8-16 strain-rate. Display similar to Figure 6-6.

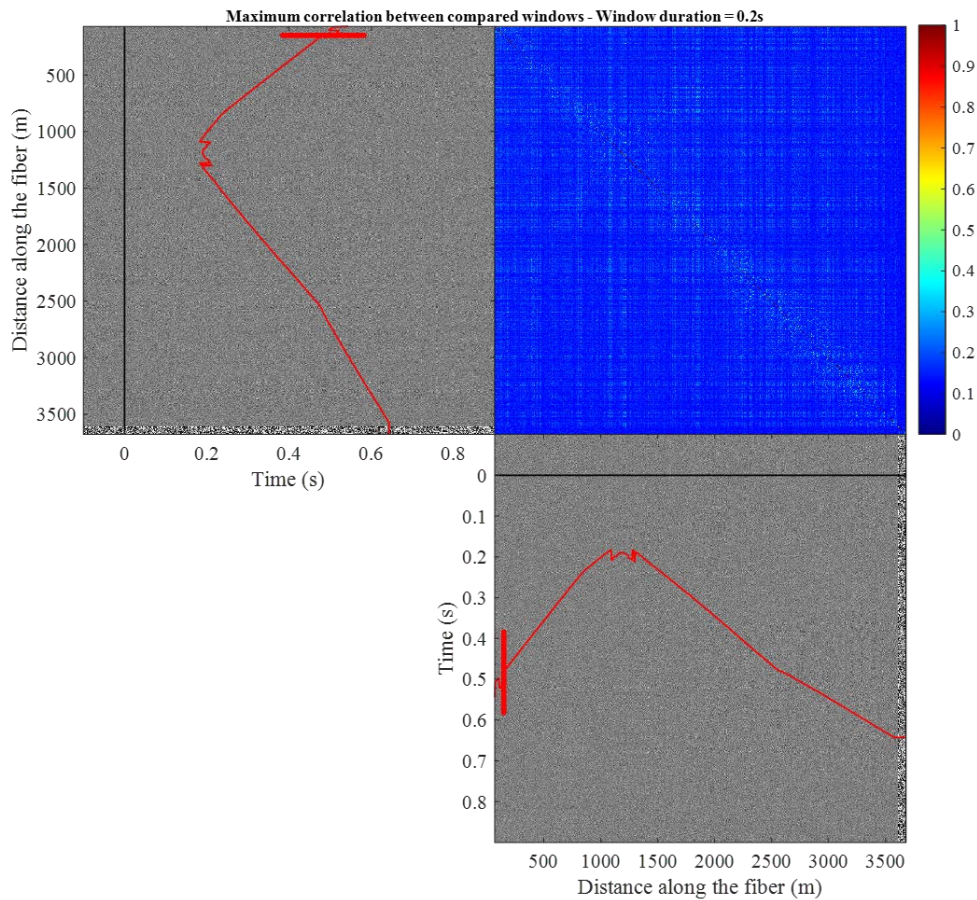


Figure 8-19: Spatial cross-correlation of Figure 8-16 strain-rate. Display similar to Figure 6-14.

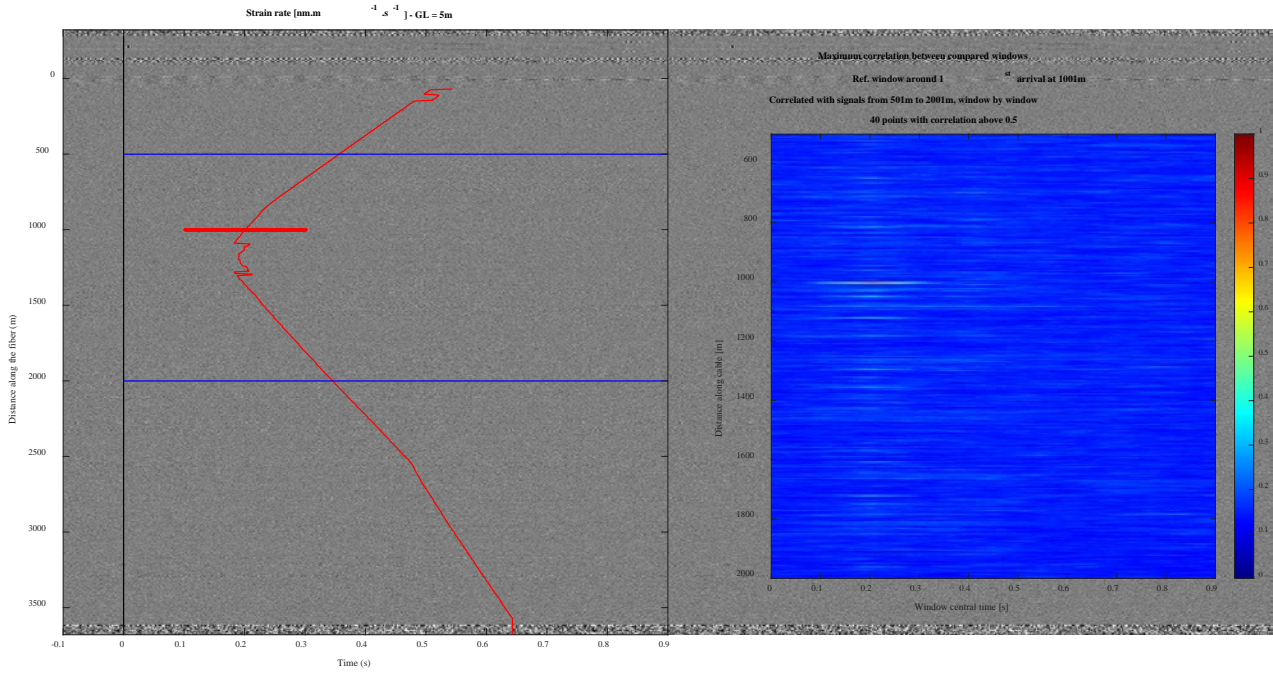


Figure 8-20: Spatial and temporal cross-correlation of Figure 8-16 strain-rate. Display similar to Figure 6-15.

8.5 APPENDIX 5: GL = 5 m, DATA ACQUIRED IN TH3 ON 19/11, SOURCE AT 920 M

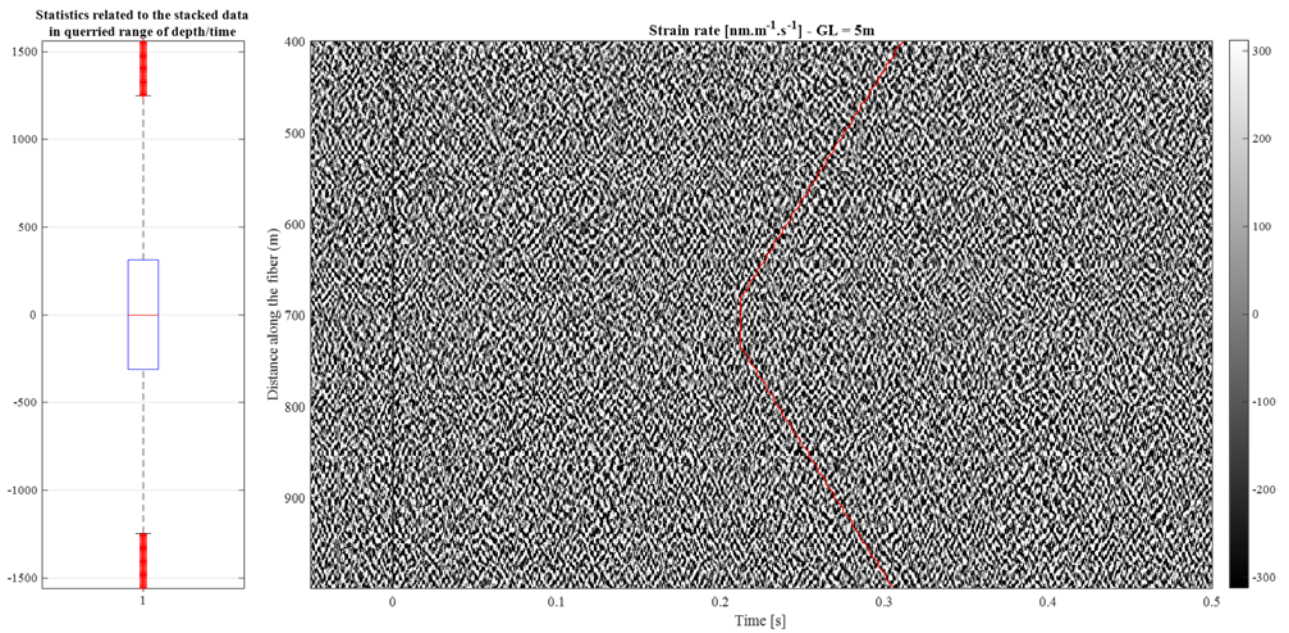


Figure 8-21: Stacked strain-rate, 545 shots, Th3, 19/11, source at 920 m, GL = 5 m. Display similar to Figure 6-11.

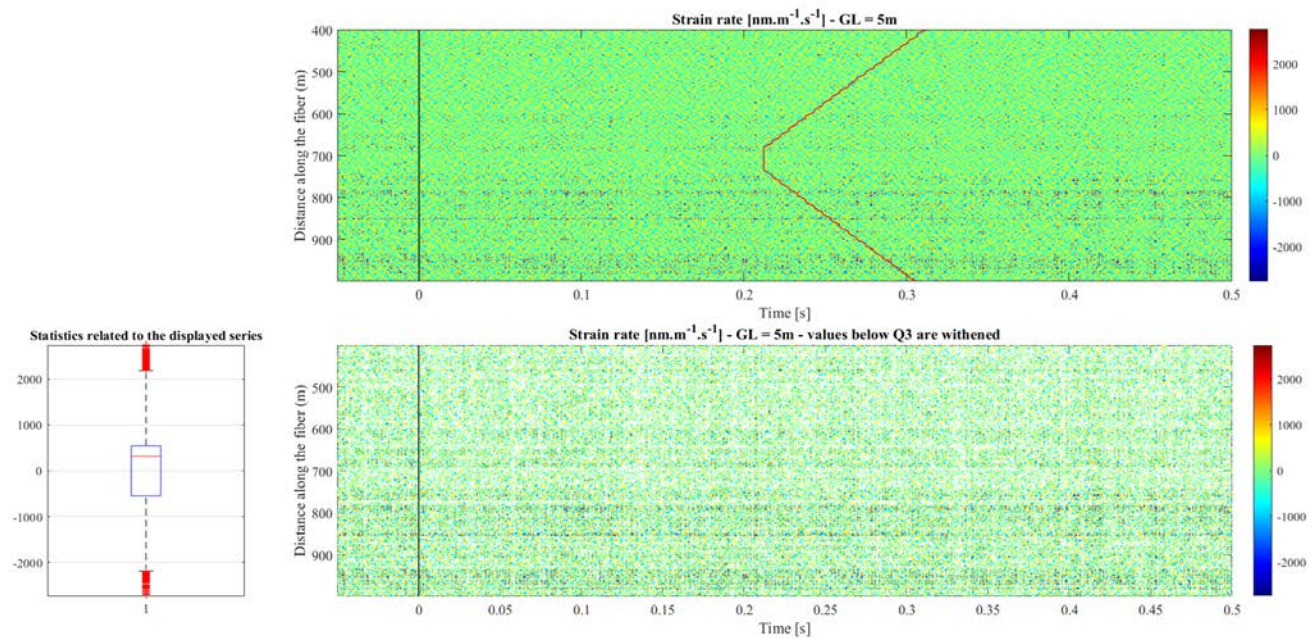


Figure 8-22: Enhanced visualisation of strain-rate of Figure 8-21. Display similar to Figure 6-12.

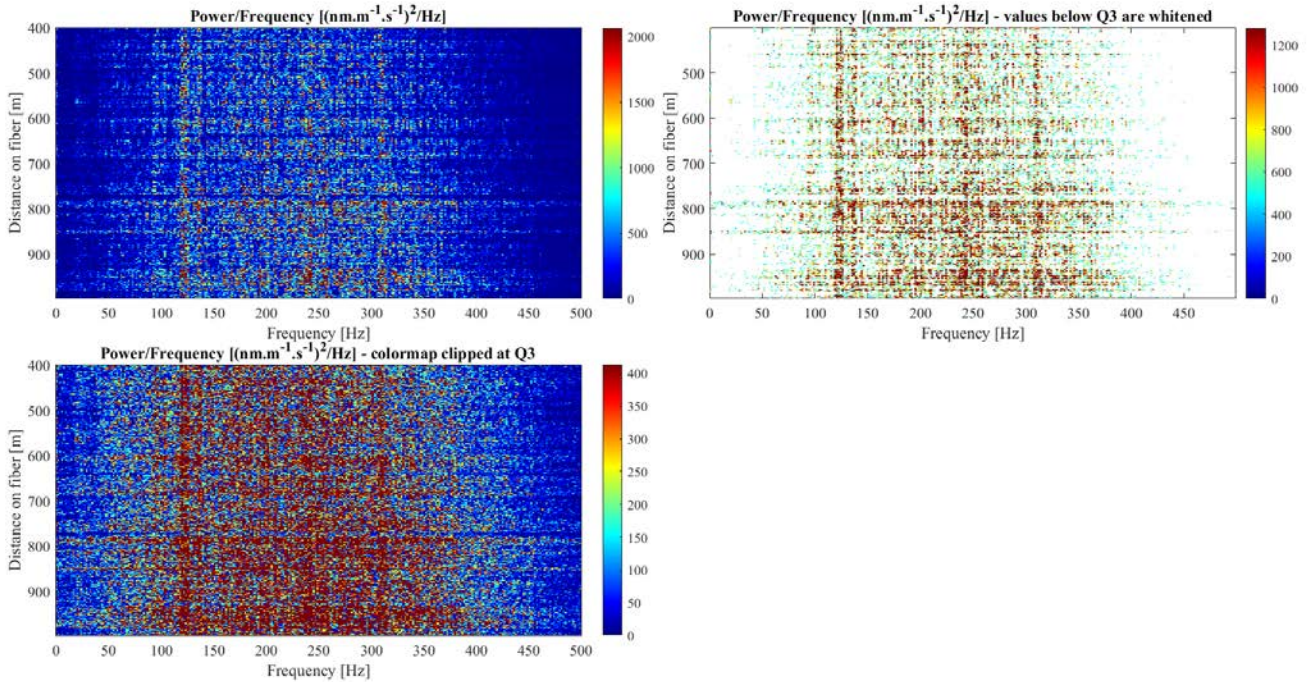


Figure 8-23: Power spectral densities of Figure 8-21 strain-rate. Display similar to Figure 6-6.

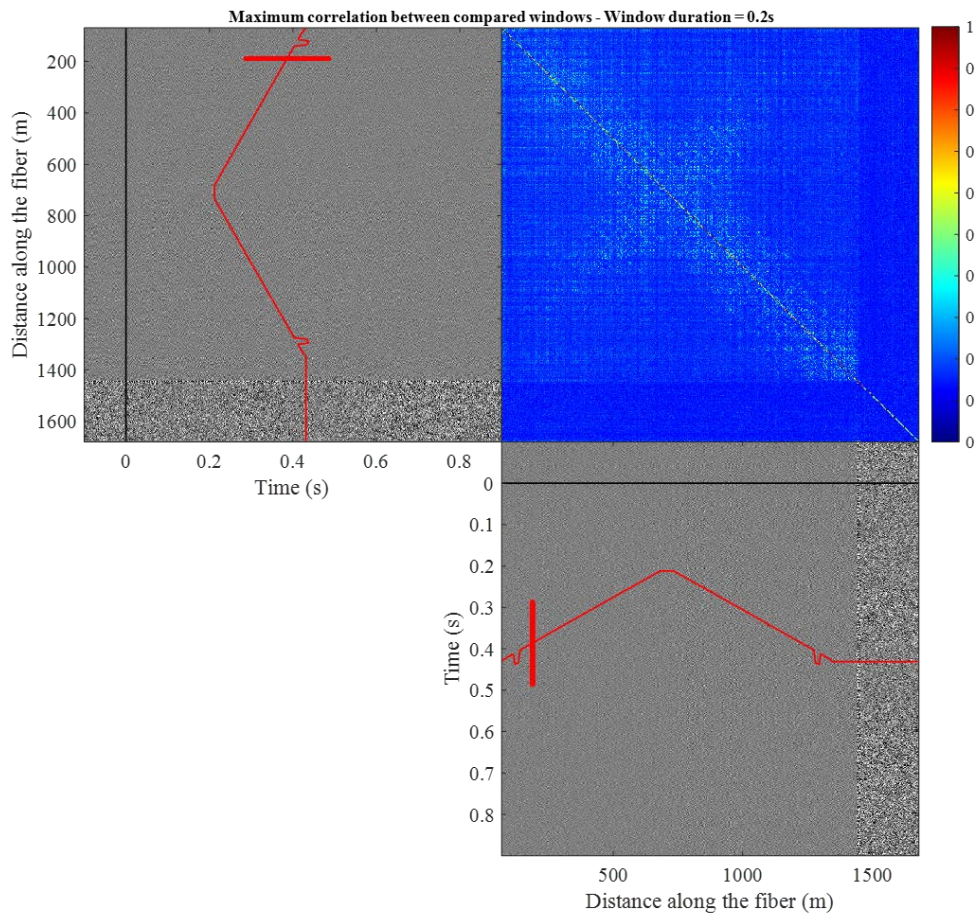


Figure 8-24: Spatial cross-correlation of Figure 8-21 strain-rate. Display similar to Figure 6-14.

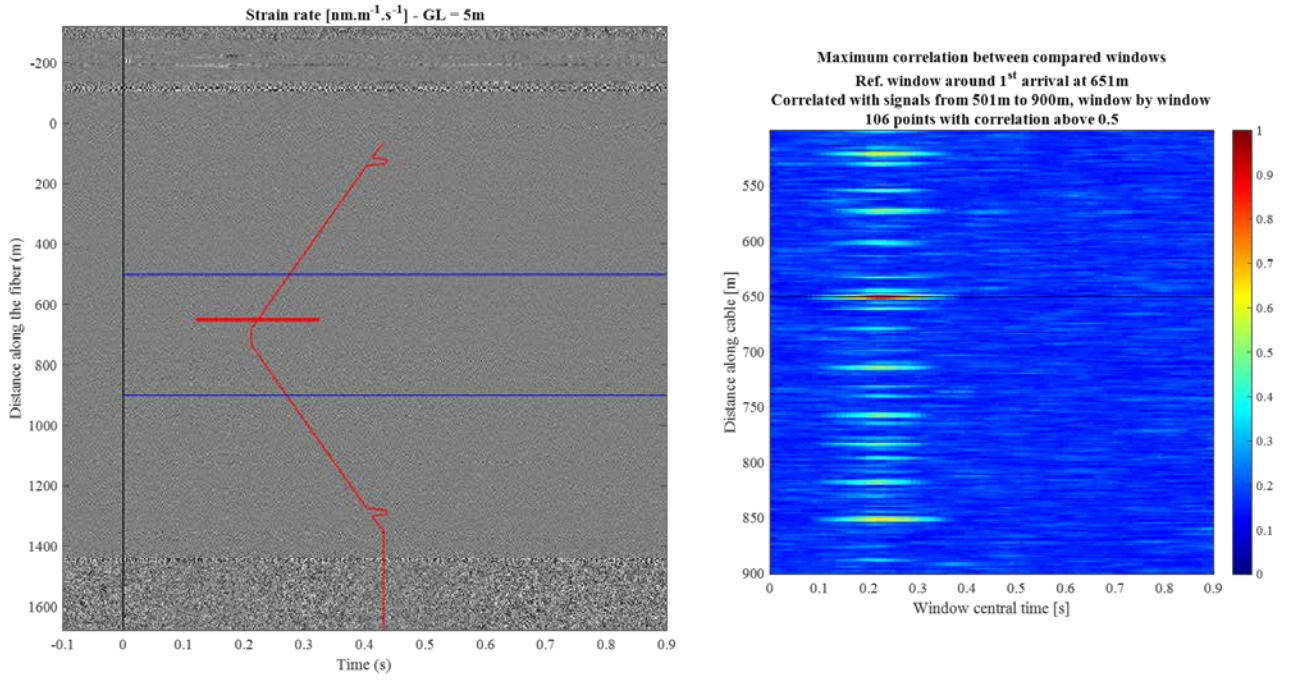


Figure 8-25: Spatial and temporal cross-correlation of Figure 8-21 strain-rate. Display similar to Figure 6-15.

8.6 APPENDIX 6: GL = 10 m, DATA ACQUIRED IN Th3 AND Th4 ON 17/11, SOURCE AT 400 m

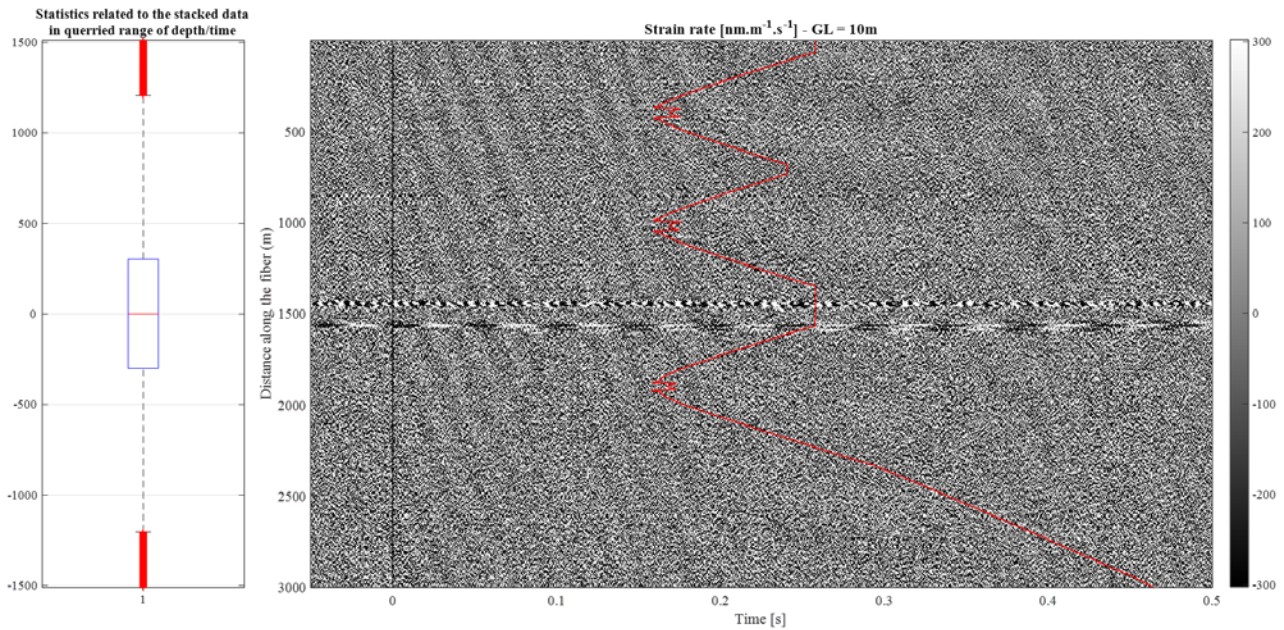


Figure 8-26: Stacked strain-rate, 9 shots, Th3 and Th4, 17/11, source at 400 m, GL = 10 m. Display similar to Figure 6-11.

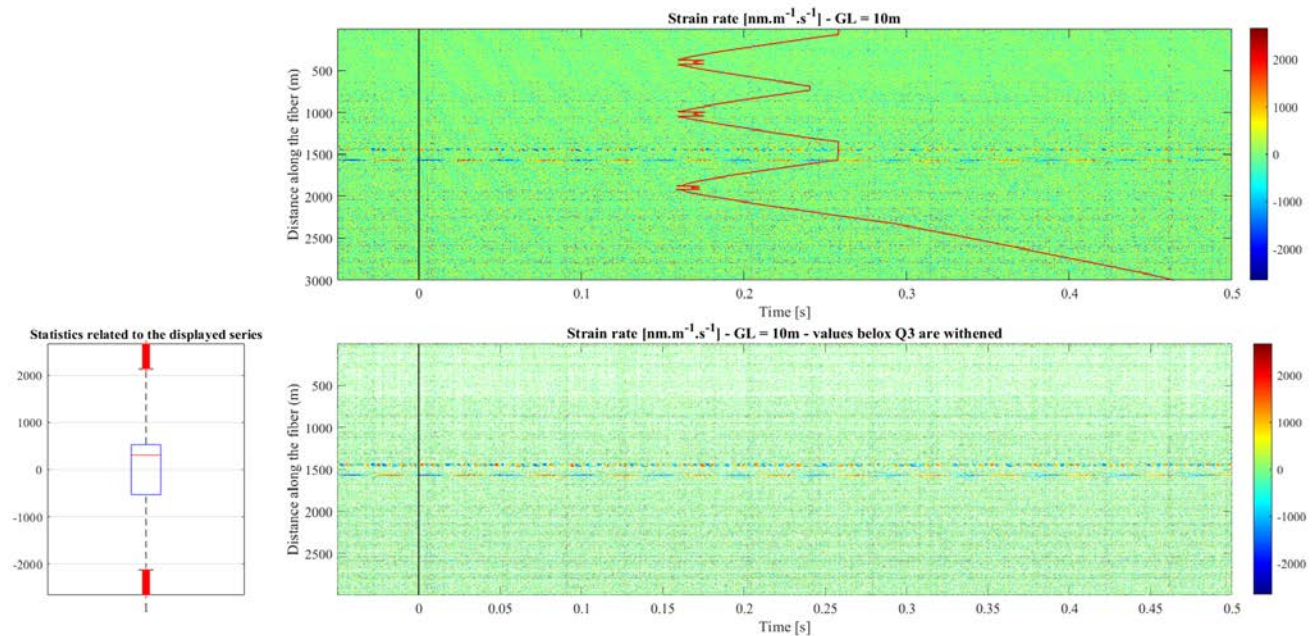


Figure 8-27: Enhanced visualisation of strain-rate of Figure 8-26. Display similar to Figure 6-12.

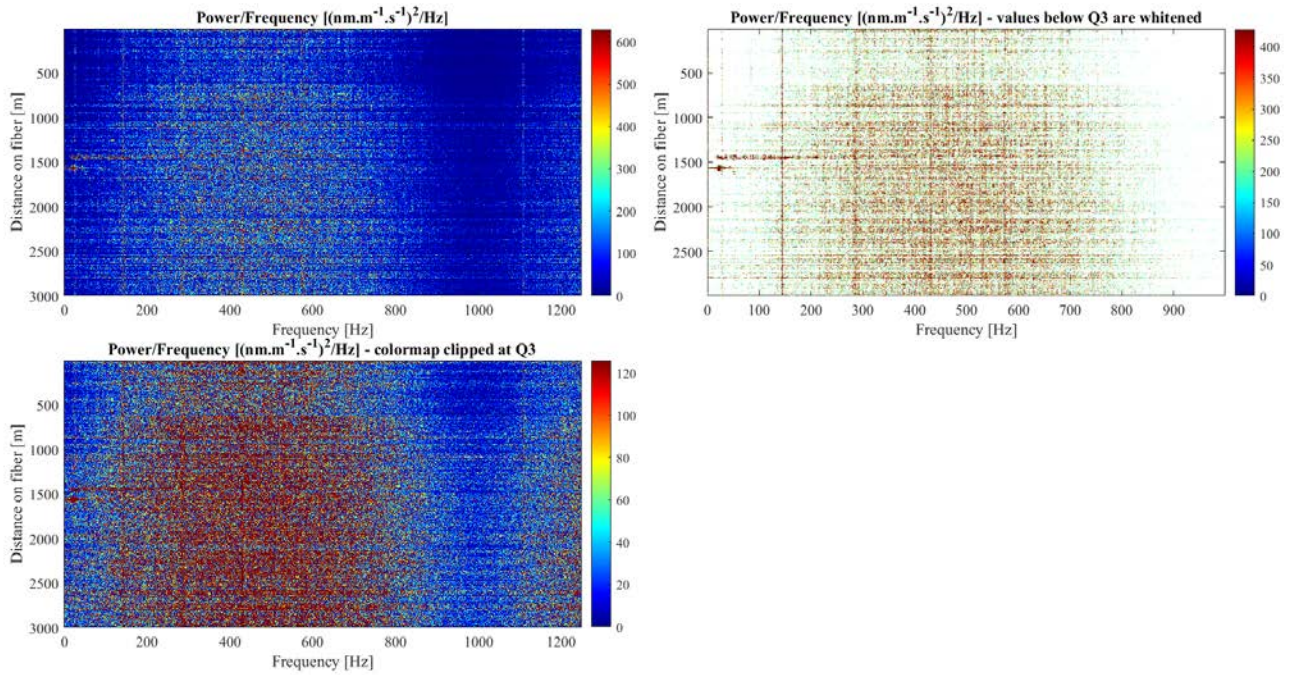


Figure 8-28: Power spectral densities of Figure 8-26 strain-rate. Display similar to Figure 6-6.

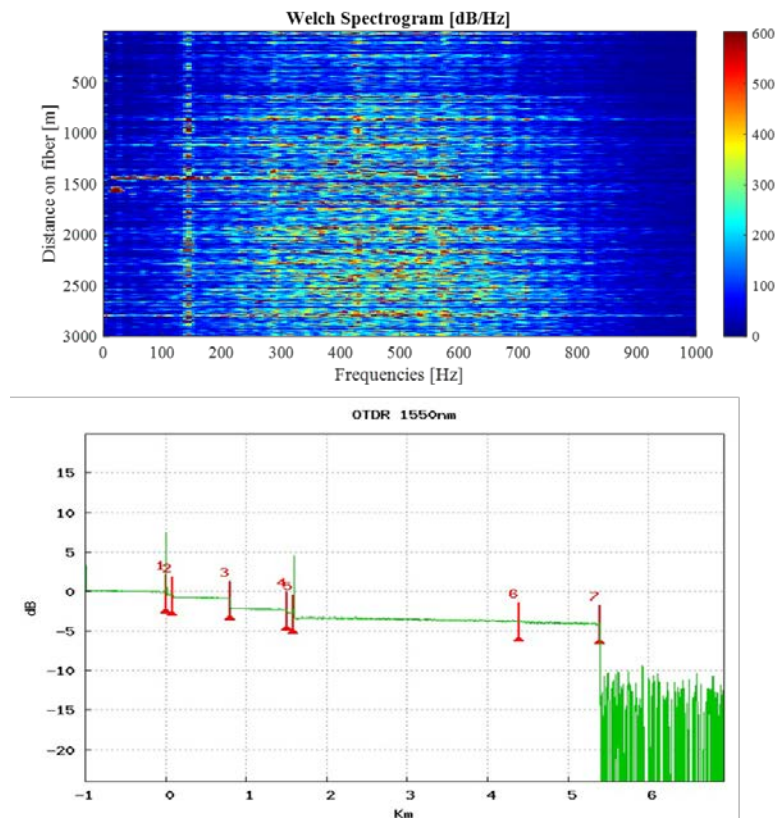


Figure 8-29: Parallel between the Welch spectrograms measured along the Th3 and Th4 FOCs put in series (top) and the OTDR report (bottom) (see “Appendix 1: OTDR measurements on the Th3 and Th4 fibres”). Each spectrogram is calculated with the Welch method to decrease the impact of noise at the cost of the frequency resolution. The depths at which the OTDR highlights strong energy losses are clearly identified on the spectrogram image by a widening of the excited frequency band, associated here with a deterioration of the measurement conditions due to strong reflexions at the connectors/splice/microbend.